Effect of Substrate Concentration and Loading and Catalyst Type on the Performance of a Microbial Fuel Cell

by

Gregory Ryan Dong

A thesis
presented to the University of Waterloo
in fulfillment of the
thesis requirement for the degree of
Master of Applied Science
in
Chemical Engineering

Waterloo, Ontario, Canada, 2009

AUTHOR'S DECLARATION

I hereby declare that I am the sole author of this thesis. This is a true copy of the thesis, including any required final revisions, as accepted by my examiners.

I understand that my thesis may be made electronically available to the public.

Gregory Dong

Abstract

The microbial fuel cell (MFC) is an innovative renewable energy technology that also serves to treat wastewater through the bacteria-driven oxidation of organic substrates. The liquid anolyte contains the organic substrate to be oxidized, while the catholyte contains the substance to be reduced. In a dual-chamber MFC, the catholyte typically contains dissolved oxygen or another easily reducible compound (e.g., ferricyanide) in an aqueous solution, while in a single-chamber MFC, gaseous airborne oxygen reacts directly at the cathode.

A single-chamber air-cathode microbial fuel cell was operated using an acetate substrate and a 0.2 mg/cm^2 platinum catalyst cathode in the initial stages of the project. The platinum catalyst was airbrushed onto a carbon paper cathode and hot-pressed onto a Nafion 117 membrane. After the platinum runs were completed, the MFC was disassembled, cleaned and reassembled with a new non-precious nitrogen-doped carbon composite catalyst replacing the platinum. Two MFCs were operated at different loading levels (1.0 mg/cm^2 and 2.0 mg/cm^2) of the new catalyst. The cell was configured to operate in a fed-batch and upflow modes.

Preliminary experiments were conducted using two non-precious catalysts synthesized with different nitrogen precursors, polyaniline and ethylenediamine (EDA). These experiments showed the ethylenediamine-based-catalyst exhibited higher catalytic activity for oxygen reduction (ORR) with a half-wave potential of 0.57 V versus 0.43 V for the polyaniline catalyst. These values were lower than the expected half-wave potential of 0.65 – 0.70 V. Consequently, the catalyst based on EDA was used in all subsequent experiments. SEM images revealed that this catalyst has a fluffy, bulbous, highly porous structure, while EDAX and XRD both detected the presence of residual iron and cobalt from the preparation procedure. Nitrogen (3.57 wt %) and oxygen (4.87 wt %) were also detected from the EDAX analysis.

Operation with a hydraulic residence time (HRT) of 24 hours and feed COD concentration of 6.44 g COD/L-day was found to produce the highest power density of 141.7 ± 2.4 mW/m^2 from the experiments conducted on the platinum catalyst. A subsequent run at a 12 hour HRT and 3.22 g COD/L-day feed produced only 104.4 ± 5.2 mW/m^2. When the cell operation was reverted to the original high HRT and high feed COD concentration, the original current was not recovered and in fact remained virtually

unchanged from the level attained at the lower HRT and COD feed level (105.7 ± 2.7 mW/m^2). It was suspected that the decreased acetate concentration in the second phase, and the biomass accumulation in the replicate third phase were the cause of the decreased currents. Overall, the COD removal in each phase was high, between 87 – 95% although only a maximum of 4.24% was due to electricity generation. A significant portion of the COD removal during operation at high HRT and feed concentration was due to methane generation (30-50%), while the effect of oxygen leakage from the cathode into the anode compartment was estimated to account for a flux of up to 3.08 g COD/L-day, leading to significant biomass accumulation within the cell.

Upon replacement of the platinum catalyst with the non-precious catalyst at the cathode, the current and power densities generated in the 1.0 mg/cm^2 and 2.0 mg/cm^2 cells rose by 50.5% and 205%, respectively, to 213.2 ± 13.9 mW/m^2 and 431.8 ± 23.6 mW/m^2. Importantly, the current generated in these cells was found to be exactly proportional to the catalyst loading level. The COD removal in these runs amounted to 79.6% and 92.2% of acetate, comparable to that achieved with the platinum catalyst. The coulombic efficiency increased as a result of the improved current densities to 6.71% and 12.18%, respectively. The improved performance with the non-precious catalyst demonstrates that it is a potentially attractive replacement for the conventional platinum as the catalyst for energy production. The proportionality between the generated current density and the catalyst loading also suggests that operation at higher catalyst loading levels will lead to further improvement in performance.

Acknowledgements

First off I would like to thank my advisor, Dr. Mark Pritzker, as well as collaborators Dr. Raymond Legge, and Dr. Wayne Parker for their support and assistance through these past two years. There were several bumps along the road and I appreciated your availability and willingness during the tougher times. Also, a big thanks is extended to Dr. Zhongwei Chen, who introduced the idea of using the non-precious catalyst and took the research in a completely new direction.

Thanks also to all my labmates who helped me along the way as well. The wastewater group was such a treat to work with; thanks to Mirzaman for always helping me whenever the IC decided to misbehave, and Weiwei for always being spunky and cheerful, and of course helpful! Also, I give a big thanks to Mark Sobon for taking care of all the technical details as well. All of the people in Zhongwei's lab were great and helpful during the times I was trying to synthesize batch after batch of catalyst. Last but certainly not least, is Megan. You came in and handled the MFC as if you had been working on it for years. I was surely impressed with the speed at which you settled in, and your poise was impeccable as well. Thanks for picking things up and I am so glad that you found the experience worthwhile.

To all my friends in the Chemical and Civil Engineering department, you made this ride a fun one! I would list all of you, but that would probably take a few pages and there are enough of those in this thesis already.

Lastly, a big thank you is extended to my family and especially my mother, who has always been supportive to the last.

Dedication

To my mother, Irene Cheng, who will begin enjoying
a well-deserved retirement very soon. Congratulations, Mom!

Table of Contents

List of Figures

List of Tables

Chapter 1
Introduction

Renewable energy technologies and environmentally sustainable solutions are gaining considerable momentum not only within the scientific community, but the general population as well. The emergence of hybrid and all-electric vehicles as well as the allocation of $78.6 billion towards green energy projects by the United States in February 2009 [1] are indicative of the awareness and recognition of renewable technologies among the mainstream population. Water treatment is a continuing issue, especially in undeveloped and developing countries where the infrastructure is not present and the energy demands for treatment cannot be met. Microbial fuel cells (MFCs) are a promising technology that combines the generation of electricity with the treatment of wastewater through the metabolic oxidation of organic and inorganic substrates by bacterial species living within a biofilm. At present, MFC designs are still at the laboratory scale. The eventual goal is to scale the technology up to provide power on an industrial or commercial level. Since power densities generated by MFCs are still significantly lower than by hydrogen proton exchange membrane fuel cells (PEMFC), significant improvements in the cell components used are needed. One component that can be especially costly is the catalyst for cathodic oxygen reduction. Platinum is presently the catalyst of choice, but the introduction of an inexpensive alternative is important for lowering the capital cost of the technology. Further research on this topic, as well as improving cell design and scale-up and evaluating long-term reliability and durability are perhaps the key areas of MFC research that will determine whether this technology is commercially viable.

In this chapter, the electrochemical and wastewater treatment principles and background behind MFC operation are described. The research objectives and finally the organization of the thesis will then be described.

1.1 MFC Background

The background to MFC operation is described under the following two sections: electrochemical power generation and wastewater treatment.

1.1.1 Electrochemical Power Generation

The MFC is a biofilm technology whereby bacteria living within a biofilm are responsible for current and power generation. Current is generated through the biocatalyzed oxidation of carbon sources such as starches, sugars, or volatile fatty acids to simpler constituents and reduction of oxygen in air. A schematic of an air-cathode single-chamber microbial fuel cell similar to the one used in this study is given in Figure 1.1.

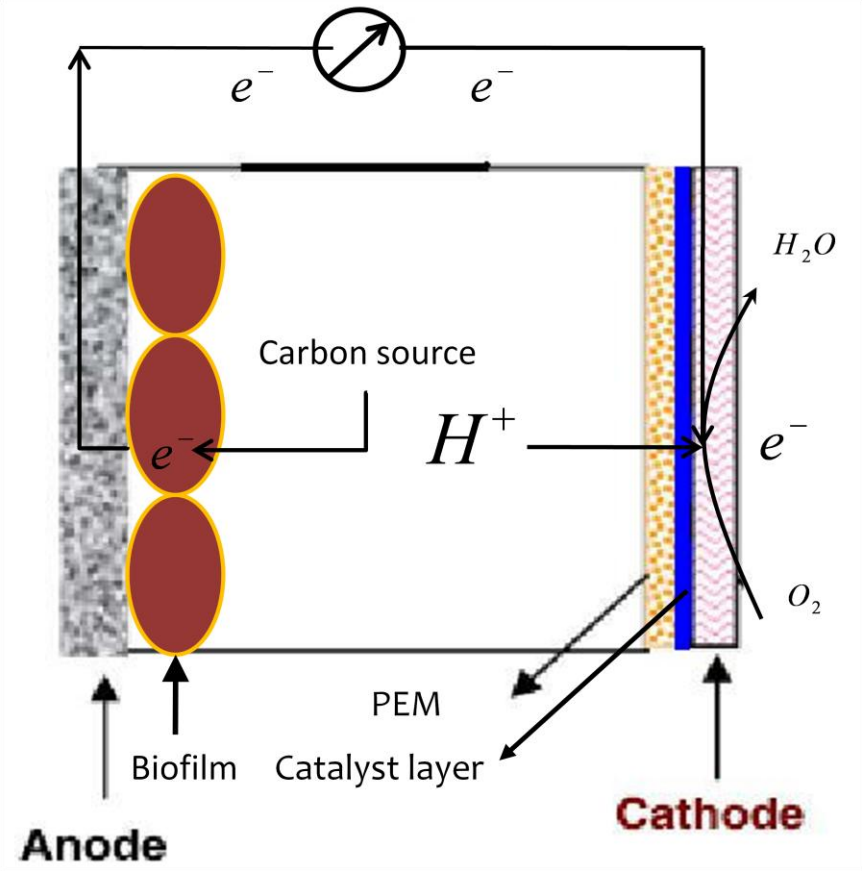

Figure 1.1 Single-chamber Microbial Fuel Cell

The substrate used in this study is acetate, the simplest of volatile fatty acids. In this type of study where an MFC is operated using a synthetic stock solution containing a known concentration of a carbon source, the cell must be first inoculated with a bacterial culture. In this case, the inoculant is a

mixture of aerobic and anaerobic wastewater. Once the MFC is inoculated, a biofilm can begin to grow on the surface of the anode.

The anode serves as the current collector for the anodic reaction, as well as the surface on which the biofilm develops. Bearing these criteria in mind, the anode must be conductive, non-toxic and provide a suitable surface for the bacteria to grow. Carbon paper fits these requirements and also has a high surface area/volume ratio which allows for more bacteria to proliferate. It has commonly been used in MFC research and is used in this study as well.

The oxidation of the carbon source liberates electrons and protons. The electrons liberated from the oxidation reaction travel through the anode, a load (potentiostat in this study) and ultimately to the cathode while the protons travel through the wastewater to the cathode. In some cases, a cation exchange membrane serves as a barrier against liquid leaving the cell and oxygen entering the cell, while allowing protons and other cations to be transported to the cathode. Finally, the protons and electrons combine with airborne oxygen at the cathode to produce water and complete the circuit.

There are two types of MFCs: dual-chamber cells where both the anolyte and catholyte are liquid-based and require containment in separate chambers, and single-chamber cells where air is contacted directly with the cathode, eliminating the need for a cathode chamber. Unlike the dual-chamber MFCs that require a catholyte chamber filled with either a low concentration of dissolved oxygen or non-renewable oxidant such as ferricyanide, the air-cathode single-chamber MFC utilizes the high concentration of oxygen in the air (21%), while minimizing reactor volume. A common problem associated with air-cathode MFCs though, is the loss of current due to oxygen diffusion through the cathode MEA into the anode compartment. Oxygen has a higher potential for reduction relative to other species such as nitrate, sulfate and ferric iron in the anolyte. If dissolved oxygen is present in the anolyte, it will be reduced by the bacteria via aerobic respiration, resulting in the consumption of substrate and aerobic biomass growth without the generation of electricity.

The air-cathode requires a catalyst to improve the slow kinetics of oxygen reduction. By far and away the most common catalyst is platinum since it exhibits the best catalytic activity and is commonly used in PEMFCs. Obviously, due to its high cost and limited availability, alternatives are being sought to improve the economical viability of the technology. An objective of this study is to compare the

current and power outputs obtained using a non-precious nitrogen-doped carbon composite catalyst to that obtained using a conventional platinum catalyst..

1.1.2 Wastewater Treatment

The oxidation of the carbon sources present in the feed stream serves the additional purpose of reducing the chemical oxygen demand (COD) of the discharged solution. Reduction of the COD of a wastewater to a regulated limit is required if it is to be discharged from an industrial plant or municipal water treatment facility. A generalized oxidation reaction for a generic carbon source is given below in reaction 1.1:

$$Carbon\ source + H_2O \rightarrow CO_2 + H^+ + HCO_3^- + e^- \quad \textbf{1.1}$$

The MFC can be considered to be both aerobic and anaerobic. It is aerobic in that the terminal electron acceptor at the cathode is oxygen, but anaerobic in that anolyte itself oxygen-free with the oxygen reduced on a cathode physically separated from the anolyte. Ideally, all of the electrons liberated by reaction 1.1 should be able to generate electricity. In practice, competing electron acceptors in the wastewater such as dissolved oxygen, nitrates, and sulfates can accept electrons before they can reach the anode, resulting in a short circuit, reducing the current generated. If acetate is the only carbon source, the final metabolic pathways are reaction 1.1 to form bicarbonate carbon dioxide and protons or methanogens that convert the acetate to methane by reactions such as:

$$CH_3COOH \rightarrow CH_4 + CO_2 \quad \textbf{1.2}$$

$$CO_2 + 4H_2 \rightarrow CH_4 + 2H_2O \quad \textbf{1.3}$$

The reduction of oxygen at the cathode occurs as follows:

$$O_2 + 4H^+ + 4e^- \rightarrow 2H_2O \quad \textbf{1.4}$$

The COD of the feed is a measure of the available electrons that can be converted into current. In this study, the current generated and the acetate COD consumed were measured to determine the coulombic efficiency, which gives the percentage of the theoretically generated electrons that were converted to current. In addition to the COD removed through current generation, several other possible COD sinks are listed below:

- electricity generation
- methane generation
- anaerobic biomass production (from methanogens or due to sulfate/nitrate reduction)
- aerobic biomass production (due to oxygen infiltration from the cathode)
- unreacted substrate leaving in the discharge stream

In environmental chemistry, the COD is an indirect measure of the amount of organic compounds in water, more specifically the amount of organic pollutants found in surface water. Since the discharge from any wastewater treatment process (including MFCs) will likely enter a body of surface water, the COD becomes a useful measure of water quality for the MFC.

The sum of all COD eliminated by these sinks should equal the COD brought into the cell in the feed stream. Another objective of this study is to close the COD balance using these COD sinks. Other wastewater parameters measured in this study include the pH, oxidative-reductive potential (ORP), dissolved oxygen (DO) level and total and volatile suspended solids content of the discharge stream.

1.2 Research Objectives

The research objectives of this thesis project are three-fold. Firstly, the operation of a single-chamber MFC is monitored under different conditions using a platinum catalyst. Secondly, the catalytic activity of two non-precious carbon composite catalysts is compared on the basis of their oxygen reduction reaction (ORR) potentials. One catalyst is then selected to be further characterized and used in MFC operation. Lastly, the selected catalyst is utilized in an MFC at different loading levels and compared to the optimum performance obtained with the platinum catalyst. During MFC runs, electrochemical

parameters such as current and power outputs are continually monitored on-line, while wastewater parameters such as COD removal are regularly measured off-line.

Specific research objectives are outlined as follows:

- Selection of a non-precious nitrogen-doped carbon composite catalyst by comparison of ORR potentials of two non-precious carbon composite catalysts - one based on a polyaniline nitrogen precursor and the other based on an ethylenediamine precursor.

- Characterization of the structure of the selected catalyst by scanning electron microscopy (SEM), elemental analysis by energy-dispersive x-ray spectroscopy (EDAX) and crystal composition by x-ray diffraction (XRD).

- Establishment of a baseline MFC performance by varying hydraulic residence times (HRTs) and substrate concentration to find the optimum feeding conditions for current production in an acetate-fed single-chamber MFC using platinum on carbon black as a cathodic catalyst.

- Assessment of the performance of the MFC to reduce the COD level of the feed stream and accounting for the fate of COD fed to the system on the basis of a COD balance.

- Characterization of the quality of the discharge by monitoring common wastewater parameters such as pH, oxidative-reductive potential (ORP), dissolved oxygen content (DO), total and volatile suspended solids (TSS/VSS).

- Comparison of the current production and wastewater treatment capability of the selected nitrogen-doped carbon composite catalyst to that achieved using the platinum catalyst.

1.3 Thesis Organization

This thesis is organized into several chapters. Chapter 1 discusses some of the basic principles involved in MFC operation along with the research objectives. Chapter 2 provides a review of the literature on the developments in MFC technology, including those related to non-precious nitrogen-doped carbon

composite catalysts. Chapter 3 assesses the catalytic activity of two nitrogen-doped carbon composite catalysts using different nitrogen precursors, followed by the characterization of the selected catalyst. Chapter 4 describes the analytical parameters and experimental design of the platinum-based MFC, followed by a discussion of the experimental results obtained with this cell. The results from this chapter establish the baseline performance which the results obtained with the non-precious metal catalyst are to be compared that are covered in Chapter 5. Chapter 6 presents the principal conclusions obtained from this study and recommendations for improvements to the system. A list of all references is presented as Chapter 7.

There are five appendices included in this thesis. Appendix A lists the abbreviations included in this thesis. Appendix B describes the procedures for synthesis and characterization of the nitrogen-doped carbon composite catalyst. Appendix C presents the sampling and solution preparation procedures followed in this project, while Appendix D outlines the analytical procedures for all wastewater parameters. Appendix E is a CD containing the experimental data collected (not available in the electronic version).

Chapter 2
Literature Review

As with any fuel cell, a main objective of the MFC is to generate electrical power. However, since it is likely to be also used for the purposes of wastewater treatment, it has the added objective of effectively treating wastewater mainly through the reduction of COD, although it may also be useful for the removal of specific inorganic species such as sulfides [2] and nitrates. [3] Given that this technology is still in its early stages of development and the addition of a biological component to a conventional fuel cell introduces a number of challenges, the research focus has been broad, covering aspects such as (but not limited to) materials, fuel cell design and configuration, substrates for metabolism, choice of inoculant (mixed culture versus pure culture) and catalyst usage. With the large range of available operating variables available, it is important to first attain a solid understanding of the history as well as the current state of MFC research.

The origin of using microorganisms to generate electricity is not a new concept and dates back to 1910 when Potter first discovered electricity production by *E.coli*. [4] These results were later substantiated in 1931 when Cohen demonstrated that a voltage of 35 V could be achieved from MFCs connected in series. [4] Although some studies in the 1950s and 1960s were conducted, the past 15 years have seen a significant push in the area of MFC research. This increased attention is no doubt due to the greater awareness and demand for renewable sources of energy as well as improved water treatment.

2.1 Evaluation of MFCs

MFC performance can generally be evaluated based on two main parameters: power generation through oxidation of organic and inorganic substrates, and COD removal capability, which is a key wastewater parameter. This section covers each aspect various aspects on minimizing polarization losses, which will improve power production, as well as the ability of MFCs to remove COD from a feed stream, thus improving water quality of the discharge.

2.1.1 Polarization Losses, Influence on Design

As stated in the introduction, all fuel cells are subject to three types of polarization losses: activation, ohmic and mass transfer. A typical polarization curve for microbial fuel cell application is shown in Figure 2.1.

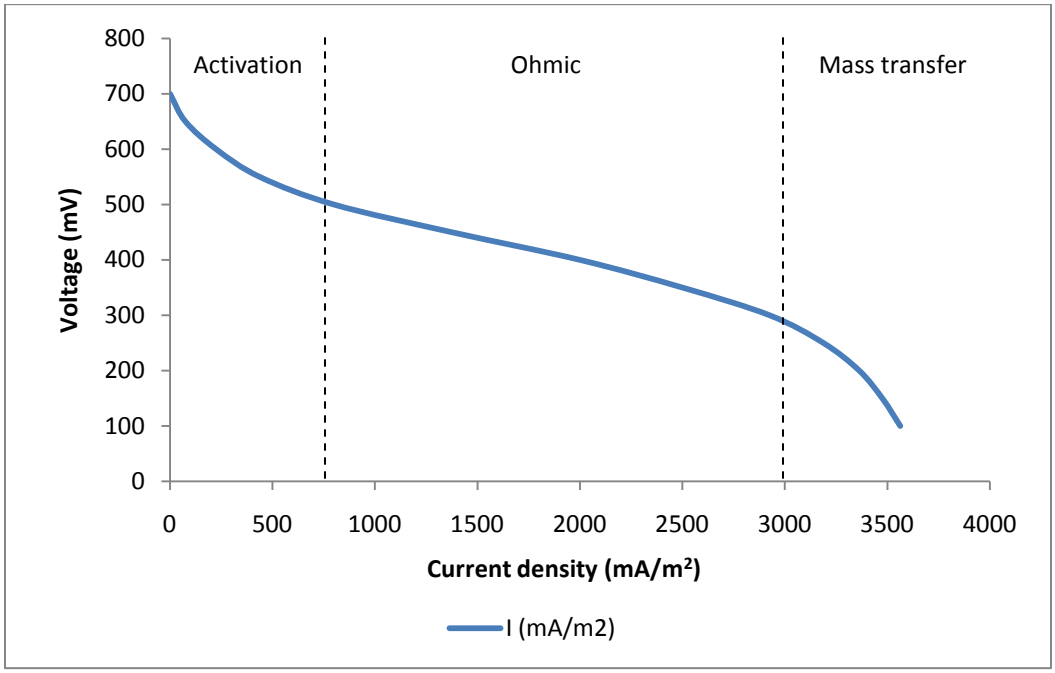

Figure 2.1 Example of a polarization curve for a MFC with overpotential regions indicated

When designing an MFC, each type of polarization loss should be minimized in order to decrease overall potential losses and thus increase the power generation. A fundamental characteristic of MFCs is that most of the biocatalytic oxidation of the substrate occurs within a biofilm attached to the anode.

Several studies have focused on delineating the activation losses occurring at the anode as well as methods by which these losses can be reduced. Ramasamy *et al.* [5] used electrochemical impedance spectroscopy (EIS) and found that the impedance associated with the anode is the dominant loss in an MFC, even with an established biofilm. They also reported that the charge transfer resistance dropped from 2.6 to 1.5 kΩ-cm^2 after 5 days of closed circuit operation and decreased further to 0.48 kΩ-cm^2

after 3 weeks of operation. This indicates that as the biofilm becomes established, biocatalytic oxidation of substrate is enhanced and thus activation losses are reduced. A modeling study by Pichoreanu *et al*. [6] found that a decrease in the initial suspended biomass concentration as inoculant appears to favour the growth of biofilm biomass within an MFC relative to suspended MFC biomass. Furthermore, this leads to an increase in biofilm thickness and density and consequently raises the maximum current that can be generated, although it is worth noting that the amount of charge obtained over a batch cycle was not affected.

As with the anode, the reduction reaction of the oxidant at the cathode of an MFC is also subject to polarization losses. In conventional PEMFCs, precious metal catalysts such as platinum are often used to decrease the activation energy required for oxygen reduction. The same is true in MFCs, although strides have been made to move away from platinum catalysts due to their cost. Further discussion regarding the use of precious and non-precious catalysts will be covered later in this literature review. The use of the ferricyanide ion as the terminal electron acceptor rather than oxygen has been investigated in some studies and found to improve cell power by up to an order of magnitude. Although the theoretical half-cell potential of oxygen reduction is higher than that of ferricyanide (1.23 V SHE vs. 0.36 V SHE), ferricyanide reduction to ferrocyanide has very fast kinetics, leading to much lower activation losses. [7] Also, the limitation associated with the low oxygen solubility is alleviated since the cell can be operated at much higher ferricyanide concentrations. A concentration of 50 mM ferricyanide is common in MFC applications. The faster electrode kinetics also eliminates the need for a catalyst at the cathode.

Similar to the case of PEMFCs, MFCs also exhibit ohmic (electrolyte) resistance associated with the transport of H^+ ions from the anode where they are liberated to the cathode. However, unlike PEMFCs which use a proton-permeable membrane (Nafion) as the solitary electrolyte, MFCs rely on the ions present in the wastewater such as Na^+, Mg^{2+}, K^+, SO_3^{2-}, NH_3^+ and NO_3^- to provide the ionic conductivity of the anolyte. [8] Given that the wastewater solution is not concentrated; its proton conductivity is much lower than that of Nafion. Although a Nafion membrane is commonly used in MFC systems to separate the anode compartment from the cathode or cathode compartment due to its proton-permeability and hydrophobicity, its importance is not likely as critical as in a conventional PEMFC. In PEMFCs, protons liberated at the anode can transfer directly to the cathode since both

electrodes are hot-pressed to the Nafion and so very closely spaced. The hydrogen source in these cells is typically gaseous and free of ionic impurities that can occupy the negatively charged sulfonic acid active groups on the Nafion structure. Thus, more active sites are available for proton transfer and ohmic losses are lower. Anolyte solutions in MFCs typically contain cation species at concentrations that are about 10^5 times higher than that of protons (at a typical operating anolyte pH of 7), resulting in fewer active sites for proton conduction and higher ohmic resistance.

In a study on a cell in which Nafion was incorporated, Rozendal *et al*. [8] found that several cationic species also are transported into the catholyte solution and that these species are responsible for the majority of positive charge transfer required to maintain electroneutrality in the anolyte and catholyte solutions. Although MFCs do not necessarily require an aqueous catholyte, this study found that proton transfer from the anolyte into the catholyte must be improved to further enhance cathodic reduction of oxygen and in turn the power densities. To help minimize this effect, phosphate buffers and to a lesser extent bicarbonate buffers can be added to anolyte solutions to increase proton conductivity. For example, Min *et al*. [9] found that the addition of a 100 mM phosphate buffer caused a four-fold increase in the maximum power density (from 70 to 320 mW/m^2) and a 25% rise in overall power density (from 70 to 98 mW/m^2) obtained from a given wastewater. Although useful for laboratory-scale experiments, the addition of phosphate buffers may not be feasible for pilot-scale and industrial-scale applications as they are non-renewable and can be expensive. Initial studies using bicarbonate buffers have shown promising results by yielding better performance than that achieved using phosphate buffers. [10] However, since very few such studies on the use of these buffers have been reported, their overall efficacy still remains questionable.

The incorporation of Nafion in an MFC also adds to its ohmic resistance and therefore tends to reduce achievable power densities. Its use in an MFC stems from its excellent success in conventional chemical fuel cells for high proton conductivity and limited oxygen diffusivity. However, as mentioned previously, since other cations are present at much higher concentration than protons in an MFC, the proton conductivity is limited. Nafion membranes are also relatively expensive. For these reasons, the future development of MFCs may entail either the removal of Nafion or substitution with another cheaper membrane which can limit oxygen permeability.

Mass transfer polarization losses occur when current densities are high enough that the oxidant (oxygen) or reductant (substrate) availability at the electrode surface becomes limiting. Since the oxidation reactions of interest occur within the biofilm at the anode, mass transfer can be limited at the bulk phase/biofilm interface due to difficulties associated with the diffusion of the substrate into or through the biofilm itself and also the competition between organisms that can consume the substrate before an anodophilic organism is encountered. Marcus *et al*. [11] developed a model for electron donor oxidation at a biofilm anode and reached several conclusions which are relevant to polarization losses. The conductivity of the biofilm (κ_{bio}) dependence on biofilm density and thickness is a key indicator of the limitations of a particular biofilm. It also strongly influences electron donor fluxes and biomass distribution. At lower κ_{bio} (~10^{-5} mS/cm), the anode potential is limiting (activation polarization). At high κ_{bio} (10^{-3} mS/cm), mass transfer of the electron donor (acetate) to the active biofilm residing near the anode becomes limiting due to lower ohmic resistance and increased substrate utilization, to the point where the transfer of the substrate to the active portion of the biofilm near the anode becomes limiting. Marcus et al. also found that biofilm thickness should be kept to a minimum so that inert biomass does not accumulate and increase biofilm thickness and thereby inhibit transport of substrate to active biomass near the anode surface.

Cathodic mass transfer losses dominate when the rate of oxidant species flux to the cathode is low. This often occurs when the oxidant is dissolved oxygen in solution due to its low solubility in water (8 mg/L at 27ºC). In addition, the amount of catalyst loading may also affect mass transfer. Since platinum is still the most widely used catalyst for oxygen reduction in an MFC, the minimization of the catalyst loading while still maintaining performance is important to reduce costs. One study revealed that only a minor drop in cathode potential by 20 mV occurred when the Pt catalyst loading was decreased from 2 mg/cm^2 to 0.1 mg/cm^2 at a current density of 1 mA/cm^2. [12] A loading of 0.5 mg/cm^2 at the same current density caused the cathodic potential to drop by only 10 mV.

2.1.2 MFCs as a Wastewater Treatment Technology

The second major function of an MFC is to convert oxidizable substrates in a feed stream to fully reduced species. By doing so, the chemical oxygen demand (COD) of the effluent is reduced. COD can be from natural sources such as domestic [13,14] or industrial [15, 16] wastewater, or by addition of

synthetic sources such as volatile fatty acids [13, 17], sugars [18, 19], or starches. [20] The COD is an important wastewater treatment parameter because any oxidizable compounds that are discharged to a body of water will then be aerobically reduced by organisms, thus reducing the dissolved oxygen concentration in the water and consequently suffocating aquatic biota.

The amount of COD removal in an MFC is a function of the complexity of the substrate, the hydraulic residence time (HRT) of the solution, and the maturity of the microbial community. Complex substrates such as sugars and starches take a longer time to fully metabolize as they are first degraded into simpler sugars, and then volatile fatty acids, before finally being oxidized to methane, hydrogen sulfide, and carbon dioxide. [21] MFCs can be operated using a wide variety of HRTs, ranging from 22 minutes [17] to several days [16] though most that are operated continuously or as fed-batch have HRTs of 2 days or less. The HRT is inversely proportional to the COD removed; the shorter the HRT, the lower the COD removal. [14, 17] For example, one study by Min and Logan varied the HRT and observed its effect on COD removal as well as power production. They found that as the HRT decreased from 4.0 hr to 1.1 hr, power production from a domestic wastewater feed increased from 43 to 72 mW/m^2, while COD removal increased from 42% to 79% (246 mg COD/L feed). [17]

Recent research has also attempted to further treat the effluent from an MFC by looping it to the cathode chamber for cathodic reduction of nitrates and nitrites. After oxidation of the carbonaceous compounds in the anolyte chamber, the ammonium-rich effluent is sent through an air stripper to convert the ammonium to nitrate. Finally, the discharge from the stripper is cycled through to the cathode chamber, where it is reduced to nitrogen gas. One study by Virdis *et al*. successfully ran this type of dual-treatment configuration, producing a maximum of 34.6 W/m^3 while removing 100% of a 1 g COD/L as acetate feed at a coulombic efficiency of 40.8%, and 58.9% of a 586 mg/L nitrate feed at a coulombic efficiency of 72.2%. [22] These types of MFCs may play a larger role in situations where wastewater treatment is of higher priority, as aeration of a stripper for conversion of ammonium requires a pump, decreasing net power production.

2.2 Current MFC Designs

Today, MFC designs are numerous and of varying complexity. The design is often dependent on the purpose of the MFC, whether it is to analyze a particular aspect of MFC operation, like microbial community analysis, or increasing power production through comparison of materials like anode/cathode electrodes, catalyst considerations, or by varying feed conditions. This section covers two main MFC designs, the dual-chamber and single-chamber configurations.

2.2.1 Shift from Dual-Chamber (DCMFC) to Single-Chamber (SCMFC) Architecture

One of the most important objectives of any MFC or fuel cell is to produce as much power as possible in the most efficient manner. The term "efficient" is very broad and can be based on not only direct efficiency relations such as coulombic efficiency and energy efficiency, but also the areal and volumetric current and power densities, material costs and design simplicity. MFCs typically are designed as either dual-chambered (DCMFC) or single-chambered (SCMFC). Dual-chambered cells, as their name suggests, comprise separate anolyte and catholyte compartments with the substrate in the anolyte and various electron acceptors in the catholyte. Examples of such DCMFCs are the H-bottle design shown in Figure 2 of reference [23], and the rectangular box configuration, separated by a cation-permeable membrane such as Nafion. An example of such a design is given in Figure 2.1 of reference [24], which utilized a dual-chamber rectangular box with graphite plates and a catholyte containing ferricyanide or dissolved oxygen.

Although DCMFCs are suitable for easy setup, sampling and monitoring of parameters such as pH, DO, and ORP, they are bulky (low area/volume ratio) and difficult to combine together in stacks efficiently, and produce low volumetric current and power densities due to the resistance of the electrolyte. The liquid-based oxidants are also either non-renewable (ferricyanide/permanganate) or require continuous dissolution of air or oxygen. Non-renewable oxidants are not compatible with the concept of "renewable" energy, making them less attractive and more expensive. The spent catholyte must also be disposed or regenerated, adding to operational costs. Continuous sparging of air in the catholyte is energy-intensive and can require more power than that generated. The approach of using an aqueous catholyte containing dissolved oxygen also suffers from the low oxygen solubility in water (~8 mg/L). Given that the oxygen concentration in air is 21% and that air is abundantly available at no cost, it stands to reason that the design of the MFC should move in the direction of an air-cathode cell where

the cathode is in direct contact with air. The first air-cathode cell was based on a design not unlike a conventional hydrogen fuel cell. A flat-plate design by Min and Logan [17] used a serpentine-channel air-catholyte chamber coupled with a similar serpentine-channel anolyte chamber, eliminating the need for a liquid catholyte and for high-volume air sparging, but still required minimal pumping of air to maintain constant gas flow through the serpentine channels. Strictly speaking, this unit was dual-chambered although the air-cathode could be easily modified to eliminate the chamber to directly expose the cathode to air.

The first single-chamber MFC (SCMFC) was designed in 2004 by Liu *et al*. as a cylindrical anolyte chamber (filled with domestic wastewater) with eight graphite rod anodes surrounding a central tubular cathode made of a carbon cloth/Pt/Nafion layer supported onto a porous plastic tube, as shown in Figure 1A of reference [14].

Although power generation was low (26 mW/m^2), it demonstrated that a catholyte compartment was not necessary to generate power. Another important finding from the study was that passive air flow appeared to yield about 25% higher power densities than when forced air flow rates of 4-5 L/min were used. A similar effect of a ~30% drop in power density with an increase in the air flow rate from 0 to 200 mL/min was observed in the earlier flat-plate cell study. [17] Although not confirmed, the authors suggested that the increased air flow enhanced the transport of oxygen through the Nafion to the anolyte chamber and thereby promoted short-circuiting or non-electricity-producing reactions.

SCMFCs also permit the cathode to be in closer, even direct, contact with the anolyte solution rather than being forced to travel through a catholyte medium to the cathode surface. Reduced distance between electrodes tends to lower the ohmic resistance and increase the cell potential. Furthermore, SCMFCs are simpler, more compact, require less material for fabrication and can be more easily stacked in series or parallel to generate larger currents/potentials than DCMFCs, they have become attractive options for scale-up. More details on specific SCMFC designs are given in the next section.

2.2.2 DCMFCs

Before describing current MFC designs, it is important to note that not the same substrate or substrate concentrations, HRT, inoculun, reactor size or electrode material was necessarily used in the various studies in which the different designs were evaluated. Therefore, comparisons must be made with caution, realizing that performance from cell to cell may vary significantly and that differences may not be due to design, but rather to operating conditions independent of cell design.

As mentioned, DCMFCs are still used although they are only known to be used for laboratory-scale experiments in which the focus is on specific performance factors rather than high power throughput. H-tubes are a popular design for studies that focus on catholyte performance. You *et al*. [25] used this type of design to compare cell performances achievable using the oxidants permanganate, ferricyanide and dissolved oxygen. They found that the use of permanganate produced 4.5-fold more power than that of ferricyanide and 11.3-fold more than that of dissolved oxygen. They attributed this difference to the higher half-cell potential of +1.70 V for the reduction of permanganate in acidic conditions compared to +0.804 V and 0.344 V for the reduction of oxygen in air and ferricyanide, respectively. As described earlier in Section 1.1, Rozendal *et al*. [8] used the same configuration to determine which cations contributed the most to positive charge transfer through a Nafion membrane into the catholyte.

Another dual-chamber design is a mini-MFC shown in Figure 1 of reference [26], in which the anode chamber was inoculated with a pure culture of *Shewanella putrefaciens* DSP10. An artificial electron mediator (AQDS) was also used to assist in electron transfer. Maximum current density of 6.3 A/m^2 and power density of 3.0 W/m^2 were attained using a 50 mM ferricyanide catholyte. The advantages of such a small cell (1.2 mL volume, 2.0 cm^2 area, ~175μm distance between anode/cathode) are the very small distance between electrodes without the need for hot pressing and the ease with which the concentration of the anolyte solution can be maintained uniform.

Although not a true SCMFC, the aforementioned flat-plate reactor by Min and Logan mimics the design of a conventional PEMFC with its serpentine plug-flow channel and membrane electrode assembly configuration, as presented in Figure 1B of reference [17].

The advantage of the two-chambered design is that the air flow through the cathode chamber can be controlled or can be operated using a liquid catholyte. The serpentine catholyte chamber can also be

removed to convert the unit into a single-chamber cell. A disadvantage is that since the reactor is operated as a plug flow, the outlet concentration of substrate may be much lower than the inlet, creating a concentration gradient along the flow path and reducing overall performance. With a 1 g/L acetate feed as a fuel source, dry air pumped through the cathode chamber, carbon paper anode and cathode and 0.7 mg/cm^2 Pt loading on the cathode, this cell produced 286 mW/m^2. Similar tests with starch, glucose, dextran and butyrate yielded power densities of 246, 212, 150, and 220 mW/m^2 respectively.

2.2.3 SCMFCs

As mentioned earlier, the first single-chamber MFC was of cylindrical design with several graphite anode rods surrounding a central carbon cloth cathode. A major problem with this design is that the anode chamber volume is much larger than the cathode surface area, leading to a lower area/volume power ratio. The cube SCMFC reactor combines the single chamber concept of the cylindrical cell with the higher surface area/volume ratio of the flat-plate cell (see Figures 1A and 1B of reference [27]).

In a study by Liu and Logan [27], a 4 cm long x 3 cm diameter cell produced 173 mW/m^2 using a 600 mg/L glucose substrate when a PEM (Nafion)-carbon paper electrode was used. The cell was also operated with a PEM-less carbon paper cathode and produced 381 mW/m^2. The removal of the PEM decreased the ohmic resistance and so increased the delivered power. At the same time, however, the oxygen flux into the anode chamber increased from 0.05 mg/h to 0.187 mg/h and caused a drop in the coulombic efficiency. With a PEM, stable power was maintained for 95 h with a coulombic efficiency of 40-55%. Without a PEM, stable power was maintained for only 20 h at a coulombic efficiency of 9-12%. Considering the high cost of Nafion ($1600/m^2) and the requirements of rapid substrate removal and high power generation, removal of the PEM may be a viable option in the future.

In fact, one study showed that relatively inexpensive materials such as J-cloth can substitute for Nafion with impressive results. Fan *et al*. [28] used a cube SCMFC design modified with J-cloth to replace the Nafion. The substitution of 2 layers of J-cloth improved the coulombic efficiency from 35% to 71% with only a slight decrease in power density from 80 to 68 W/m^3 in a cell where the anode and cathode were spaced 1.7 cm apart (11.9 mL volume). Further modification of the cell design was done by

sandwiching the J-cloth layers between the anode and cathode, effectively creating a cloth-electrode-assembly (CEA) and reducing cell spacing to 0.4 cm (2.5 mL volume). These modifications significantly increased power density to 627 W/m^3 (fed-batch) and 1010 W/m^3 (continuous). Normally in a membrane-less cell, the increased oxygen diffusion into the anolyte would create a local short-circuit, resulting in some of the substrate being consumed by non-electrogenic means. In turn, the width of the anolyte chamber would have to be such that oxygen cross-over would not significantly affect current and power densities. The addition of J-cloth appears to have solved this problem by effectively limiting oxygen diffusivity, permitting further reduction in electrode spacing while maintaining high coulombic efficiencies.

2.2.4 Stacked MFCs

Although recent advances in MFC architecture have shown great promise, the viability of this technology on a large scale requires that these cells be stacked so that either voltage or current is increased to the point where it can be distributed to the power grid or practicably usable. As MFCs research progresses, recent efforts are beginning to focus on stacked cell architectures. An early design by Aelterman *et al*. used a 12-chambered cell split into 6 dual-chambered flat-plate cells (no serpentine flow), as shown in Figure 1 of reference [29].

Both anode and cathode consisted of graphite granules supported on a graphite rod inserted for current collection. The chambers were separated by Ultrex, a cation-exchange membrane which is thicker than Nafion and often used in dual-chamber cells. The catholyte was a 50 mM ferricyanide solution. The cell was operated in both series and parallel modes and power densities were reported on a volumetric basis since the active area of the carbon granules was not known. The researchers found that parallel operation yielded higher hourly power density performance than series operation (248 W/m^3 vs. 228 W/m^3). Also of note, it was observed that a stack configuration resulted in polarity reversal in three of the six cells. Polarity reversal occurs when the anodic overpotential increases to the point that the anodic potential rises above the cathodic potential. Consequently, the directions of both electrode reactions become reversed from what is intended. This can occur if a cell is starved of fuel or if too much current is drawn. The limited biocatalytic properties of the microbial consortia residing in the biofilm were cited as the explanation for this phenomenon. Based on polarization curves shown in the

literature, an increase in concentration overpotential likely caused a rise of the anode potential, resulting in voltage reversal. Upon disconnection of the stack configuration and reconnection as individual cells, performance returned to normal.

Another MFC stack developed by Shimoyama *et al*. (Figures 1A and 1B of reference [20]) utilized a practical submersible stack of 12 "cassettes" arranged into six cathode boxes and operated in parallel. The anodes were made of graphite-felt (non-catalyzed), while the cathodes were also made of carbon cloth with a 30 wt.% PTFE loading, 4 gas diffusion layers containing 4 mg/cm^2 PTFE on the air-facing side to reduce water loss and oxygen diffusion and 0.7 mg/cm^2 Pt sprayed onto the water-facing side. The substrate was a model organic waste composed of starch, bacto-peptone and fish extract (289 g COD/L). Based on a COD loading rate of 5.8 g/L-day, 93% of the COD loading was removed to lower the effluent tCOD level to 20.5 g/L from an inlet concentration of 26.3 g/L. The overall power density generated by the stack was 899 mW/m^2 with a coulombic efficiency of 28%. It was also found that the volumetric power density of the stack as a whole was only 63% of the sum of the individual cell power densities if they were operated separately (115 vs. 182 W/m^3). Since the anodes from one cassette were connected to those from other cassettes, it was postulated that the neighbouring anodes contributed electrons to the current generation from one cassette.

2.3 Importance of the Catalyst in an MFC

Cathodic reduction of oxygen in an air-cathode MFC is one of the potential major limiting factors for power production. This is due to the slow reaction kinetics of oxygen reduction to water. As is the case with PEMFCs, a catalyst is required to improve reaction kinetics for oxygen reduction in MFCs. Significant improvement in power production, up to 3 to 4 times, has been found with the addition of a catalyst (platinum or cobalt tetramethoxyphenylporyphrin) over a plain carbon cathode. [12] Almost all studies with air-cathode MFCs now include some sort of catalyst, whether it is platinum or another compound. This section will cover the theory of catalysts and how they improve oxygen kinetics, as well as a history of common catalysts in MFC applications.

2.3.1 Catalyst Theory

In fuel cells, the catalyzed reduction of oxygen at the cathode is not limited to one simple reaction. Several steps are required, each with their own specific reaction kinetics. Determination of the molecules in the individual reactions can be difficult, especially for non-precious catalysts given that the actual sites for catalysis are not entirely understood themselves. A simplified mechanism of oxygen reduction to water and hydrogen peroxide on any catalyst can be given by the following reaction:

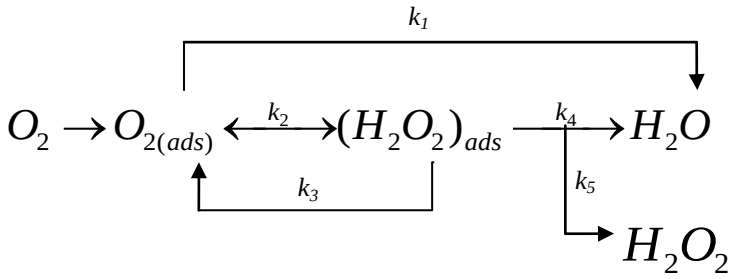

The reduction of oxygen can either produce water or hydrogen peroxide. The water-producing pathway is a 4-electron reaction, meaning that 4 electrons are required per molecule oxygen, while the hydrogen peroxide-producing pathway is a 2-electron reaction. [30] From an efficiency standpoint, the water-producing pathway is preferable since more electrons are consumed per oxygen molecule. Hydrogen peroxide is also reactive, potentially causing degradation of the Nafion membrane [31], consequently limiting proton transfer.

For a given catalyst, the geometry and key parameters that determine the rate of the electrochemical reaction are the exchange current density and the Tafel slope. The exchange current density is a measure of the catalyst's background current for a given electrochemical reaction, and is defined as the current density when the forward and backward reactions are at equilibrium, the net current is zero, and at zero overpotential. The Tafel slope is based on the Butler-Volmer equation and represents the effect of current density on the overpotential in a given reaction. As current density increase, so too does the overpotential. This relationship is given by equation 2.1 [32], also known as the Tafel equation.

$$n_A = \pm\beta \log \frac{i}{i_o} \qquad \textbf{2.1}$$

n_A = Overpotential (V)
± = Sign convention for reaction (+ for anodic reaction, - for cathodic reaction)
β = Charge transfer coefficient (between 0 and 1)
i = Current density (mA/m^2)
i_o = Exchange current density(mA/m^2)

In fuel cells, a higher exchange current density and lower Tafel slope are desired. Higher exchange current densities indicate faster exchange of charge and ions and therefore lower ohmic losses, while a lower Tafel slope indicates a lower overpotential gain as the current density rises. This leads to a higher cell potential for a given current density and consequently a higher power density.

The cathodic catalyst for fuel cell applications is either a noble or transition metal that is adsorbed onto a conductive but inert support like carbon black, or is a carbon composite derived from a carbon support that has been doped with nitrogen compounds and transition metals, and heat treated such that the entire surface area of the carbon is catalytically active for oxygen reduction rather than just the surface area of the adsorbed metal particle. The next section presents an overview of platinum, the most common catalyst. The sections following that document the progression of non-precious catalysts in MFCs, to the carbon composite catalyst that is the focus of this study.

2.3.2 Platinum – Pros and Cons

Platinum is the primary catalyst choice in PEMFC applications and is also extensively used for air-cathode MFCs. One of the reasons for this preference is due to its high ORR exchange current density (2.8×10^{-3} mA/cm^2). Platinum in fact has the highest exchange current densities of any metal, making it a suitable choice. [33] Another advantage of platinum is that it has a high selectivity for the 4-electron reduction pathway to water (99.5%) , as opposed to the 2-electron reduction pathway to hydrogen peroxide (0.5%). [34] Despite this advantage, the platinum must also be easily incorporated into the carbon electrode in a manner that would maximize its surface area but maintain good contact and durability with the electrode. A technique which adsorbed platinum onto a high surface area carbon black substrate with a Nafion binder was developed in the early 1990s, revolutionizing PEMFC technology. [35] Carbon black was chosen due to several factors such as high surface areas, high electronic conductivity, availability, cost, and being inert. By using this technique, the platinum

loading has significantly reduced from 3-4 mg/cm^2 to as low as 0.15 mg/cm^2 while increasing the active surface area from 10-40 to 80 m^2/g. [35, 36] In doing so, the catalyst layer thickness was also significantly reduced, increasing gas diffusion through to the active sites.

Despite the vast increase in platinum-based fuel cell technology over the past 20 years, there are two main drawbacks to using platinum. The most critical drawback of platinum to the commercialization of the fuel cell is cost. The cost of platinum is extremely high (>$1300/ounce) and can contribute approximately $1,500 to the capital cost of an 80 kW PEMFC ($18/kW) stack, based on figures from a 2008 DOE report. Overall, the cost of the fuel cell is now estimated to be $73/kW, or $5,840 for an 80 kW stack. [37] Based on these numbers, the platinum cost is 25% of the total, a significant portion. Finding a cheaper catalyst that will produce similar power densities will be a priority.

With respect to MFCs, the power densities are significantly lower than PEMFCs, up to 2-4 orders of magnitude. Given that the area required to produce practical power from an MFC stack will be significantly higher than a PEMFC, the cost of the catalyst will contribute a greater portion of the overall capital cost, especially if Pt is required. It is known that oxygen reduction at the cathode is a bottleneck to increasing power densities, however in one study by Cheng *et al*., increasing the platinum loading from 0.1 to 0.5 mg/cm^2 only increased power densities by 19%. [12] This suggests that the bottleneck lies less in the catalyst used but other factors like the active surface area for catalysis.

2.3.3 Previous Use of Non-Precious Catalysts in MFCs

There have not been many studies using non-precious catalysts, however the preliminary results seem promising. The first known study using a non-precious catalyst was by Cheng *et al*. in 2006, where a ~0.6 mg/cm^2 cobalt tetramethoxyphenylporyphyrin (CoTMPP) catalyst was found to produce only 12% less power than a 0.5 mg/cm^2 Pt catalyst (369 vs. 414 mW/m^2) at similar coulombic efficiencies of 8-18%. [12]

Another study by HaoYu *et al*. [38] compared several different non-precious catalyst such as pyrolyzed iron phthalocyanine (FePc), CoTMPP, and manganese phthalocyanine (MnPc). They found that FePc (634 mW/m^2) outperformed the other catalysts, including platinum (593 mW/m^2), with comparable

coulombic efficiencies of ~20%. They also compared the electrochemical performance of FePc using two different carbon black substrates, Vulcan XC-72 and KetjenBlack EC 300J. KetjenBlack was found to have a higher OCP (0.319 V vs. 0.289 V (vs. Ag/AgCl electrode)). Although no further testing was done to determine the exact reason behind this increase, it was suspected that the increased surface area of the KetjenBlack allowed for more adsorption of oxygen to the catalyst/carbon surface. [38].

2.3.4 Background on N-doped Pyrolyzed Carbon Composite Catalysts

The group of nitrogen doped non-precious metal catalysts is synthesized through the pyrolysis of transition metal and nitrogen precursors on a carbon support. Synthesis of these complexes usually involves adsorption of the metal and nitrogen precursors to a high surface area carbon support under vigourous stirring, followed by high temperature pyrolysis using Ar, H_2, or NH_4 gas. Catalyst synthesis may also include the acid leaching of the pyrolyzed material to remove excess metal impurities. The metal component can be in the form of different salts like iron sulfate and cobalt acetate, metallic complexes like ferrocene and iron phenanthroline, or N_4-macrocyclic complexes like iron phthalocyanine and iron porphyrin that contain chelated nitrogen complexes and don't require separate nitrogen precursors. Nitrogen precursors can be either ammonia, acetonitrile, ethylenediamine, or other N-containing materials. [39] Carbon black substrates can be Vulcan XC-72, which is commonly used as the carbon support for precious metal catalysts, or KetjenBlack, which has been increasingly used in studies due to its surface area being significantly higher than XC-72 (800 m^2/g vs. 250 m^2/g). [38]

Research on the catalytic properties of metal N_4-chelates began in 1976, where Jahnke *et al*. first postulated that these chelates could remarkably increase catalytic stability and activity for oxygen reduction. [40] More recent research [41] revealed that the optimum pyrolysis temperature that gave the highest oxygen reduction activity for N_4-chelates was between 500-700ºC, although it was also found that pyrolysis temperatures of >800ºC were required for stable operation in PEM fuel cells. [42] Of importance was the the fact that at these higher temperatures, the structure of the N_4-chelate complex was degraded due to pyrolysis. [43] This suggested that the active site had changed from the chelate complex to another site and that the use of chelated precursors may not be required to produce a high activity catalyst.

The nature of this/these active site(s) is still not well defined, although it has been postulated that several nitrogen containing carbon alloys may exhibit catalytic activity for oxygen reduction, such as pyridine-like, pyrrole-like, and graphite-like nitrogen, with graphite-like exhibiting a higher ORR activity than pyridine-like. [44] The nitrogen content as well as the source of the nitrogen have also been shown to be critical in the degree of catalytic activity. Increased nitrogen content has been shown to yield higher catalytic ORR activity. [45] Inexpensive nitrogen precursors such as ethylenediamine and 1,2-phenylenediamine have also proven to yield ORR activity surpassing that of the more expensive cobalt phthalocyanine, an N_4-chelate, [46] which is significant for reducing the capital cost of a fuel cell stack while maintaining high ORR activity. There is also debate as to whether the transition metals remaining in the carbon support contribute to ORR activity or if they are more so required only for the incorporation of the nitrogen precursor into the carbon support. Metal and metal complexes have been suggested to be more of an impurity rather than catalytically active, and that the nitrogen groups are the major active species. [47] Their addition as a precursor however, is critical to increasing the nitrogen content of the catalyst (from 1.9 to 3.9%) and subsequently increasing ORR catalytic activity. [48]

Longevity of the catalyst in a PEMFC application has been tested as well with promising results. A 480 hr continuous test by Nallathambi *et al.* [48] used a selenourea-formaldehyde modified carbon sprayed onto a gas diffusion layer carbon paper and hotpressed onto a Nafion 112 sheet forming a membrane electrode assembly (MEA). They found only a slight (10%) maximum decrease in power over the cycle. Additionally, the fuel cell performance was fully recovered after purging with O_2 gas, indicating that the reduction in performance was likely due more so to ineffective water management rather than catalyst degradation. [48]

There is considerable potential for nitrogen-doped catalysts to replace precious metal and transition metal chelate catalysts as a cost-effective alternative in PEMFCs and especially MFCs where the capital cost per unit power is weighted more to the materials as a consequence of the lower power densities (and subsequently larger reactor size requirements). This chapter provided a brief coverage of the progression of such non-precious catalysts.

Chapter 3
Synthesis and Characterization of a Non-Precious Catalyst

As MFCs and PEMFCs continue to gain momentum towards commercialization, the replacement of platinum with an inexpensive catalyst for oxygen reduction becomes more important. Not only have strides been taken to replace the platinum with other transition metal complexes such as CoTMPP on a conductive but inert carbon backbone, but novel nitrogen-doped carbon composite catalysts have eliminated the surface area limitations of the inert carbon backbone by changing the chemical structure of carbon substrate itself through the introduction of nitrogen groups, heat treatment, and acid leaching. The new carbon composite itself becomes entirely catalytically active for oxygen reduction.

This chapter focused on the synthesis of two N-doped carbon composite catalysts, one using a polyaniline (PANI) precursor, and another using an ethylenediamine (EDA) precursor. The two catalysts were compared for their cathodic oxygen reduction potentials through their half-wave ORR potentials. The catalyst exhibiting a higher half-wave ORR potential was then further characterized through imaging via SEM, elemental composition via EDAX, and identification of surficial crystalline structures via XRD. It was found that the EDA catalyst exhibited a higher ORR half-wave potential at 0.57 V. SEM imaging of the EDA catalyst showed a fluffy, amorphous, and bulbous structure. Elemental composition via EDAX found 3.57 wt. % nitrogen and 4.87 wt. % oxygen, which are likely bound directly to the carbon black, as well as 1.25 wt. % iron and 1.26 wt. % cobalt, the transition metals used for incorporation of the nitrogen groups. XRD analysis of the surface structure confirmed the presence of iron and cobalt. The detection of these metals through XRD indicated that at least some of the metal was exposed at the surface, and not entirely encased in the carbon composite catalyst.

3.1 Introduction

Platinum remains the best choice for catalysis of oxygen reduction in fuel cells based on its high cathodic potential, however cost remains one of its major drawbacks. PEMFCs have recently focused on decreasing platinum loadings on carbon supports, decreasing platinum particle size, and improving dispersion of Pt onto carbon supports [39] in order to reduce capital costs while minimizing power loss.

Although these methods may help improve the cost/power ratio, the room for improvement is limited since as platinum particles become smaller, the chances for inactivation due to either inability of protons to reach platinum particles isolated from Nafion, or due to platinum being isolated from oxygen in the carbon support, increase. Platinum catalyst cathodes also suffer from the fact that aside from the catalyst itself, the carbon black support and GDL are not suitable for oxygen reduction, reducing the active/total surface area ratio of the cathode as a whole. Eventually, PEMFCs and fuel cells in general will need to replace platinum entirely to improve financial viability.

Nitrogen-doped carbon composite catalysts represent a novel approach to catalyst technology, by utilizing inexpensive transition metals such as iron and cobalt, nitrogen precursors like pyrrole and ethylenediamine, high surface area carbon nanoparticles, and heat treatment to create a nitrogen-containing carbon composite that is catalytically active for oxygen reduction. Although the oxygen reduction overpotentials are greater than platinum [48] resulting in a decreased cathodic oxygen reduction potential, an advantage of this catalyst is that unlike a platinum-based cathode, the entire surface area is catalytically active. These catalysts are also significantly less expensive than platinum, therefore allowing for increased catalytic loadings. Since the power density of MFCs is significantly less than PEMFCs, the capital cost will be higher per unit power generated, and therefore finding an inexpensive catalyst is critical to the commercialization of air-cathode MFCs. The use of N-doped carbon composite catalysts has not been explored in MFCs as of yet, and may represent a possible alternative to platinum for single chamber air-cathode cells.

This chapter focuses first on the synthesis of two N-doped carbon composite catalysts, each using different nitrogen precursors, polyaniline and ethylenediamine. Each catalyst was then analyzed for its oxygen reducing capability through oxygen reduction reaction (ORR) experiments. Based on the half-wave potential of the generated ORR curve, the catalyst with the higher potential was then selected for further characterization through imaging via scanning electron microscope (SEM), elemental composition through energy dispersive x-ray spectroscopy (EDAX), and identification of crystalline compounds through powder x-ray diffraction (XRD).

3.2 Materials & Experimental Design

Synthesis and characterization of non-precious catalyst batches were completed according to procedures outlined by Dr. Zhongwei Chen. Two types of non-precious catalysts produced using different nitrogen-containing precursors (polyaniline and ethylenediamine) were prepared. This section will describe the procedures, materials and equipment involved in synthesis and characterization of these catalysts.

3.2.1 Synthesis

The support for the polyaniline-based catalyst was a highly porous carbon support (Ketjen Black EC-600JD) that was pre-treated by contacting with 6 M HCl for 3 hours, rinsed with DI water, air-dried overnight and then refluxed in 250 mL of 70% HNO_3 at 80ºC for 8 hours to introduce carboxyl groups into the carbon surface. The treated carbon support was then added to a solution obtained by combining 200 mL of 1 M HCl and 1 mL of pure aniline and sonicated/mixed thoroughly. Polymerization of the aniline was then initiated through drop-wise addition of ammonium persulfate into the mixture. Once the polymerization process was completed, a metal precursor in the form of cobalt acetate was added with ethanol to form metal-nitrogen complexes. After the solution was heated to dryness, the resulting powder was ground using a mortar and pestle and then pyrolyzed in argon gas at 850ºC for 1 hour to form the carbon composite catalyst. Finally, the metals were leached from the catalyst in 0.5 M H_2SO_4 and the remaining solid catalyst was washed, filtered and dried before being stored in a clean, tightly sealed vial to prevent oxidative degradation of the catalyst.

The support for the ethylenediamine-based catalyst was also Ketjen Black EC-600JD although it was not pretreated beforehand. After sonication and mixing with ethanol, the support was added to equal masses of cobalt nitrate and iron sulfate dissolved in ethanol. The nitrogen precursor, ethylenediamine, dissolved in ethanol was added to the mixture to initiate formation of the carbon-metal-nitrogen complex. This mixture was boiled to dryness and then the residue was ground and pyrolyzed in argon gas at 900ºC for 1 hour before being acid-leached in 0.5 M H_2SO_4 to remove the transition metals. Finally, the remaining solid catalyst was washed, filtered and dried before storage.

A list of materials and equipment used for synthesis of the polyaniline-based and ethylenediamine-based catalysts is given in Table 2.1. A more detailed procedure for synthesis of both catalysts including the reagent quantities can be found in Appendix B.

Table 3.1 Materials and Equipment in Synthesis of Carbon Composite Catalysts

	Polyaniline	Ethylenediamine
Carbon support	Ketjen Black EC-600JD Pre-treated in 6 M HCl, and 70% HNO_3	Ketjen Black EC-600JD Untreated
Nitrogen precursor	Aniline	Ethylenediamine (in ethanol)
Polymerizing reagent	Ammonium persulfate (in ethanol)	--
Metal precursor	Cobalt acetate (in ethanol)	Cobalt nitrate and ferrous sulfate (in ethanol)
Acid leaching	0.5 M H_2SO_4	
Pyrolysis furnace & process tube	Mini-Mite Tube Furnace TF55035A • 16 segment programmable control, 12" heated length x 1" diameter • 25-1100ºC operating temperature • Ceramic process tube, 18" length x 1" diameter • Ceramic sample boat, 4" x 0.5" x 0.25"	
Sonicator	Branson 2510 Tabletop Ultrasonic Cleaner 40 kHz frequency	

3.2.2 Characterization

The ability to promote oxygen reduction was chosen as the benchmark test to assess and compare catalyst quality. This is a reasonable choice since the objective of the catalyst is to provide the highest potential for oxygen reduction in the fuel cell. In particular, the catalyst which yielded a voltammogram with the most positive half-wave for the oxygen reduction reaction (ORR) was considered to exhibit the highest performance and so chosen for use in the fuel cell. Once selected, this catalyst was further characterized for its chemical composition, microstructure and morphology.

The ORR experiment requires the use of a 3-electrode rotating disk electrode (RDE) system controlled by a potentiostat, as shown in Figure 3.1. The catalyst film was applied to a glassy carbon working electrode insulated by a Teflon shroud. The potentiostat controlled or measured the potential difference between the working electrode and Ag/AgCl reference electrode. A separate loop within the electric circuit connected the working electrode to the Pt counter electrode. The high impedance between the working electrode and reference electrode ensured that all the current flowed between the working

electrode and counter electrode. All electrodes were placed in a glass jar containing an acidic electrolyte solution (0.5 M H_2SO_4 in this case) constantly sparged with oxygen to ensure oxygen-saturated conditions. During operation, the working electrode was rotated at a specified velocity by a remote control unit. This type of agitation is preferred during electrochemical experiments since it provides well-defined and controlled hydrodynamic conditions that can be linked to mass transfer to the electrode based on the analysis originally carried out by Levich. [49]

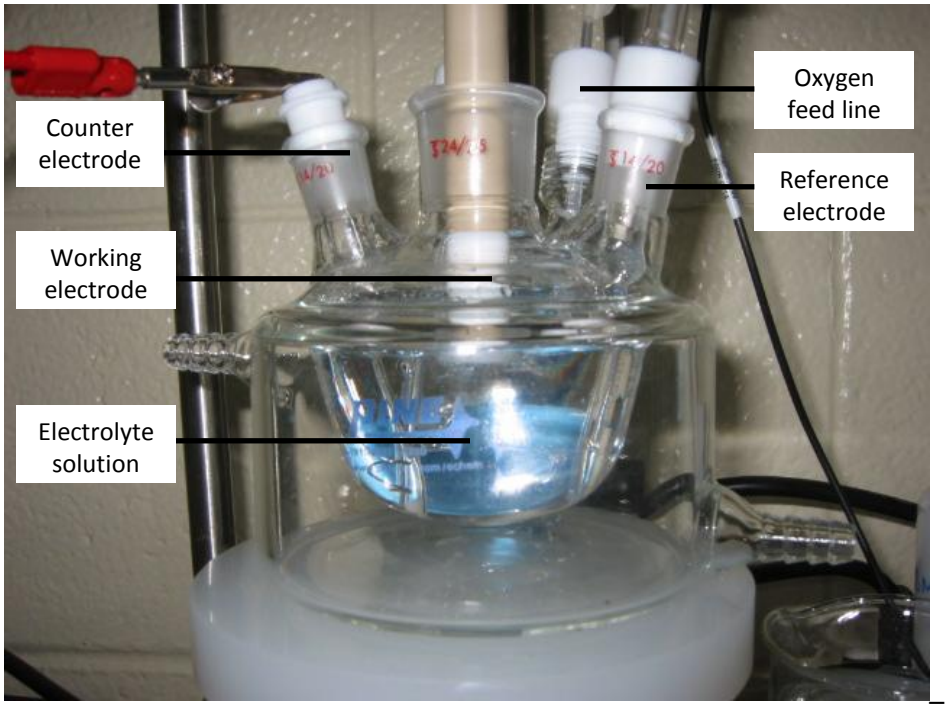

Figure 3.1 3-electrode-setup for ORR experiment

To produce the catalyst film for these ORR experiments, 4 mg of catalyst and 2 mL of ethanol were combined and sonicated for 30 min to form a catalyst ink. Forty μL of the catalyst ink was then extracted using a micropipette and deposited onto the glassy carbon electrode in 10 μL aliquots. Each aliquot of ink was allowed to completely dry before the next one was added to prevent any ink from escaping the electrode. Afterwards, 10 μL of 0.05 wt% Nafion in isopropanol solution was also added on top of the dried catalyst film to enable better adhesion of the catalyst to the electrode. The catalyst-doped working electrode was then attached to the rotator for ORR measurements.

All ORR tests were run as a three-electrode setup using a platinum wire encased in a glass frit as the counter electrode, while a double-junction Ag/AgCl electrode (+0.199 V vs. NHE @ 25ºC) served as the reference electrode. The electrodes were immersed in a 0.5 M H_2SO_4 (99.999% pure) electrolyte solution along with a 1/16" tube to allow for oxygen gas sparging. The potentiostat was run in linear sweep voltammetry mode over the range from +1.0 V to -0.2 V (vs. Ag/AgCl) at a sweep rate of 10 mV/s, and then in the reverse direction from -0.2 V to +1.0 V. Experiments were conducted at rotation speeds of 400, 900 and 1600 rpm to observe the effect of agitation on the ORR response. For each experimental run, the electrode response was allowed to stabilize by completing 2 cycles first before obtaining the electrode response from +1.0 to -0.2V to characterize the ORR. A specific list of materials and equipment used for the ORR tests is given in Table 3.2. A detailed procedure outlining the steps for electrode preparation and ORR measurement is given in Appendix B.

Table 3.2 Materials and Equipment for ORR Measurements

Potentiostat	Pine AFCBP1 Bipotentiostat • Sweep range: 0 - ±9.999 V • Sweep rate: 0 - 99.99 mV/s
Rotator	Pine AFMSRCE Rotator Control Box • 0-10,000 rpm range • Analog knob control
Working electrode	Pine E3 Tip Series Glassy carbon electrode • Area: 0.19625 cm^2 • Teflon shroud insulation
Reference electrode	Pine AFREF3 Double-Junction Ag/AgCl electrode • +0.199 V vs. NHE @ 25ºC • Inner solution: 4 M KCl saturated with AgCl • Outer solution: 0.1 M KNO_3
Counter electrode	Platinum wire encased in glass frit
Electrolyte	99.999% pure 0.5 M H_2SO_4 (Sigma-Aldrich)

Scanning electron microscopy (SEM) enabled observation of the catalyst powder and the composite morphology of the catalyst at a nanometer scale (~100 nm). In scanning electron microscopy, a highly focused electron beam (< 10 nm spot size) is directed towards a sample and causes a number of interactions to occur. This leads to the emission of several different types of radiation, including secondary electrons, backscattering electrons, characteristic X-rays and other photons. The intensities of these emissions at different frequencies are measured by detectors and the signal is amplified to allow observation on a monitor. The emitted radiations of most importance for obtaining images are

secondary and backscattered electrons since their energy levels are affected primarily by surface topography. [50] All SEM images were obtained using the LEO FESEM 1530 electron microscope located in the WATLabs facility in the Department of Chemistry at the University of Waterloo. The sample was prepared by airbrushing a pre-made catalyst ink (via a similar procedure to that used for the ORR experiments) onto a piece of carbon tape adhered to a metallic holder. This method was found to be more effective than simple spreading of dry catalyst powder onto the carbon tape by hand which caused particles to agglomerate and the images to be unclear.

Powder X-ray diffraction (XRD) analysis was used to identify crystalline compounds present in the various samples, while energy-dispersive x-ray spectroscopy (EDAX) was used to determine their elemental composition. In powder XRD analysis, a disc sample is located in a diffractometer while an X-ray tube and scintillation counter detector rotate around it at a tube-detector angle of 2θ, where 2θ is the scattering angle. A beam of X-rays emitted by the X-ray tube reach the electron cloud of the material and diffract at different intensities according to unique diffraction patterns associated with the electrons of atoms within each crystalline solid present. [51] The diffraction intensity is finally detected by a scintillation counter and displayed as a function of the scattering angle in the form of a diffractogram. Peaks appearing in the sample diffractogram can then be compared to standards or to a database (Powder Diffraction File (PDF) from the International Centre for Diffraction Data (ICDD)) for compound identification.

All XRD analyses were run using a PANalytical Xpert Pro Materials Research Diffractometer located in the WATLab facility. For analysis of the catalyst powder, a small amount of the powder was applied to a shallow flat metal disc holder and flattened using a glass slide. The analysis was run for 15 minutes to improve the peak resolution and to minimize noise.

EDAX is coupled with the SEM unit and distinguishes elements based on the number and energy of X-rays emitted when an atom is hit with high energy electrons, protons, or X-rays, causing an electron in an inner shell to become excited and ejected from its shell. An electron from an outer shell of higher energy then drops into the inner shell of the ejected electron and releases energy in the form of an X-ray photon. The energy of the X-ray is then measured by creating “electron-hole” pairs in a semi-conductive crystal detector (silicon-based). The number of electron-holes generated is directly proportional to the energy of the incident X-ray. The energy emitted from an X-ray is atom-specific

and thus enables identification and measurement of the concentration of specific elements. [52] In this case, a high energy electron beam was used as the energy source. After obtaining SEM images, EDAX readings were taken at specific locations on the surface by focusing the electron beam on a highlighted section of the sample, using the image as a guide.

3.3 Results

The results from ORR experiments determined the catalyst to be used for this study. After the preferred catalyst was chosen, it was further characterized by SEM, EDAX and XRD. The preferred catalyst was also used in the MFCs, as will be described in Chapter 5. The comparison of ORR obtained for two non-precious carbon composite catalysts are presented first, followed by SEM, EDAX and XRD analyses of the catalyst with the highest half-wave ORR potential.

3.3.1 ORR Response

The electrode response was obtained for the oxygen reduction reaction on two synthesized non-precious catalysts using different nitrogen-containing precursors, polyaniline (PANI) and ethylenediamine (EDA). The scans for these two catalysts obtained at 400 rpm are presented in Figure 3.2. Note that the potential range shown has been shifted to the standard hydrogen electrode scale.

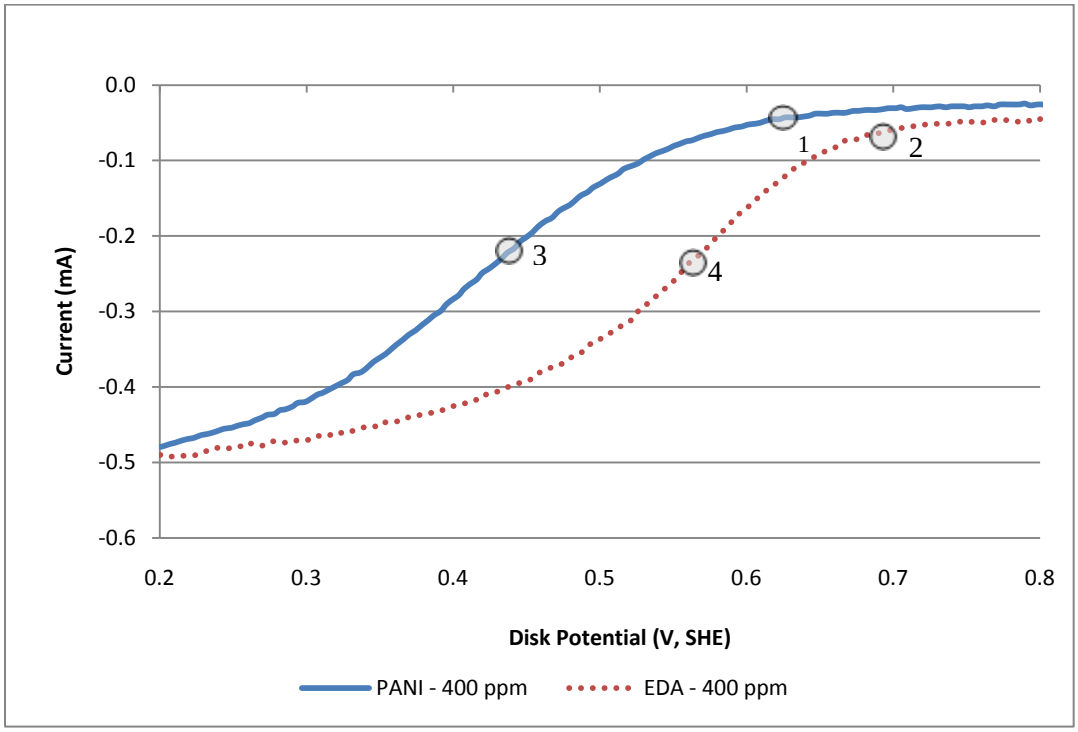

Figure 3.2 Comparison of the ORR scans obtained on two non-precious catalysts prepared with different nitrogen-containing precursors (PANI, EDA)

As expected, by the end of the scans, both electrode responses approach the same limiting current which is determined by the dissolved concentration in the bulk solution. However, the catalyst based on the EDA precursor clearly exhibits faster kinetics for the ORR. The onset potential at which oxygen reduction commences is estimated from the scans from the potential at which the current due to the ORR has reached -0.05 mA. In this way, the onset potentials using the EDA and PANI catalysts are determined to be 0.69 V(denoted as 2) and 0.62 V, respectively. The half-wave potential, defined as the potential at which the current due to ORR reaches half of the maximum (limiting) current, [53] and denoted as the potential at the inflection point of the curve, is also shown for the electrodes based on the PANI and EDA catalysts. The half-wave potential obtained with the EDA catalyst (0.57 V) is also higher than that with PANI (0.43 V) indicating that the EDA catalyst exhibits faster kinetics for ORR. ORR scans at higher rotation speeds of 900 and 1600 rpm were also obtained on the EDA catalyst to observe the effect of agitation and are compared in Figure 3.3 with the response at 400 rpm presented previously.

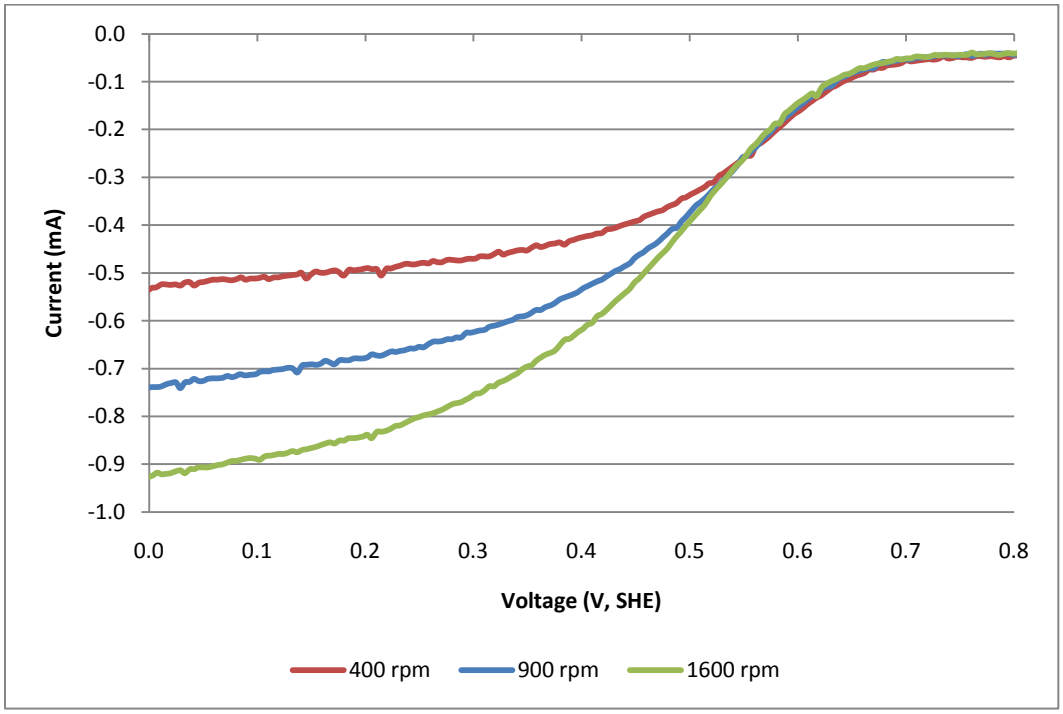

Figure 3.3 Effect of working electrode rotation speed on the response for ORR on the EDA catalyst.

From theory, the limiting current for the reaction should vary proportionally to the square root of the rotation speed [54]. In this case, the ratio of the limiting current for 400, 900, and 1600 rpm should be 2:3:4. Although the scans did not proceed far enough to the limiting current, the relative currents at higher overpotentials appear to fit this ratio.

Although the difference is significant, the half-wave potentials still were not as high as expected, as the expected half-wave potential for the non-precious catalysts was to be between 0.65 – 0.70 V, while the onset potential was expected to be 0.87 V. [48] Note that further improvements to the synthesis procedure for both non-precious metal catalysts could be made. However, it was not possible to focus more on this aspect of the research due to time constraints. Several factors could have contributed to limiting the ORR response such as incomplete dissolution of metal from the solids by ethanol prior to their incorporation into the carbon black, leakage of some oxygen into the pyrolysis chamber and termination of the flow of inert gas in the pyrolysis furnace before the temperature had dropped below 70ºC.

3.3.2 SEM Analysis

A sample of the selected EDA catalyst was examined by SEM. An image obtained at 10,000X magnification is presented in Figure 3.4. Also shown in the inset in the lower left corner is a smaller portion at 100,000X magnification.

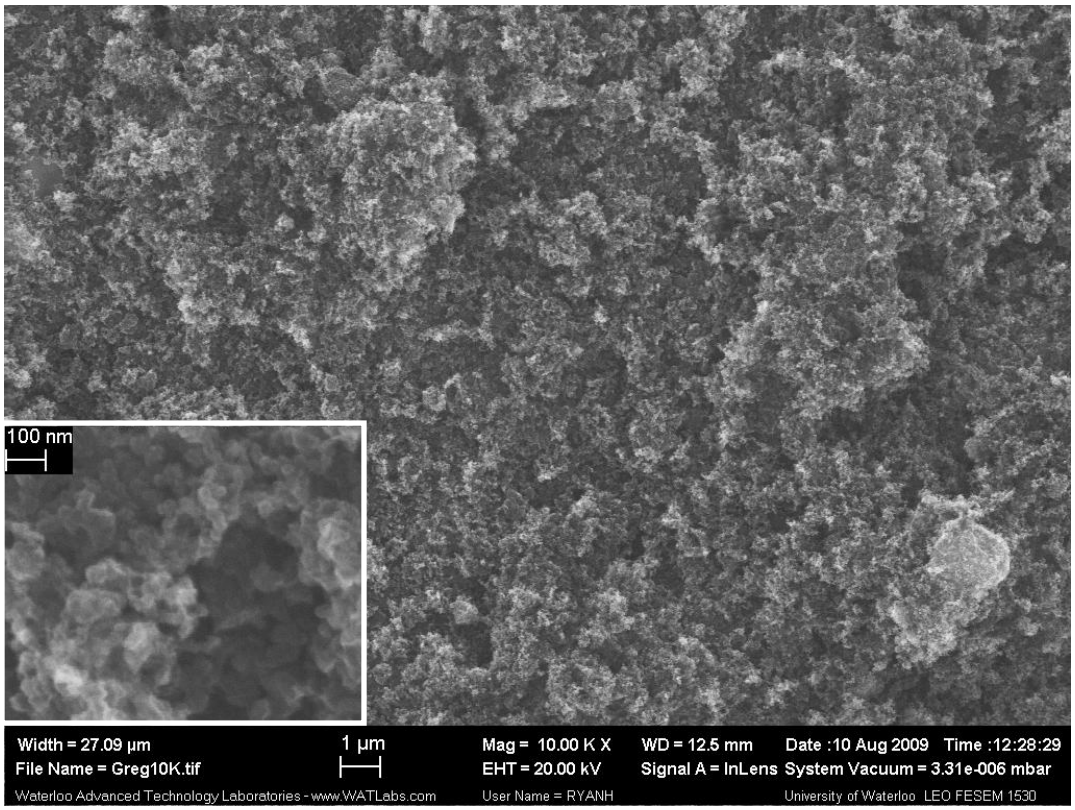

Figure 3.4 SEM image of EDA catalyst (10,000X) with a portion at higher magnification (100,000X) in the inset in the lower left corner.

The surface of the catalyst appears to be fluffy, indicative of a highly porous structure. This is expected as the catalyst is derived from a carbon black powder. A previous study found that the structure of a similar catalyst synthesized using PANI was fibrous prior to pyrolysis, but became more bulbous after pyrolysis [55]. As seen in the 100,000X inset, the structure of the catalyst appears bulbous. Due to its rounder structure in its final form, it appears that the pyrolysis step also tends to increase the surface area of the catalyst.

3.3.3 EDAX/XRD

After SEM images were taken, the sample was then analyzed for elemental composition by EDAX. A screenshot of the elemental composition along with the graphical display from the X-ray detector is shown in Figure 3.5.

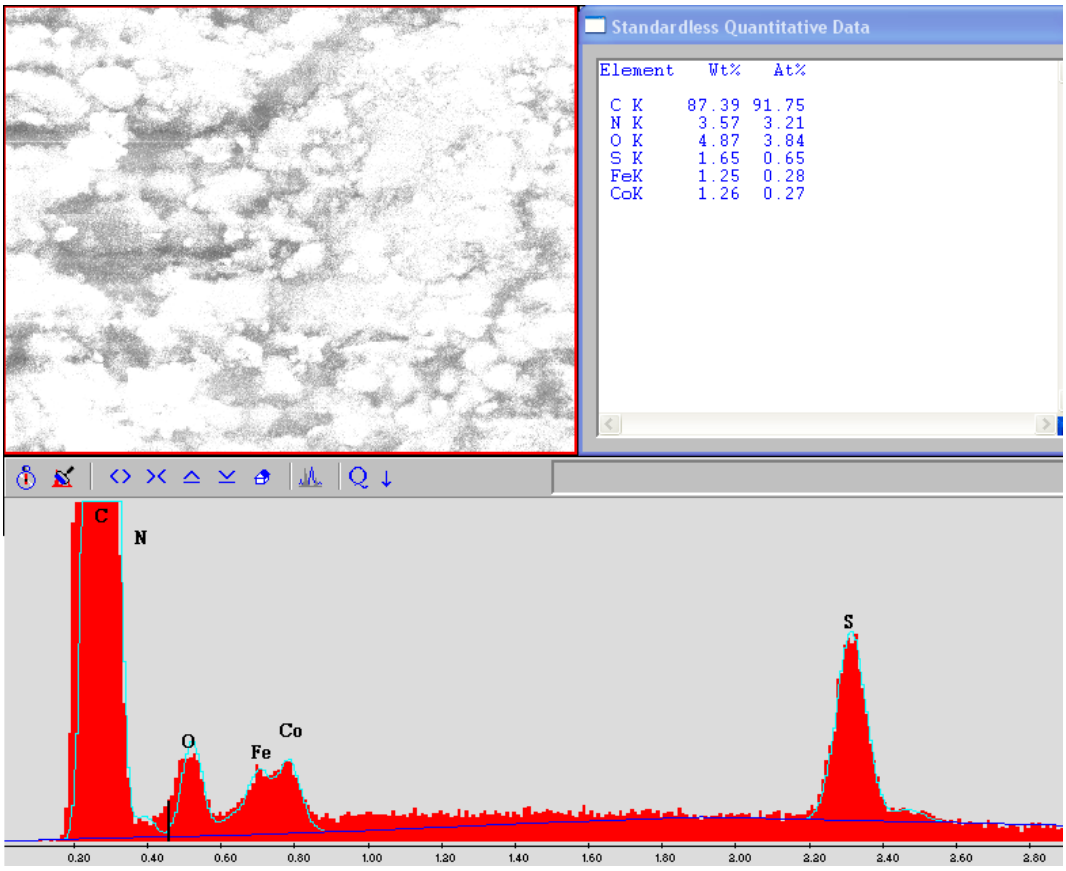

Figure 3.5 EDAX analysis of elemental composition of EDA catalyst

From EDAX, the elemental composition of the catalyst sample consists mostly of carbon, as obviously expected. The other elements detected were oxygen (4.87 wt %), nitrogen (3.57 wt %), sulfur (1.65 wt %), iron (1.25 wt %) and cobalt (1.26 wt %). Nitrogen is incorporated into the carbon structure through the EDA precursor, while the transition metals (Fe, Co) are bound to the nitrogen groups, which in turn are bound to carbon. The metal-nitrogen-carbon catalysts for ORR can be divided into two structure types: pyrrole-like (MeN_4/C, where Me is the transition metal) and pyridinic-like (MeN_2/C) structures. The iron content in our catalyst is similar to that reported by Nallathambi *et al.* [48] of ICP-mass

spectrometry measurements (i.e., 1.4 wt %), although the cobalt content was found to be significantly higher (4.6 wt %). The oxygen content on an atomic basis was slightly higher than that of nitrogen. The presence of sulfur in the catalyst likely occurred due to the use of sulfuric acid during the leaching process since no sulfur-containing species was used in any other preparation step.

Determine of the crystalline structure of the catalyst was carried out by XRD. The diffractogram obtained for the EDA catalyst sample is shown in Figure 3.6. All peaks were identified based on the Powder Diffraction File 2.0 provided by the International Centre for Diffraction Data.

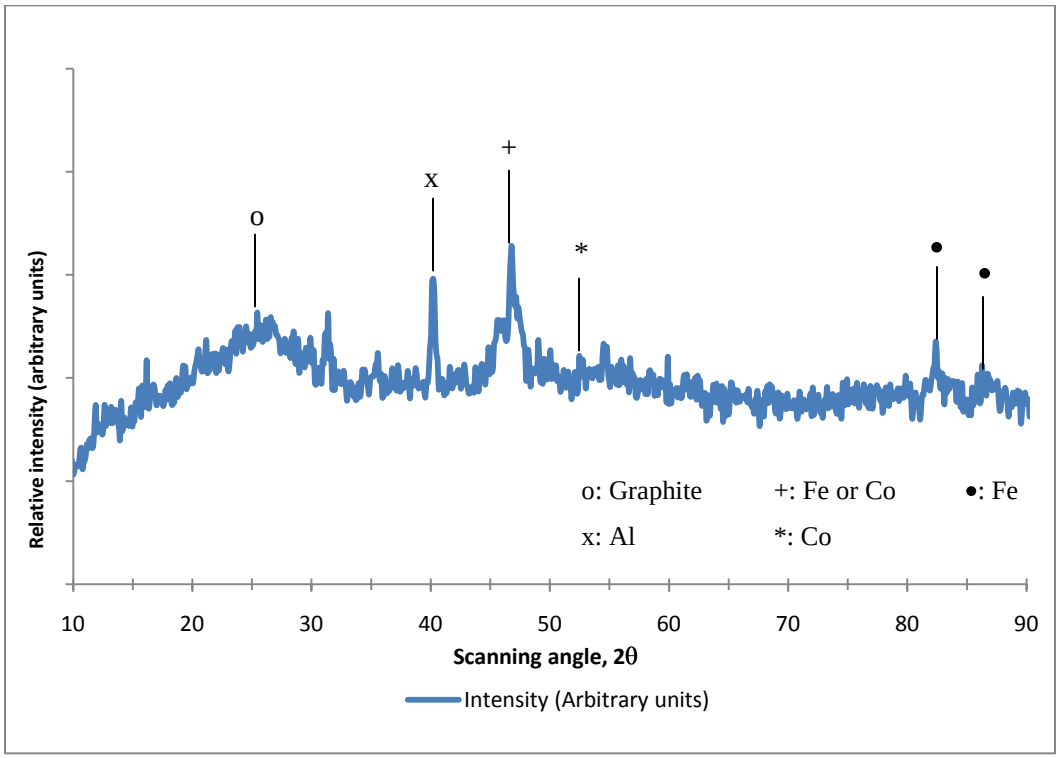

Figure 3.6 XRD diffractogram of EDA catalyst sample

From Figure 3.6, the most intense peak at 46.79º (denoted by +) is attributed as either Fe, Co or Fe_xCo_y, while the less intense peaks are assigned to Co at 51.45º (*) and Fe at 64.38º and 81.58º (●). The broad peak at about 25º is indicative of the carbon composite catalyst, while the sharp peak at 40.11º can be attributed to aluminum in the sample dish. A small unknown peak was detected at approximately 31º, possibly due to an organic or organometallic compound that may have formed during synthesis. A peak at 45.6º that is partially confounded by the more intense peak at 46.79º also appears. In their earlier study, Nallathambi *et al*. [48] also observed this peak and assigned it to Fe_3C (cementite). They also

found peaks similar in intensity to the "+" peak (for Fe, Co or Fe_xCo_y) and the "o" peak (carbon composite) appearing in Figure 3.6. [48] The detection of Fe and Co by both EDAX and XRD is not surprising given the synthesis procedure. The detection of these metal compounds by XRD provides more evidence that these compounds were present in the catalyst.

3.4 Conclusions

Two carbon composites synthesized from different nitrogen-containing precursors were compared for their ability to catalyze the oxygen reduction reaction. It was determined that the catalyst prepared using ethylenediamine (EDA) performed better (half-wave potential of 0.57 V) than the one prepared using polyaniline (PANI) (half-wave potential of 0.43 V). This value was still lower than the value of 0.65 – 0.7 V. Some aspects of the synthesis procedure causing the poorer ORR performance could be the incomplete dissolution of Fe from the catalyst and leaks in the furnace tube.

A sample of the EDA catalyst was subsequently examined using SEM and found to have a bulbous structure, similar to SEMs for similar type catalysts reported in the literature. The catalyst was then analyzed by EDAX to contain 1.25 wt. % Fe and 1.26 wt. % Co. The presence of these transition metals was expected since species containing these metals were used in the synthesis of the catalyst. Nitrogen comprised 3.57 wt. % of the catalyst sample, while oxygen comprised 4.87 wt. %. Although it was not possible to determine if the nitrogen was incorporated into a pyridine-like or pyrrole-like structure, the presence of nitrogen in the catalyst and its catalysis of oxygen reduction based on the ORR experiments suggest that these structures had formed. Some sulfur was also detected in the catalyst. It is suspected that it originated from the sulfuric acid used to leach out the metals during the synthesis procedure. XRD analysis confirmed the presence of both Fe and Co metal as well as carbon itself. Detection of the metals by XRD indicated that at least some of the metal was exposed to the surface rather than being completely encased in the bulk of the carbon composite catalyst.

Chapter 4

Effect of Substrate Feed Conditions and HRT on Power Generation in a Microbial Fuel Cell

Microbial fuel cells (MFC) are an emerging technology that may play an important role in the development of renewable sources of energy. Since it serves the dual purpose of directly generating electricity in conjunction with the treatment of wastewater, its potential for practical application are encouraging. Many aspects of their design and operation are still to be optimized to improve their power densities.

This chapter focuses on investigating the effect of varying the feed conditions of an acetate substrate (feed concentration, hydraulic retention time - HRT) on the performance of a single-chambered MFC with a common platinum cathode catalyst. The MFC was operated in three phases - first with a higher concentration feed and longer HRT (Phase 1), then at a lower concentration but lower HRT (Phase 2). Finally, the system was converted in Phase 3 back to the higher concentration/higher HRT feed conditions of Phase 1 to observe the ability of the system to respond to changes in the feed conditions after prolonged operation under other conditions. It was found that operation during Phase 1 produced the highest current and power densities (472.2 mA/m^2, 141.7 mW/m^2), although this only amounted to 4.24% of the entire reduction in the total feed soluble COD that was achieved by the cell. This indicated that most of the COD was removed by non-electrogenic processes. During the course of this study, the MFC proved to be very effective at COD reduction by removing 87- 95% of the inlet COD. Analysis of the total suspended and volatile suspended solids from the feed and discharge, as well as comparison of the discharge total and soluble COD levels and visual observations of the interior of the cell upon disassembly all indicated that significant amounts of biomass accumulated within the cell over prolonged operation, and may have contributed to the lower power densities achieved towards the end of Phase 2 and into Phase 3. COD balances over the cell indicated that a large portion of the COD was converted into methane (33.4 – 44.7%), while a minimum of 38% of the COD could not be accounted for directly. Calculated estimate of the oxygen diffusion flux through the Nafion membrane at the cathode into the anolyte indicates that it can account for 7.9 – 47.5 % of COD removed depending on the assumptions made. Thus, it is likely that oxidation of the substrate by dissolved oxygen that has leaked into the anolyte and biomass accumulation within the cell that cannot be measured account for most of this unaccounted COD removal. Lastly, analysis by ion chromatography

(IC) of the concentration of soluble COD in the form of acetate yielded concentrations similar to that obtained using standard digestion techniques and did so with less sample-to-sample variability.

4.1 Introduction

As demand for fossil fuels continues to rise with the emergence of India and China as significant consumers, the necessity for developing new sources of renewable energy and expanding existing sources grows as well as the need to reduce the anthropogenic carbon footprint. In addition, with the growing worldwide population and industrialization, improved methods for wastewater treatment are required. The use of MFCs presents a novel method of tackling both problems by producing electricity directly through the biocatalytic degradation of oxidizable organic and inorganic substrates and thereby lowers the chemical oxygen demand (COD) of the discharge.

However, at present, MFC technology remains at the laboratory scale, primarily due to the low power densities that have been achieved (several orders of magnitude lower than chemical fuel cells) [56]. Since it is still a relatively new technology, the focus of MFC research has been more on the determination of the operating conditions and reactor design that optimize cell performance than on scale up to commercial units. Optimization can be considered to be based on several criteria such as reactor design, substrate utilization for current generation, high throughput treatment of wastewater and long-term reliability and durability to name a few. Over the course of the past decade, MFCs have evolved in design, with focus shifting toward high-throughput single-chambered cells [12, 14, 20]. The flat-plate design used in proton-exchange membrane fuel cells (PEMFC) is a good benchmark since it has been proven to produce high power densities with relatively small reactor volumes. One study by Min and Logan [14] used this type of design with some success, while recent advances have modified the flat-plate design to an immersible cassette-type design, which are more suitable for implementation into existing wastewater treatment plants. [20]

At present, feed sources for MFCs vary from complex domestic and industrial wastewaters for practical applications to simple synthetic feeds comprised of acetate or other carbon sources that allow for easier characterization of substrate consumption and reaction pathways. Characterization of an MFC system can include the monitoring of water quality parameters such as pH, dissolved oxygen (DO), nitrogen

content, COD removal, power production for a specific carbon source or for a specific bacterial species (pure culture) and measurement of resistances that lower power production.

The focus of this chapter is to investigate the effect of substrate concentration and HRT on the performance of a SCMFC resembling those used in PEMFCs. Therefore, a flat-plate cell similar to that by Min and Logan [14] was constructed to treat a stream containing acetate as the substrate. In order to carry out a COD balance over the cell, the COD level in several streams was measured: the total and soluble COD of the feed and discharge streams, COD equivalence of the electrical current generated by the cell and the COD equivalence of the methane produced. Although not directly measureable, the amount of COD removed by dissolved oxygen that had leaked from the cathode side to the anolyte by diffusion through the Nafion membrane was estimated from information obtained from the literature. The combination of these parameters was included in attempting to close the COD balance. In addition, the discharge and feed were analyzed for various wastewater parameters such as pH, DO, oxidative-reductive potential (ORP) and total/volatile suspended solids content (TSS/VSS). A description of the materials and methods used is given first, providing details concerning the construction of the MFC, methodology for its operation and the analytical techniques used. This is followed by presentation of the experimental results in the following order: electrochemical parameters (current/power, polarization curves), then wastewater parameters (pH, ORP, DO, TSS/VSS, total and soluble COD) and finally parameters which involve both electrochemical and wastewater parameters (coulombic efficiency, COD balance). As a check against the soluble COD measurement, the acetate concentration was specifically analyzed using ion chromatography as well. Finally, conclusions are drawn based on overall performance indicators such as current/power densities, COD reduction and closure of the overall COD balance.

4.2 Materials

The section is divided into four main sub- sections that describe the following aspects of the MFC experiments: i) construction of the microbial fuel cell, ii) auxiliary equipment for MFC operation, iii) equipment for control of electrochemical experiments, and iv) constituents of inoculant and feed solutions. Although the original intent was to operate the system as a two-cell stack operating in

parallel, one cell (MFC #1) was discontinued due to inconsistent current generation and so data were collected from only the MFC #2 cell.

4.2.1 Materials - MFC Construction

The microbial fuel cell was originally constructed in June 2008 as a two-cell stack with a flat-plate design similar to the dual-chamber flat-plate cell in Figure 1B of reference [17].. In this design, no catholyte compartment was used and the cathode was exposed directly to ambient air.

Each anolyte chamber, which held the wastewater inoculants or synthetic feed stream, contained an inlet line, outlet line and baffles designed to help prevent short-circuiting of the flow and to increase the tortuosity of the flow path through the reactor. The original design consisted of a common graphite plate in the middle to serve as the common anode for the two cells. On the other side of the two cells were commercially made platinum-coated Nafion membranes. However, during preliminary operation, one cell was essentially short-circuited and produced little or no current. Consequently, the MFC design was modified.

The MFC was re-designed so that the graphite plate anode was replaced with two plain carbon paper anodes and a non-conductive plate placed between them to electrically and physically separate the two cells. The cathodes were also replaced with single-sided membrane-electrode assemblies (MEA). Each MEA was comprised of two layers: i) carbon paper impregnated with hydrophobic PTFE (5% weight) to reduce water loss, a carbon/PTFE microporous layer to improve oxygen diffusion and a home-made Pt-coated or non-precious polypyrrole-based carbon composite catalyst airbrushed onto the GDL, and ii) a pre-treated sheet of the proton-exchange membrane (Nafion). The Nafion sheet was pre-treated by boiling in 3% hydrogen peroxide for 1 hr to remove organic contaminants, rinsing with DI water for 1 hr, boiling in 0.5 M sulphuric acid for 1 hour to convert from the Na-form to H-form of the ionomer and finally rinsing for another 1 hr in DI water to remove any free acid remaining in the membrane. The two layers of the MEA were annealed by hot-pressing at 1780 kPa and 140ºC for 3 min. [14]

The connections of each cell to the external circuit were made directly at the carbon paper anode and at a stainless steel mesh pressed to the cathode using a perforated stainless steel plate. All liquid-

containing parts of the cell were sealed using rubber gaskets. The anodes of both cells were separated by a non-conductive plate. The MFC stack as a whole was constructed as a plate-and-frame design fastened together by threaded Nylon screws. The overall nominal flat-plane area of each anode and cathode was both 80 cm^2 and the overall anolyte chamber volume in each cell was 120 mL. In the original series of experiments with this design, MFC #1 operated with a non-precious metal catalyst polypyrrole, while MFC #2 operated with a platinum catalyst. Although both cells originally functioned properly, the current from MFC #1 became inconsistent during the first week of January 2009. This cell was electrically disconnected on January 13, 2009 and only the platinum cell was operated for the duration of this run (until May 2009). Specific information regarding the materials of construction of the MFC is given in Table 4.1. Photographs of the baffled anolyte chamber along with the fuel cell (shown as the two-cell stack) are presented in Figure 4.1 and Figure 4.23.2, respectively.

Table 4.1 MFC Construction Materials

Anode	Provides surface for biofilm formation and oxidation reactions • Dimensions: 14 x 13 cm • Effective surface area: 80 cm^2 • Sigracet 34 AA carbon paper • Non wet-proofed, no catalyst • Twelve 0.25" holes punched 0.75 cm from edges for screws • Aluminum tape adhered to exposed surface for improved contact to external load
Cathode MEA	Provides surface for oxygen reduction and serves as a liquid barrier Cathode: • Dimensions: 10 x 10 cm - 235 μm depth • Sigracet 25 BC carbon paper • Contains 5 wt. % PTFE for wet-proofing and a, microporous layer • 0.2 mg/cm^2 Pt catalyst - 10% Pt on activated charcoal support (Sigma-Aldrich) • Catalyst ink airbrushed onto cathode microporous layer (Paasche VL series airbrush), weighed and dried • Placed at center of Nafion sheet Nafion: • 13 x 13 cm - 178 μm depth • Twelve 0.25" holes punched 0.75 cm from edges for screws Cathode MEA: • Effective surface area: 80 cm^2 (20 cm^2 subtracted due to baffles) • H.ot=pressed cathode to Nafion at 140ºC, 1780 kPa for 3 min
Anolyte chamber	Contains bioreactor liquid where oxidative reactions can occur • Frame material: non-conductive Delrin • Frame dimensions: 13 x 13 cm – 1.5 cm depth, 1.5 cm thick • 10 x 10 cm inner area exposed (except for baffles) • 4 baffles: 9 cm long x 0.5 cm thick extending inwards from exterior frame to prevent preferential flow • Two 0.25" threads tapped into top and bottom of chamber to permit flow Effective anolyte volume: 120 mL
Cathode current collector	Provides a convenient area for attachment of alligator clips to external load • Stainless steel mesh • 100 x 100 mesh/inch, 14 μm aperture, 114 μm wire diameter • Dimensions: 14 x 13 cm • Twelve 0.25" holes punched 0.75 cm from edges for screws
Delrin support plate – Anode	Adds structural support to carbon paper anode • Plate dimensions: 13 x 13 cm – 5 mm depth • Twelve 0.25" holes punched 0.75 cm from edges for screws
Delrin support frame – Cathode	Adds additional structural support to cell • Frame dimensions: 13 x 13 cm – 5 mm depth, 1.5 cm thick exterior frame • 10 x 10 cm inner area exposed Twelve 0.25" holes punched 0.75 cm from edges for screws
Rubber gasket frames	Provides water & gas-tight seal for anolyte chamber • Frame dimensions: 13 x 13 cm, 1.5 cm thick exterior frame • 10 x 10 cm inner area exposed • Twelve 0.25" holes punched 0.75 cm from edges for screws Gaskets placed between: (i) anode & anode support plate, (ii) anode & anolyte chamber, (iii) anolyte chamber & Nafion sheet

Stainless steel supports	Improves contact between current collector and cathode • Perforated stainless steel plate • Dimensions: 9.5 x 9.5 cm – 3 mm depth • Perforation dimensions: 0.25" holes, 0.125" spacing between holes
Screws, nuts, washers	Fastens anode, cathode MEA, support frames & plates, current collector and rubber gaskets • Screws: 0.25" ID x 3"L x 20 threads (NPT), hex head, non-conductive nylon • Nuts: 0.25" ID threaded NPT, non-conductive nylon • Washers: 0.25" ID, non-conductive nylon

Figure 4.1 Baffled anolyte chamber of MFC

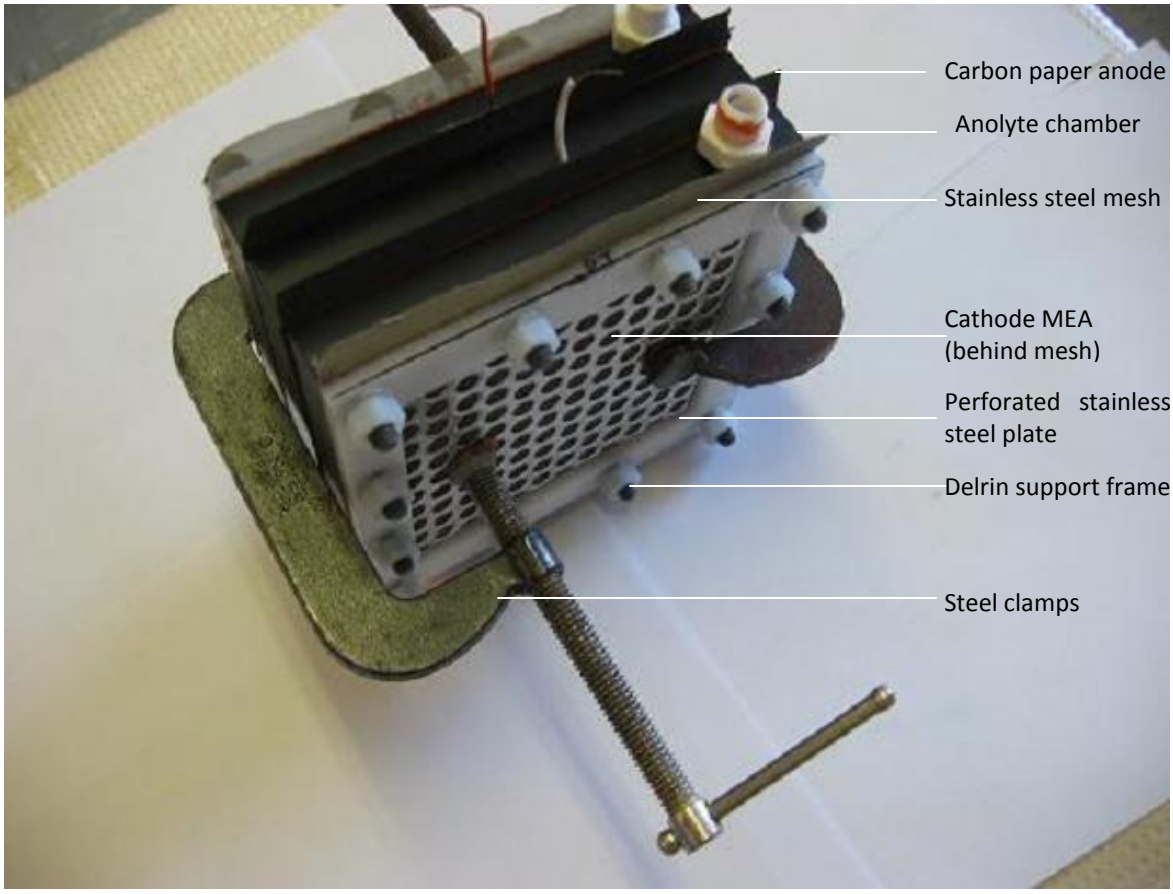

Figure 4.2 Constructed MFC

4.2.2 Materials – Auxiliary Equipment

In addition to the structure of the MFC, other auxiliary equipment was also required to maintain proper operation of the system. An incubator controlled the temperature of the MFC to 30ºC while an indoor house fan placed inside the incubator circulated air. The inlet stream was fed from an external chiller controlled at 4ºC to reduce microbial degradation of the substrate. The feeding system consisted of a peristaltic pump controlled by two remote timers – one that controlled the time at which the pump was switched on and the other which controlled the time interval over which the pump was left on. Process tubing provided a means for liquid to flow in and out of the MFC, while Tedlar bags (Chromatographic Specialities, Brockville, ON) hooked downstream of the MFC enabled any gas generated by the process to be collected and analyzed. A detailed list of auxiliary equipment used in the operation of the MFC is

listed in Table 4.2. The complete MFC setup and auxiliary equipment in the incubator are shown in Figure 4.3.

Table 4.2 Auxiliary Equipment for System Operation

Incubator	Controls temperature of MFC to 30ºC • Thelco GCA Precision Scientific Model 6M • Metal racks for multi-level shelving • Ceiling vent provided access for wiring, potentiostat electroprobe and overhead compartment for Tedlar bag storage
Air circulation fan	Provides circulation of ambient air • Airworks 1500W fan heater • Fan-only setting for air circulation without heating
Tedlar bags	Permits collection of head gases for GC analysis • Attached downstream of MFC • 1 – 2 L volume • 0.125" nipple, lockable • Rubber septum for sampling
Peristaltic pump	Controls liquid flow into fuel cell • Masterflex Pump Model #: 7520-35 • Pump head Model #: 7017-21 • 2.8 – 1700 mL/min liquid flow rate controlled by analog knob
Pump interval timer	Sets the time interval during which the pump operates • Remote clockless analog timer • 2 knobs for interval time (1 s – 60 min) and cycle time (1 min – 8 hrs) • Manual override button
Pump cycle timers	Sets the time for activation of interval timer and the number of feeding cycles per day • For 24 hr HRT sampling: - Woods TD 1300-2 Indoor 7-Day Electronic Lighting Timer - 10 programmable on/off functions per day - Minimum 1 minute intervals - Manual operation mode available • For 12 hr HRT sampling: - Woods TIM 1200 Heavy Duty Appliance Timer – 24 hr - Minimum 30 min intervals, up to 24 settings per day - Timer/Manual operation switch
Waste jar	Collects fuel cell discharge • 2 L narrow mouth glass bottle, sealed with rubber stopper • Spigot at bottom for discharge discharge, flow controlled with C-clamp
External feed chiller	Controls feed temperature at 4ºC to minimize acetate degradation • Fisher Isotemp 3016 Refrigerated Circulator • 6 L volume, -20ºC - 200ºC range • Filled with 50% ethylene glycol, 50% water mixture to prevent freezing
Process tubing	Provides conduit for liquid flow • 0.25" OD Poly tubing - Main liquid flow • 0.25" ID Flexible tubing – Provides pinch point for C-clamps for flow diversion (i.e. during sampling, purging)
Electrical wiring	Provided electrical connection between cell and external load • Copper wire, 1 mm diameter • Electrical connection to MFC via alligator clips • Electrical connection to potentiostat via 2 BNC connections

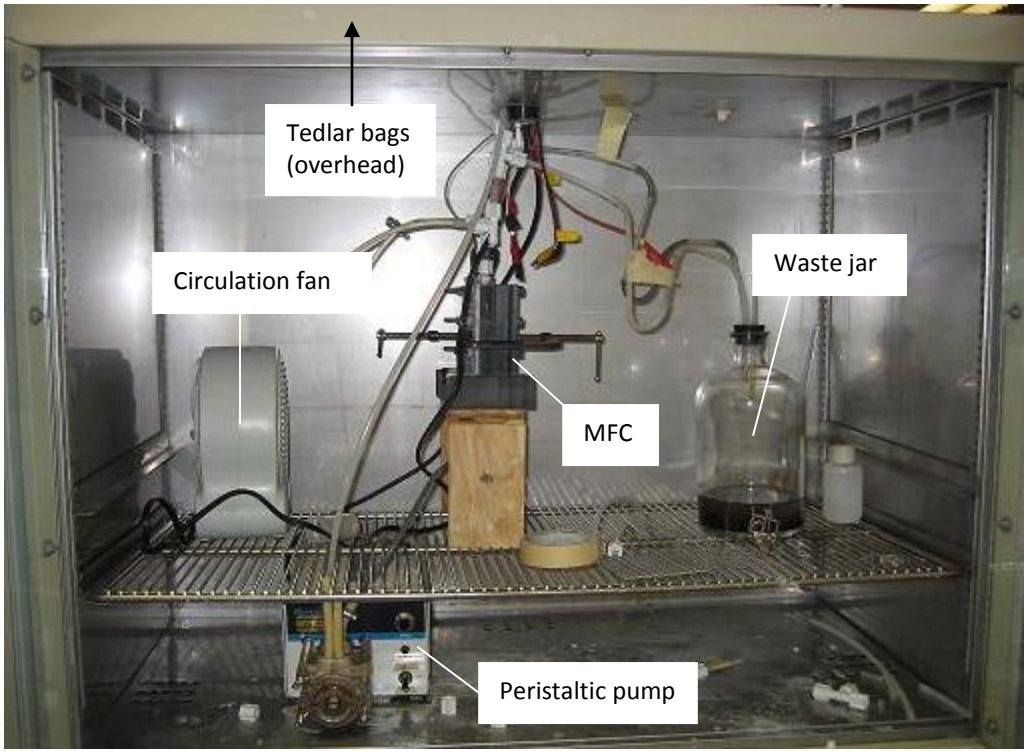

Figure 4.3 System components housed in incubator.

4.2.3 Materials – Electrical

A potentiostat was used to control the cell potential and measure the current generated by each cell. The charge was measured by a digital coulometer connected to the potentiostat, converted into a current signal and sent to the data logger. The analog output measurements from the potentiostat were then converted by an eDAQ E-corder Model 401 datalogger into a digital signal that was relayed to a PC computer for real-time data monitoring and collection. When the system was operated as a two-cell stack in parallel, a separate digital multimeter was connected to record the current from MFC #1. This was necessary since the potentiostat was only able to measure the total current produced from the stack. The current from MFC #1 was then subtracted from the total current to yield the current from MFC #2. However as mentioned in subsection 3.2.1, MFC #1 was disconnected on January 13, 2009. From then on, only the current from MFC #2 was measured. A detailed list of electrical equipment used for MFC #2 after January 13th is given in Table 4.3, while a basic circuit diagram for MFC #2 is given in Figure 4.4.

Table 4.3 Electrical Equipment for System Operation

Potentiostat/galvanostat	Controls potential of cell at 0.3 V • EG&G PAR 173, dual channel • Current range: 10 μA - 1 A • Voltage range: 0 - 2 V, electroprobe voltage control through 2 cable sets with standard banana plugs connected to alligator clips • EG&G PAR 179 Digital coulometer installed for current output • Analog BNC connection outputs
eDAQ E-corder	Converts analog BNC outputs to digital signal • Model 401 • Signal inputs: Two BNC connections used (voltage output, current output) • Signal output: USB 2.0 A/B to lab computer
Lab computer	Displays and saves data from eDAQ as voltage and current • USB signal input • Associated software: eDAQ Chart 5.0 software allows for continuous monitoring of voltage and current and analysis of data to display coulombs, current density and power density

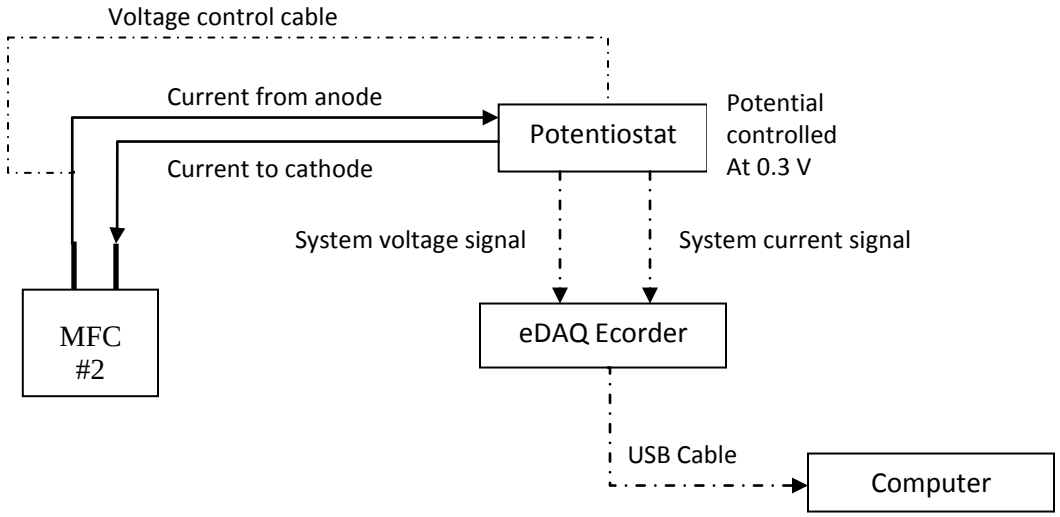

Figure 4.4 Basic circuit diagram of MFC #2

4.2.4 Materials - Feed solution

The MFC required inoculation of a bacterial culture to establish the biofilm before introducing the synthetic feed solution. The choice of an inoculum culture was based on three factors. Firstly, the culture should be diverse and resilient enough to adapt to changes in environmental conditions. Secondly, it should be rich in facultative anaerobes (bacteria that can function in both anaerobic and

aerobic conditions). Thirdly, it should be generated from a wastewater source that is likely to benefit from MFC technology. Based on these three criteria, the selected inoculum was a mixture of the digester overflow and aeration basin collected from the Waterloo domestic wastewater treatment plant (WWTP). The complex bacterial diversity of the digester overflow and aeration basins satisfied the first condition above, while the mixture of the aerobic consortia from the aeration basin and the anaerobic consortia from the digester overflow increased the likelihood that the facultative anaerobes would satisfy the second condition. Obviously, since this inoculum consists of domestic wastewater, it satisfies the third condition.

The synthetic feed solution consisted of acetate (the nutrient source), a phosphate buffer (to maintain pH and increase proton transport from the biofilm to the cathode) and several minerals (micronutrients for the bacteria). The final feed solution was titrated to pH 7 using sodium hydroxide. The mineral composition in the feed solution remained the same in all experiments in order to maintain the ionic strength and the conductivity of the solution as constant as possible. The mineral solution recipe obtained from a study by Mohan *et al*. [57] and scaled for a 6.44 g COD/L-day feed is shown in Table 4.4. The acetate concentration was varied depending on the experimental run, as will be described in Section 4.3. A more detailed description of the feed solution preparation for each experimental run is given in Appendix C.

Table 4.4 Mineral Solution Recipe for MFC

Compound	Concentration (g/L)
NH_4Cl	1.073
$FeCl_3*6H_2O$	0.030
KH_2PO_4**	0.265
K_2HPO_4**	0.531
$MgCl_2*6H_2O$	0.644
$CoCl_2$	0.054
$ZnSO_4$	0.029
$CuSO_4$	0.027
$CaCl_2$	0.011
$MnCl_2*4H_2O$	0.051

** 5 mM phosphate buffer

4.3 Experimental Design

This section on overall experimental design is separated into four subsections: i) overall system operation, ii) sampling and feeding procedure, iii) electrochemical analyses and iv) wastewater characterization analyses. The analytical methods are described in Section 4.4.

4.3.1 Overall System Operation

The description of the constructed MFC and all associated equipment was given in Section 4.2. All experiments were conducted in an incubator set at 30ºC at a controlled potential of 0.3 V between the anode and cathode. This potential was chosen based on previous MFC experiments done in our group [24]. The peristaltic pump, MFC and waste jar were all located within the incubator while the pump timers, potentiostat, data logger, chiller and Tedlar bags were all located outside the incubator.

Operation of the fuel cell was split into three experimental runs or phases based on the chemical oxygen demand (COD) concentration (as acetate) and hydraulic retention time (HRT) of the feed stream, as defined in Table 4.5. The COD is a measurement of the oxidative capacity of a given solution and is a key wastewater quality parameter commonly measured in MFCs. The HRT refers to the amount of time that one reactor volume of solution resides in the reactor. As previously shown in Table 4.1, the effective volume of the anolyte contained within the reactor was 120 mL. Based on the sample volume required for wastewater analyses, a minimum sample volume of approximately 15 mL was required. To provide a safety measure against insufficient sample volumes and depleting the solution within the anolyte, a feed rate of 20 mL/cycle was chosen.

Table 4.5 Operational Parameters for Phases 1-3

	Phase 1	Phase 2	Phase 3
COD concentration (g/L as acetate)	6.44	3.22	6.44
HRT (hr)	24	12	24
COD loading (g/Lday as acetate)	6.44	6.44	6.44
Feed frequency	20 mL/4 hr 6 cycles/day	20 mL/2 hr 12 cycles/day	20 mL/4 hr 6 cycles/day

Phase 1 operated at a higher acetate concentration and longer HRT (0.1 M, 24 hr HRT) from December 12th, 2008 to March 3rd, 2009 (81 days). Phase 2 operated at a lower acetate concentration and a lower HRT (0.05M, 12 hr HRT) from March 5th to April 9th (35 days). The objective of Phase 3 was to

investigate the robustness of the cell power generation and COD removal by returning the operating conditions to those of Phase 1. This run began on April 9th and ended on May 13th, 2009 (34 days). Each phase was operated until acceptably stable cell performance was achieved (criteria used are described later in Section 4.5). The duration of Phase 1 was much longer than that of the other two since it took longer for the cell performance to stabilize due to several changes to the sampling procedure and some inadvertent external disturbances. It was only on February 17th, 2009 after the addition of the feed chiller that the final desired sampling/feeding procedure was established.

As mentioned in Section 4.1, the MFC system was originally operated as a 2-cell stack. Both cells were originally inoculated with a mixed culture wastewater on December 12, 2008 collected from the digester overflow and aeration basin at the Waterloo Wastewater Treatment Plant. After inoculation for 4 days, the feed was shifted to the Phase 1 synthetic feed (see Table 4.5). The introduction of this feed was continued until December 23rd, at which point the waste jar was cleaned, filled with fresh solution and converted into a recycle jar by rerouting the jar to the feed line. A concentrated acetate solution was periodically added every 3-4 days to the jar, equivalent to an initial COD loading of 6.44 g/L-day. This change in feed was implemented as the normal operator was away from the laboratory for 2 weeks. Normal operation resumed on January 8th, 2009. After disconnection of MFC #1 on January 13th, 2009, the cell operated without interruption until January 29th, 2009, when a leak caused the anolyte chamber to completely drain. It was refilled the following day and current recovered completely within 2-3 days. The feed bottle was also placed in a separate chiller at 4ºC on February 17th to limit premature microbial degradation of the feed. A timeline showing the course of events for Phase 1 is given in Figure 4.5

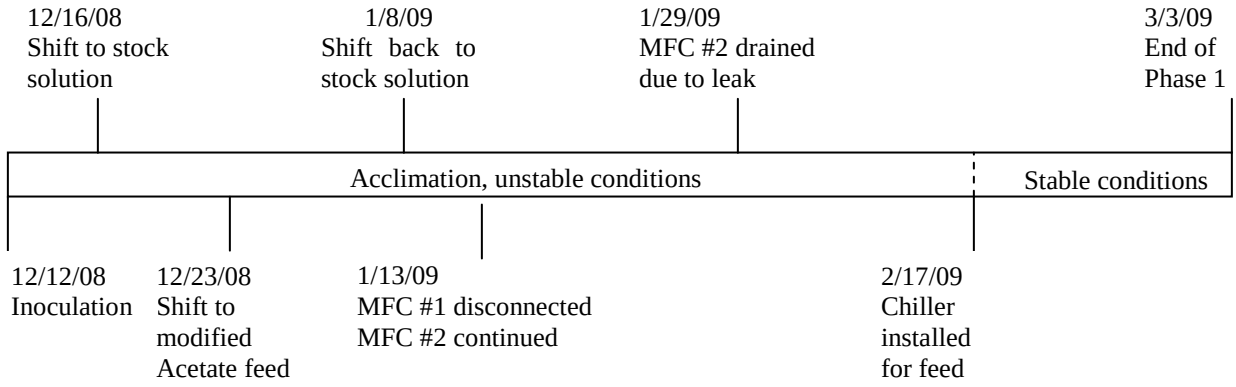

Figure 4.5 Timeline of Phase 1 acclimation

The only disturbance encountered during Phase 2 occurred on March 29th, 2009, when the feed line was accidentally raised above the liquid level which caused air bubbles to be introduced into the system. No disturbances were encountered during Phase 3.

4.3.2 Feed and Sampling Procedure

As previously described, fresh stock solution was fed in 20 mL increments every 2-4 hours depending on the HRT. Fresh stock solution was prepared once a week. If any stock solution was left unused at the end of the week, it was not used in the next feed batch. Instead, it was discarded and a new complete batch of fresh stock solution was prepared. Samples from the MFC were collected every 48 ± 4 hours. The MFC was equipped with bypass ports for upstream and downstream sampling in the reactor. The bypass ports were comprised of tees with flexible tubing attached to/from the line leading to the cell and to the sample bypass port. Under normal operation, the sample bypass port was closed using a C-clamp. When a sample was taken, the line leading to/from the cell was closed and the sample bypass port opened up. The pump timer was also set to manual for convenient pump control. A sample was then collected by manually activating the pump to transport discharge into a 40 mL glass sample vial. In most cases, an insufficient volume of discharge was collected from one cycle. In these cases, the pump would then be manually activated again to collect more samples. In all cases, less than 10 mL of extra feed was added to the reactor per sample cycle. It should be noted that samples of the feed and discharge streams were originally collected from these sample ports. However, after the reactor leak on January 29th, feed samples were subsequently taken directly from the feed bottle.

Samples obtained were immediately analyzed for pH, ORP and DO before being homogenized and diluted. After homogenization and dilution, the portion of the sample to be used for total COD analysis was removed. The remaining sample was then filtered through a 1.5 μm glass fibre filter (Whatman 934-AH). The residue on the filter was analyzed for the mass of solids present (used to determine the total suspended solids and volatile suspended solids of the original sample collected), while the filtrate was collected in a glass vial. The filtrate was preserved with sulfuric acid before being stored at 4ºC for further analyses. Once a week, a portion of the filtrate was removed for soluble COD determination, while the remaining sample was stored at < -14ºC for acetate analysis via ion chromatography (IC) at a later date.

Gas samples from the Tedlar bags were collected once every 4 days. Before being attached to the head gas port of the MFC, the bag was emptied of any residual gas by a vacuum pump and locked using the adjustable nipple. Once locked, the bag was immersed into a 500 mL graduated cylinder filled to 400 mL (5 mL gradations) to determine its empty volume. The bag was then connected to the head gas port and sealed using a hose clamp before being opened to enable gas collection. At the end of the 4-day collection period, the bag was re-locked and removed and a new bag of known empty volume was then installed. The filled bag was then immersed into a 2000 mL graduated cylinder filled to 1300 mL (20 mL gradations) to measure its filled volume. The gas volume generated by the MFC was then obtained from the difference between the filled gas volume and the empty gas volume. The composition of the gas was measured by gas chromatography (GC). Detailed procedures for sampling, feeding and sample preservation can be found in Appendix C.

4.3.3 Electrochemical Analysis

During all runs, the cell voltage was continuously controlled to be 0.3 V. The cell current and voltage were recorded continuously by a data logger. From these data, the current density, power density and total coulombs could be determined. Calculation of these quantities is covered in Section 4.4.

A polarization curve showing the variation of current with cell voltage was determined at the end of each experimental phase. Polarization curves are a good indicator of MFC performance.. After waiting for 80-90 minutes and the open-circuit voltage had stabilized, the voltage was changed in a step-wise pattern beginning at the highest value of 0.55 V. The cell was held at this potential for 20 minutes and the resulting current over this time was monitored. The final current at the end of this 20-minute period was taken as the value to be plotted on the polarization curve. Although this interval was not long enough for steady state to be reached, it was found to be sufficient to provide a good measure of cell performance. After the 20 minute interval, the voltage was decreased to 0.5 V and held for another 20 minutes while the corresponding current was measured. Voltage was continually decreased in this way in 50 mV steps until 0.1 V was reached, at which point the cell was reset to 0.3 V and normal operation resumed. From these polarization curves, the corresponding power densities were obtained from the

product of the voltage and current density and plotted versus the current density. Lastly, the internal resistance of the cell was estimated from the slope of the polarization curve in the linear ohmic region.

4.3.4 Water Analysis

The various samples were analyzed every 2 days soon after they were collected. Some of these analyses were done immediately following sampling, while others were begun on the same day but required preparation steps or were preserved and done at a later date. Immediate analyses focused more on monitoring the system environment, while later analyses focused more at system performance.

Immediate analyses included pH, oxidative-reductive potential (ORP) and dissolved oxygen (DO) measurement. The pH provided a general indication of the proton transfer capability of the internal solution, capability of the phosphate buffer to maintain the pH at 7 and the general microbial environment. Since it is known that a drop in pH below 6 can inhibit microbial metabolism and also increase the anode potential [58], it was important to control pH so that it did not drop below 6. The ORP and DO were both monitored as qualitative measures of the reactor anaerobicity. Preferably, the ORP should be negative (-100 to -400 mV) which puts it in the anaerobic range where no molecular oxygen is present. Higher ORP values (+50 mV) indicate the presence of free molecular oxygen which can metabolize substrate without producing current. [59]

The chemical oxygen demand (COD) is a key indicator of water quality that is a measure of the amount of oxidizable material within a solution. For this study, it was taken as the measure of wastewater remediation achieved by the MFC. The MFC(s) were fed with a known COD concentration (6.44 g/L) in the form of sodium acetate. This substrate would then be metabolized into several products and ultimately generate electrical current, methane and biomass. The electrical charge generated is proportional to a COD equivalent based on the oxygen reduction reaction (see Equation 4.10). Total COD (tCOD) and soluble COD (sCOD) of both the feed and discharge were measured every 2 days to determine the amount of suspended biomass produced, while head gas samples were collected every 4-6 days and characterized by GC for their methane compositions. The amount of methane produced was then converted into a COD equivalent. From knowledge of these COD equivalents, the coulombic efficiency could be determined and an accounting for the COD balance in the entire process made. A

description of these analyses is covered in Section 4.4. Lastly, as a check of the soluble COD measurements, the acetate concentration in the feed and discharge was also directly obtained by IC analysis.

4.4 Analytical Measurements

The following section outlines some of the principles of the analytical parameters and techniques used in this study. The section is divided into three categories: electrochemical measurements, wastewater characterization (pH, ORP, DO, solids content) and wastewater treatment indicators. The description of wastewater treatment indicators is further sub-divided into subsections on COD analysis, head gas analysis and acetate determination. Specific analytical methods and procedures are given in Appendix D.

4.4.1 Electrochemical Measurements

All electrochemical parameters were recorded using the eDAQ eCorder Model 401 data logger. The raw data collected included the current and cell voltage. Using the measured average current (I) as a function of time between current readings, the coulombic charge Q generated over this interval is determined from Equation 4.1:

$$Q = \int_{t_1}^{t_2} I \cdot dt \qquad \textbf{4.1}$$

The power P(t) generated by the cell can also be calculated from the cell voltage and current according to Equation 4.2:

$$P = I \cdot V \qquad \textbf{4.2}$$

Since the voltage was held constant at 0.3 V throughout this study, the power was directly proportional to the current.

In most studies, current and power are typically normalized with respect to the anode and/or cathode geometric surface area (80 cm^2) or the liquid volume of the reactor (120 mL) as the current and power densities. Although normalization with respect to the liquid or total reactor volume enables evaluation of the power as a function of the overall reactor volume, it includes parts of the system which do not actively participate in generating current (i.e. support structures, bulk phase of liquid volume). Normalization with respect to the surface area of an electrode is more meaningful since an electrochemical reaction is a surface phenomenon that occurs at a rate proportional to the exposed electrode area. For purposes of this study, the current and power were normalized to the area of the anode.

In the analysis of fuel cell performance, polarization curves present cell voltage as a function of current density and are a powerful tool for delineating the relative effect of the activation, ohmic and mass transfer overpotentials associated with a particular cell. Once a polarization curve is obtained, the power density can also be plotted as a function of the current density in what is called a power curve.

Internal (or ohmic) resistance is an important electrochemical parameter since it represents the loss arising from ionic transport through the electrolyte separating the anode and cathode. In the case of an MFC, this loss can be significant due to the 1 cm or more inter-electrode spacing, the aqueous nature of the anolyte solution and the low ionic strength of the solution. As a result, the internal or ohmic resistance of an MFC anolyte solution is much higher than in the case of a hydrogen PEMFC. With the MFC configuration used in this project, it was not possible to use advanced methods for determining internal resistance such as electrical impedance spectroscopy (EIS), nor was it possible to use other potentiostat-based techniques such as the current interrupt method due to the analog potentiostat used. Therefore, only an approximation of the internal resistance could be obtained. Using the power curve obtained, the internal resistance can be estimated from measurement of the maximum power (P_{max}) generated by the cell. The equation governing this property is given in Equation 4.3 [60]:

$$P_{max} = \frac{OCV^2 R_{ext}}{(R_{int} + R_{ext})^2} \qquad \textbf{4.3}$$

In an air-cathode MFC, the open circuit voltage (OCV) does not vary appreciably from run to run and the external resistance R_{ext} to the current generated by the cell is controlled manually by the potentiostat. Therefore, the internal resistance is the main factor affecting the maximum power. [60] In order to

obtain a power curve, the external resistance is varied and the current and voltage are determined. It follows that the peak of the power curve is the point where the total resistance ($R_{int} + R_{ext}$) is minimized. It is assumed that the maximum power density is attained at the point where mass transfer resistances become dominant, or at the end of the ohmic region. The voltage in the ohmic region can be defined as follows:

$$IR_{ext} = OCV^{*} - IR_{int} \quad \textbf{4.4}$$

IR	=	Cell voltage within ohmic region (V)
OCV^{*}	=	Open circuit voltage extrapolated based on linear ohmic region (V)
IR_{int}	=	Voltage drop due to internal resistance (V)

Based on the relationships given in Equations 4.3 and 4.4, it is possible to derive the maximum power density by taking the derivative of Equation 4.3 with respect to the current. It turns out from this analysis that the maximum power density occurs when $R_{int} = R_{ext}$. Using this relationship, one can use the power curve to find the internal resistance of the system.

4.4.2 Wastewater Characterization – pH, ORP, DO, Solids (TSS/VSS)

The pH, ORP and DO of both feed and discharge samples were measured immediately following a sampling event. Since it was impossible to obtain samples in an oxygen-free environment, DO and ORP measurements were recorded first to assess whether significant leakage of oxygen into the anolyte sample was occurring. DO was measured first by immersing the probe (VWR SympHony DO probe) into the solution that was stirred lightly while maintaining minimal oxygen contamination. ORP of the anolyte was measured next by immersing the redox electrode (VWR SympHony epoxy combination redox electrode, Ag/AgCl reference) into the solution while being stirred vigorously. Lastly, the pH was measured using a pH electrode.

'Solids' analysis consisted of the total suspended solids (TSS) and volatile suspended solids (VSS) contents. After the original sample was mixed and diluted, it was passed through a pre-weighed and pre-dried glass fiber filter (Whatman Grade 934-AH, 1.5 μm). The filter residue was collected for TSS measurement, while the filtrate was retained for analysis of the soluble component. After drying for 24 hrs in an oven, the filter paper (contained in aluminum dishes) was weighed to determine the amount of TSS and then burned in a muffle furnace for 12 minutes to remove the volatile component. From the

difference in weight before and after the volatile component was removed, the VSS concentration was determined. Before any samples were weighed, they were cooled in a dessicator at room temperature for a minimum of 30 minutes. Steps for sample preparation are listed below and the detailed procedure for TSS and VSS determination can be found in Appendix D.

1. **Sample dilution:** 1:2 (10 mL/sample) in duplicate
2. **TSS Drying time/temperature:** > 24 hr/105ºC
3. **Soluble sample preservation:** pH <2 using H_2SO_4, stored in refrigerator @ 4ºC
4. **VSS Flaming time/temperature:** 12 min/550ºC

Using the recorded weights, the TSS and VSS concentrations can then be found using Equations 4.5 and 4.6, respectively.

$$[TSS] = \frac{m_{postTSS} - m_{preTSS}}{\frac{10\ mL}{dilution}} \quad \textbf{4.5}$$

$$[VSS] = \frac{m_{postVSS} - m_{postTSS}}{\left(\frac{10\ mL}{dilution}\right)} \quad \textbf{4.6}$$

m_{preTSS} = mass of clean pre-dried filter paper (g)
$m_{postTSS}$ = mass of oven-dried filter paper (g)
$m_{postVSS}$ = mass of furnace-flamed filter paper (g)
[TSS] = TSS concentration (g/L)
[VSS] = VSS concentration (g/L)

4.4.3 Wastewater Performance Indicators – Head Gas Analysis via GC

The volume of the head gas collected downstream of the MFC was measured before using GC analysis to determine its methane composition. The GC system consisted of a GC unit (SRI 310C Gas Chromatograph) with a thermoconductivity detector (TCD) and helium gas carrier. The system was remotely controlled using a lab computer with Peaksimple 3.29 software for data collection and analysis. The GC analysis measured the methane, nitrogen/oxygen (the two are indistinguishable from each other for this GC setup) and carbon dioxide fractions of the sample. Only the methane fraction was of interest since nitrogen is considered inert and carbon dioxide is fully oxidized and so has zero COD content.

As described in Subsection 4.3.2, Tedlar bags were used to collect head gas samples over a 48-hour period. After measurement of the gas volume, chemical analysis was carried out by drawing out a 1 mL gas sample from the bag using a gas-tight needle and injecting into the GC unit. Three separate 1 ml gas portions were drawn from each head gas sample and analyzed. The gas fraction of methane reported in this study represents the average of these three measurements. From this average gas fraction y_{CH4} (mol CH_4/mol gas), the volume of methane V_{CH4} can be easily determined as:

$$V_{CH4} = V_{gas} \cdot y_{CH4} \quad \textbf{4.7}$$

The volume can then be easily converted into a mass m_{CH4} (g) using the ideal gas law (Equation 4.8) and finally converted to a COD equivalence (g/L) (COD_{CH4}) using Equation 4.9, i.e.

$$m_{CH4} = \frac{V_{CH4} \cdot P_{bag}}{R \cdot T_{bag}} M_{CH4} \quad \textbf{4.8}$$

P_{bag} = Tedlar bag pressure (1 atm)
R = gas constant (0.08206 atm*L/mol-K)
T_{bag} = Tedlar bag temperature (298.15 K)
M_{CH4} = molecular mass of methane (16 g/mol)

$$COD_{CH4} = \frac{4 \cdot m_{CH4}}{n_{HRT} \cdot \upsilon_{An}} \quad \textbf{4.9}$$

4 = Molecular mass ratio of O_2 to CH_4 (64 g O_2 / 16 g CH_4)
n_{HRT} = # of HRTs per sample period
ν_{An} = liquid volume of anolyte (L)

4.4.4 Wastewater Performance Parameters – COD and COD balances

Each COD sample was sub-divided into two – one for total COD analysis and the other for soluble COD analysis. Total COD samples from the feed and discharge of MFC #2 collected at each sampling time were added to the digestion solution immediately following homogenization of the raw sample, while the soluble samples were stored in a refrigerator until approximately one week of soluble samples were collected. Then, a portion of each sample was removed for separate analysis by adding to the digestion solution. The steps for analysis of feed and discharge COD are given below:

1. **Sample dilution:** 1:10 for all feed, 1:10 or 1:5 for discharge
2. **Digestion solution:** 1.5 mL digestion solution, 3.5 mL sulfuric acid solution, 2.5 mL diluted sample (as per standard methods)
3. **Digestion conditions:** 3 hours @ 150ºC
4. **Colourimetric analysis:** Optical density readings at λ = 600 nm, compared against calibration curves

All samples were diluted up to a final volume of 10 mL with deionized water. Triplicate samples of 2.5 mL each were added to COD sample vials containing the digestion reagent solutions (1.5 mL digestion solution, 3.5 mL sulfuric acid solution). Standards of 50, 100, 200, 300, 500, 750, and 1000 mg COD/L were also prepared to generate a calibration curve. As with the sample solutions, 2.5 mL of a standard were added to each sample vial. All vials were then capped, shaken and placed in a block heater for 3 hours at a temperature of 150ºC for digestion. After cooling to room temperature, the exterior of the glass vials were cleaned using ethanol. The vials were then inserted into a UV-Vis spectrophotometer (Hach DR/2010 Portable Datalogging Spectrophotometer). The COD absorbance was measured at a wavelength of 600 nm and the COD concentration determined from the calibration curve obtained from the standards.

The same calibration curve was used as long as the stock standard solution remained the same. A blank and 1000 mg/L standard were included in every digestion to check the previous calibration curve. Based on the new absorbance for 1000 mg/L, the calibration curve would be adjusted to reflect the new result. For example, if the previous 1000 mg/L standard read an absorbance of 0.400 and the new standard read 0.395 (difference of 1.25%), all calibration curve points were adjusted by the same 1.25%. See Appendix D for the detailed procedure for COD analysis and the reagents used for digestion. The Standard Methods for Water and Wastewater Analysis 5220D (closed reflux, colourimetric method) published by the American Public Health Association, American Water Works Association, and Water Environment Federation should be consulted for details regarding the technique for COD analysis.

A useful parameter that is related to COD removal and measures the ability of an MFC to convert an available substrate to current is the coulombic efficiency. The first step is to calculate the COD equivalence of the generated current as shown in Equation 4.10 for a fed batch reactor.

$$COD_{Elec} = \frac{8 \int_0^{t_b} I \cdot dt}{F \cdot \upsilon_{An}} \qquad \textbf{4.10}$$

COD_{Elec} = COD equivalence of electricity generated in MFC (g/L)
8 = molecular mass of oxygen (32 g/mol O_2) / moles of electrons generated per mole of oxygen (4 mol e^-/mol O_2)
F = Faraday's constant (96485 C/mol)
ν_{An} = liquid volume of anolyte chamber (L)

The soluble COD is used in this equation since we are interested only in the conversion of acetate, the main substrate. Once the COD_{Elec} is found, the coulombic efficiency (C_E) can then be determined as follows:

$$C_E = \frac{COD_{Elec}}{\Delta COD} \quad \textbf{4.11}$$

where ΔCOD = feed sCOD – discharge sCOD (g/L)

The coulombic efficiency is one of the key parameters in measuring the performance of an MFC and is commonly applied in literature.

Another principle goal was to carry out a COD mass balance in the reactor. The COD balance involves the total feed COD, total discharge COD and COD consumption as reflected in the generated current, evolved methane, accumulated biomass and reaction with oxygen that leaks into the anolyte, as shown below in Equation 4.12:

$$COD_{Acc} = COD_{Feed} - COD_{Sample} - COD_{Elec} - COD_{CH4} - COD_{O2Dif} \quad \textbf{4.12}$$

COD_{Acc} = COD of solid biomass accumulated inside MFC (g/L)
COD_{Feed} = total COD of acetate feed (g/L)
COD_{Sample} = total COD of discharge sample (g/L)
COD_{Elec} = COD equivalence of current generated from MFC (g/L)
COD_{CH4} = COD equivalence of methane evolved in head gas from MFC (g/L)
COD_{O2Dif} = COD removal due to reaction with oxygen leaking into anolyte (g/L)

The COD levels of the feed and sample were obtained from bi-daily analysis as described earlier in this sub-section, while the COD consumptions associated with the current and methane evolution were obtained as shown earlier in Equations 4.10 and sub-section 4.4.3, respectively. Finally, the COD due to leakage of oxygen from the cathode side into the anolyte was estimated based on oxygen fluxes for cathode MEAs reported in the literature.

The oxygen flux through the cathode MEA can be estimated using measurements on hydrogen fuel cells. A simple equation for the oxygen mass flow rate W (mg/s) relating the oxygen diffusion coefficient D (cm^2/s), MEA cross-sectional area A (cm^2), concentration difference (C - C*) (mg/cm^3) and MEA thickness Δx (cm) is given in Equation 4.13 [14]:

$$W = -D \cdot A \frac{C - C^*}{\Delta X} \qquad \textbf{4.13}$$

In this case, the value for D was taken to be between 1 to 6 x 10^{-6} cm^2/s from literature data for oxygen diffusion through a Nafion membrane in a PEMFC. [14], the MEA area was taken to be the active cathode surface area (80 cm^2), C is the DO concentration in the discharge sample. For purposes of calculating the oxygen flux, the DO concentration in the anolyte is assumed to be the same as the DO concentration in the cell discharge and C* is the saturated oxygen concentration in Nafion. Assuming no DO remains in the discharge and C* has a value of 4.9 x 10^{-6} mol/mL [61], (C – C*) is determined to be -4.9 x 10^{-6} mol/mL.

4.4.5 Wastewater Performance Parameters – Acetate Determination via IC

Acetate is the simplest and final metabolic product in acidogenesis/acetogenesis. Through methanogenesis, it is split to form methane directly through aceticlastic cleavage or by the initial conversion to carbon dioxide and subsequent reduction to methane in the presence of hydrogen [59]. There are no known metabolic pathways which convert acetic acid to formic acid, the simplest volatile fatty acid (VFA). As a result, essentially all of the soluble COD remaining in the discharge is present as acetate. Therefore, the measurement of the acetate concentration is a good check of the soluble COD readings.

The feed and discharge acetate concentrations were analyzed using the IC unit Dionex DX 300 (Acclaim Organic Acid Column - 5 μm x 210 mm, Dionex VDM-2 Variable Wavelength Detector – deuterium UV lamp @ 210 nm). All samples for IC analysis were taken from previously preserved soluble samples as per sub-section 4.4.2 and thawed from their frozen state. The IC column was operated using a mixture of 2-20% acetonitrile and 0.005 M 1-methanesulfonic acid (MSA) as eluents. Both eluents were degassed using helium gas before operation and held under pressure (12-15 psig)

with helium. MSA served to maintain the pH necessary to keep VFAs in their acid form (2.7 < pH < 3.0), while the acetonitrile concentration gradient served to separate species based on hydrophobicity (higher chain VFAs requiring more acetonitrile to elute from the column). A calibration curve using dilutions from a standard VFA solution was generated beforehand.

Samples were prepared according to the following steps:

- **Sample dilution for IC**: 1:40 (Feed), 1:10 (Discharge)
- **pH adjustment:** between 2.7 and 3 using NaOH and HCl
- **Supplemental preparation:** 2-3 mL/sample vial, filtered using 0.45 μm Nylon syringe filter and 3 mL syringe, capped with 0.2 μm filter cap to remove bacteria

Preparation of the samples began with the initial dilution using the appropriate amount of MilliQ water. Afterwards, the pH of each diluted sample was adjusted to be 2.7 – 3 using NaOH and HCl. Then, about 3 mL of each sample was extracted using a syringe and injected into an autosampler vial through a 0.45 μm Nylon syringe filter. Solutions collected from 3 or 4 sample dates were analyzed during each IC run, along with one standard solution sample to verify the calibration curve. All samples were prepared in duplicate (two sample vials per sample date). Blank and wash samples of MilliQ water were also added at regular intervals to minimize contamination of the column.
All acetate concentrations were then converted to a COD equivalence based on the stoichiometric coefficients of the acetate oxidation reaction:

$$C_2H_4O_2 + 2O_2 \rightarrow 2CO_2 + 2H_2O \qquad \textbf{4.14}$$

From this reaction, 2 moles of oxygen (64 g) react with 1 mole of acetate. Therefore, the COD equivalence is 64/60 or 1.067 g COD/1 g acetate.

4.5 Results

This section covers all results from experimental Phases 1 through 3. The results are split into six sub-sections: i) current production, ii) immediate analyses (pH, ORP, DO), iii) solids analysis– TSS/VSS, iv) methane production, v) COD measurement and COD balance, and vi) acetate concentration determination. "Stable" data for each Phase were obtained for comparison purposes. For the purposes

of this study, the system is considered to have stabilized when the current production varies by roughly less than 5% over a minimum of three sampling periods (≥ 6 days) and after at least 2 weeks of acclimation. A 2-week acclimation period was chosen on the basis of a preliminary trial run (July 2008) that this was the minimum amount of time required for acclimation of the biofilm to the acetate feed.

4.5.1 Electrochemical Performance

In all experiments, the cell potential was held at 0.3 V using the potentiostat. The MFC was operated in fed-batch mode with acetate as the feed after an initial inoculation with wastewater before Phase 1. A plot of the current and power production over the 3 phases is given in Figure 4.6. The dotted lines denote the end of each phase and the shaded regions indicate the periods when "stable" performance during the three phases was attained. Since the potential is held constant during the entire run, it follows that the power produced is proportional to the current produced. No data were collected on April 15th, 2009 during Phase 3 due to a malfunction in the pump that prevented the cell from being fed for one night.

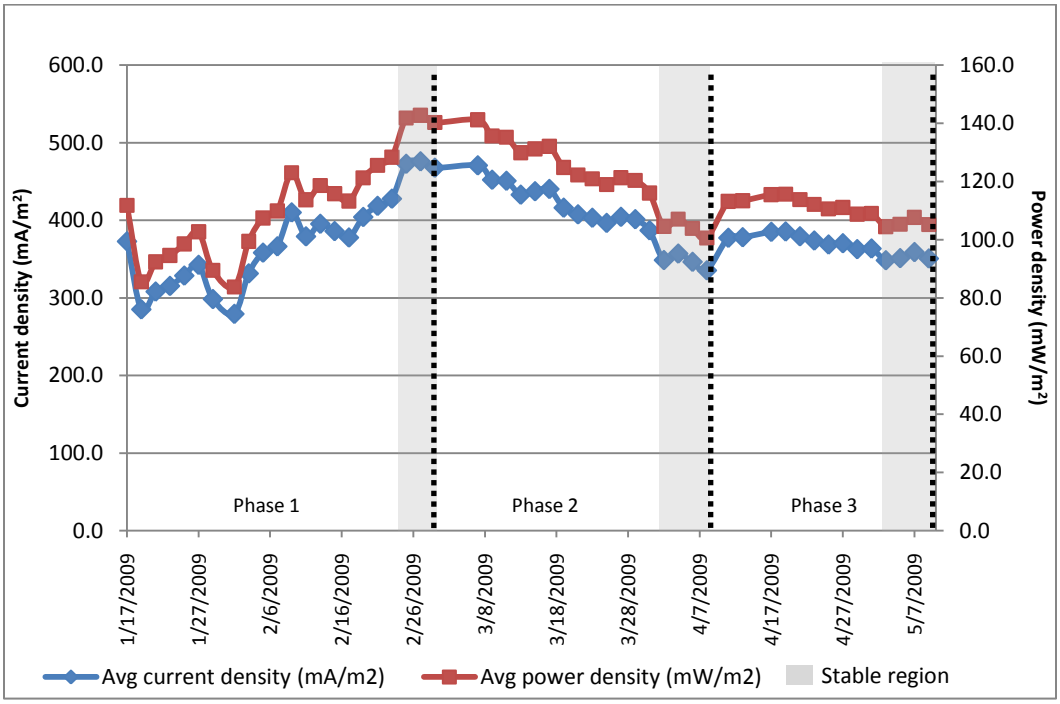

Figure 4.6 Current and power production – Phases 1-3 at 0.3 Volts

A summary of the averaged current and power densities obtained (with 95% confidence intervals) once stable behaviour is attained during Phases 1-3 is shown in Table 4.6.

Table 4.6 Current and power production once stable behavior is reached during Phases 1-3 at 0.3 Volts

	Avg current density (mA/m^2)	Avg power density (mW/m^2)	COD equivalent (mg/L-HRT)
Phase 1	472.2 ± 8.2	141.7 ± 2.4	225.5 ± 3.9
Phase 2	346.8 ± 17.5	104.0 ± 5.2	82.8 ± 4.1
Phase 3	352.3 ± 9.0	105.7 ± 2.7	168.2 ± 4.3

As mentioned in Subsection 4.3.1, Phase 1 was run for much longer than the other two phases due mainly to changes in operating conditions and sampling procedures. On January 29th, the MFC appeared to have been drained due to a leak in the tubing underneath. Over that time, the current dropped to near zero and even became negative (i.e., polarity reversal). After the cell was refilled with the feed solution, current production recovered fully within 3-5 days, demonstrating the resiliency of

the biofilm. A rapid increase in the current from 377 mA/m^2 to 404 mA/m^2 occurred after the chiller was installed on February 17th. It is likely that moving the feed reservoir from inside the incubator to the chiller inhibited bacterial growth and thus prevented acetate from being consumed prior to entry into the cell. Current then continued to rise more gradually until it stabilized near the end of the run.

The results in Table 4.6 show that the stable current obtained during Phase 1 is considerably higher than that during Phase 2. Since the contributions to the ionic strength from the other components of the solution were kept the same in Phases 1 and 2, the factors that could have caused the lower current during Phase 2 were: i) kinetics of the electron transfer reaction(s) increases with acetate concentration, ii) current production had become substrate-limited at the lower acetate concentration in the feed stream or ii) the decrease in the buffering capacity and/or ionic strength at the lower acetate concentration caused a significant rise in the ohmic resistance. A study by Torres *et al*. on phosphate buffers found that the current produced was almost directly proportional to the buffer strength, while an increase in the ionic strength through the addition of NaCl did not produce as large an effect. [58] To determine if substrate limitations due to the lower acetate concentration in Phase 2 were playing a role, the half-saturation concentration (K_s) value is required. The half-saturation concentration is defined as the concentration at which one-half the maximum rate of reaction occurs, in this case, the current generation. In a study on an MFC fed by acetate, K_s was found to vary from 9 – 141 mg/L. [62] Another study on a common electrogenic species *Geobacter sulfurreducens* found a K_s of 0.03 mM with fumarate as an electron acceptor in a non-MFC application. [63] Since the influent feed concentration in Phase 2 was ~50 mM (3220 mg/L), it is unlikely that the acetate concentration in the active biofilm was limiting. Therefore, it is likely that the current drop during Phase 2 was primarily due to the decrease in buffer concentration.

One would have expected the current production during Phase 3 to be similar to that during Phase 1 since the feed conditions were the same. However, the results in Table 4.6 indicate that this was not the case. Although the current did rise between April 8th and 11th, it gradually decreased to nearly the same level as in Phase 2. Based on the average current density alone, it is difficult to explain the cause of this phenomenon. However, a comparison of the current generated over a single feed cycle (2 or 4 hours) during the period when the response of the system had stabilized, as shown in Figure 4.7, may provide a possible reason.

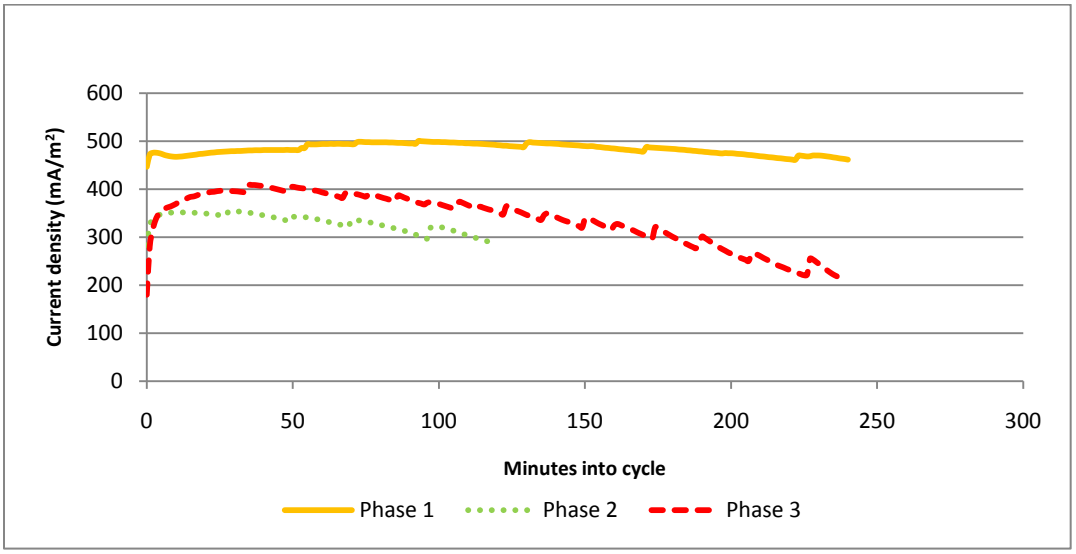

Figure 4.7 **Variation of current with time during a single feed cycle when the response of the system had stabilized during Phases 1-3**

As stated above, one would expect that increasing the feed acetate concentration when going from Phase 2 to Phase 3 would significantly increase the maximum current. However, Figure 4.7 shows that the transient current response during each feed cycle in Phase 3 is only slightly higher than that observed during Phase 2 and remains well below that observed during Phase 1. This poorer than expected performance during Phase 3 may have been due to biomass accumulation within the cell and mass transfer limitations at lower current densities, particularly due to the non-continuous mode of operation and upflow feed path. It is also possible that the baffles in the anolyte compartment may have made the removal of biosolids from the cell more difficult and contributed to a buildup of biomass in the bulk phase that suppressed current generation. This effect could inhibit current in three ways. Firstly, a thicker inactive biomass layer along with accumulated biomass in the bulk phase could attenuate the transport of acetate between the bulk solution to the active biomass closest to the anode. Secondly, some of the acetate may be consumed by the biomass by a process that does not generate current. Finally, the presence of these biosolids would tend to increase the ohmic resistance of the cell. This effect will be discussed with respect to COD removal in sub-section 4.5.5. Another possibility is that the microbial community may have irreversibly changed after the acetate concentration was decreased during Phase 2 and so could not respond to the increase in acetate concentration in Phase 3. No reported studies have explored the effect of changing the substrate concentration in such a manner on subsequent current production.

The polarization (Figure 4.8) and power density (Figure 4.9) curves generated for the three phases appear to be consistent with the results shown in Table 4.6 and Figure 4.7. Note that the curves for Phases 1 and 3 were obtained within one full feed cycle. Two full cycles were required to collect the data for Phase 2 required since the cycle time was half that of the other two phases. It is important to note that the ideal polarization curve would require the conditions at the anode (except the potential) and in the bulk solution be exactly the same for each point on the curve. Since the biofilm at the anode is continually changing, it would be impossible to maintain the biofilm and anode in the same state from point to point on the curve regardless of the procedure used to obtain the polarization curve. Another important factor is keeping the substrate concentration constant for each point on the curve. Also, since the cell was operated in fed-batch mode throughout this study, it would not be consistent to change cell operation to continuous mode for the purpose of obtaining the polarization curves. The best approach might be for each data point to be obtained at the start of a new batch-feed cycle. However, this would still not guarantee a constant substrate concentration in the bulk solution from point to point given the complex nature of the biofilm and process and would also greatly increase the time to obtain an entire polarization curve. Since our experience had shown that the variation in current over any single cycle was only about 10%, the approach followed was to obtain an entire polarization curve over the course of one or two feed cycles. The curves obtained during Phases 1 and 3 are most directly comparable since they were both obtained over a single cycle. On the other hand, the curve for Phase 2 required 2 full cycles to obtain. However, since the variation in current over a cycle was small, this difference was considered small enough that a reason comparison of the polarization curves for the three phases could be made.

The steeper drop in voltage at low current densities in the polarization curves which is indicative of activation losses, is similar for all three phases. However, once the current density increases above 200 mA/m^2 and the system moves into the ohmic resistance domain, the cell voltages during Phases 2 and 3 decrease more rapidly with current than it does in the case of Phase 1. This observation is consistent with the above proposal that the ohmic resistance during Phases 2 and 3 is higher than that during Phase 1. At first, it appears that there is no difference in the ohmic region for Phases 2 and 3 between 200 – 500 mA/m^2. However, since each polarization curve was attained during the course of at least one feed cycle, the shape of the curve was somewhat dependent on the time at which a reading was taken. Because the beginning of the curve (activation region) was obtained near the start of a cycle and since

little current was lost in the first hour of each cycle, there was little difference in the activation region of all three Phases. During the next 2 hours, current in Phase 3 began to drop more rapidly, approaching that of Phase 2. Because this current region was where ohmic resistance would be dominant, it would appear as though the ohmic resistance was higher when in fact the current was beginning to be limited by the substrate (acetate) concentration in the reactor. This hypothesis is further substantiated based on the rapid drop and even reversal in current below 250 mV. Mass transfer losses already occurring due to the high current throughput were further amplified by the already low bulk phase substrate concentration.

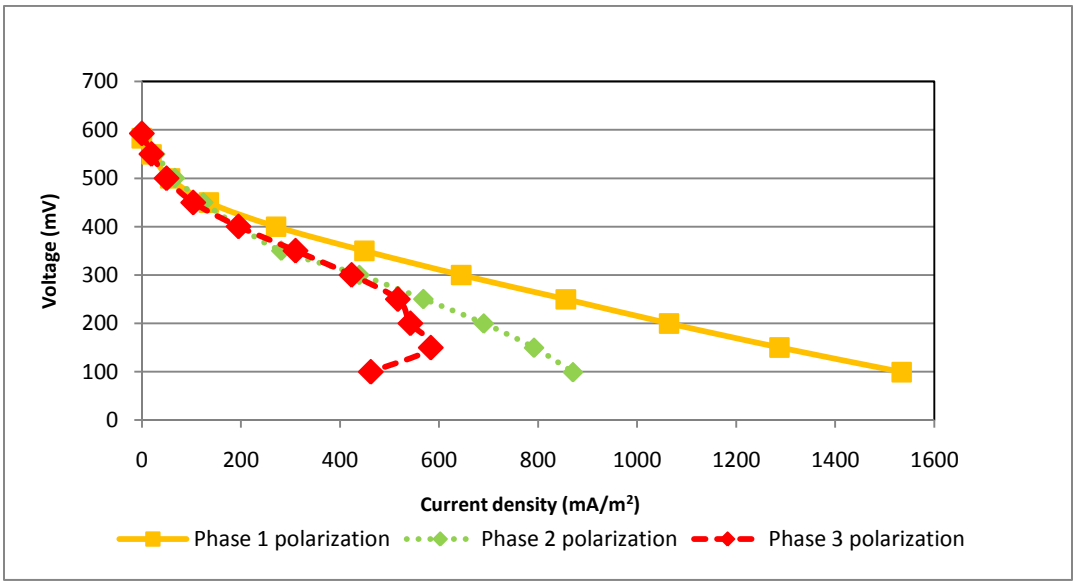

Figure 4.8 Variation of cell voltage as a function of current density during Phases 1-3

The effect of mass transfer losses was also clearly evident from the power curves generated, as well as the estimated internal resistance of the cell in each phase (Table 4.7) based on the peak power of the curve as per Equation 4.3.

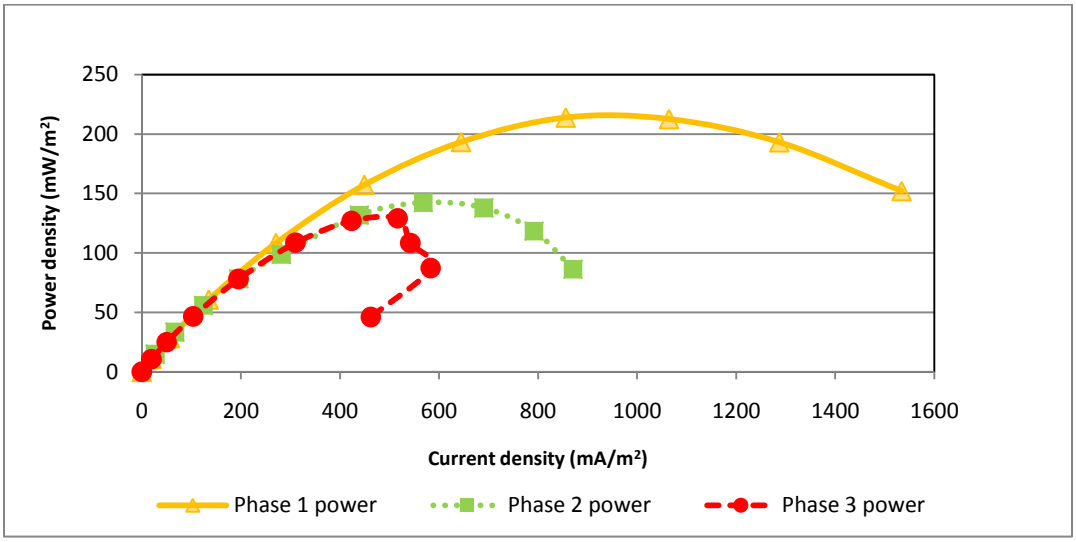

Figure 4.9 **Variation of power density generated as a function of current density during Phases 1-3.**

Table 4.7 **Estimates of ohmic resistance within cell during Phases 1-3**

	Phase 1	**Phase 2**	**Phase 3**
Internal resistance (Ω)	37.4	55.0	90.9

Because mass transfer losses were not as evident during Phases 1 and 2, the difference in the peak power and estimated internal resistance was due mainly to differences in the electrolyte solution, such as the suggested change in the buffering capacity of acetate in the solution. This can be further substantiated by correlating the relative current and the relative estimated internal resistance ratio between Phases 1 and 2. The average current during a feed cycle in Phase 2 was 68% of that observed during Phase 1, while the internal resistance during Phase 1 was 71% of that for Phase 2. These ratios are relatively close, indicative of the linear dependence between cell voltage and current in the ohmically controlled region. On the other hand, significant mass transfer losses in Phase 3 resulted in the collapsing of the tent shape right of the peak. Because the increased mass transfer losses also decreased the solution's buffering capacity, the estimated internal resistance in Phase 3 was in fact a combination of internal and mass transfer resistances.

It is evident that Phase 1 produced the highest current and power densities (472 mA/m^2, 141.7 mW/m^2) among the three phases, resulting from a higher buffering capacity and less limitation in substrate

transport due to biomass accumulation within the cell. As a comparison to literature values, Phase 1 produced about 50% of the power of a dual-chamber flat-plate MFC designed by Min and Logan using 1 g COD/L as acetate, although their feed conditions were significantly different (0.68 hr HRT - continuous flow, 50 mM phosphate buffer, lateral serpentine flow – no biomass buildup, 0.7 mg/cm^2 Pt catalyst). [17]

4.5.2 Characteristic Analyses – pH, ORP, DO

As a measure of the properties of the reactor discharge and feed, the pH, oxidative-reduction potential (ORP) and the dissolved oxygen (DO) content were measured. One set of measurements was carried out for the feed and discharge immediately after sampling to minimize leakage of oxygen. The variation of the pH, ORP and DO over the course of Phases 1-3 are presented in Figures 4.10, 4.11 and 4.12, respectively. Shaded regions indicate the stable period of each phase, while the dotted vertical lines indicate the end of a phase. A summary of the average pH, ORP and DO in the stable period of each phase is given in Table 4.8. Recall that the criterion for stability was based on current generation only. Therefore, other parameters may exhibit more variability the current. Also note that DO measurements only began on February 5th during Phase 1 as a check against the ORP, which was high in the discharge up until that point. Lastly, it should be noted that due to the upflow flow path in the MFC, some stratification likely occurred within the reactor so that the bottom of the cell behaved more anaerobically, while the upper part of the cell behaved aerobically. Details on how stratification may have affected specific discharge properties are discussed in subsequent sections.

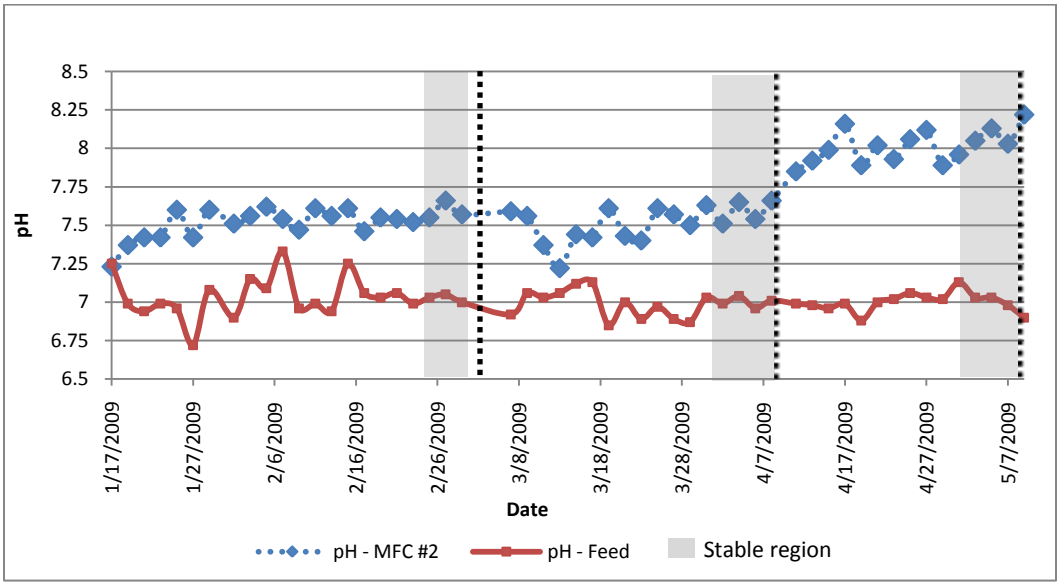

Figure 4.10 Variation of pH of the cell feed and discharge during Phases 1-3.

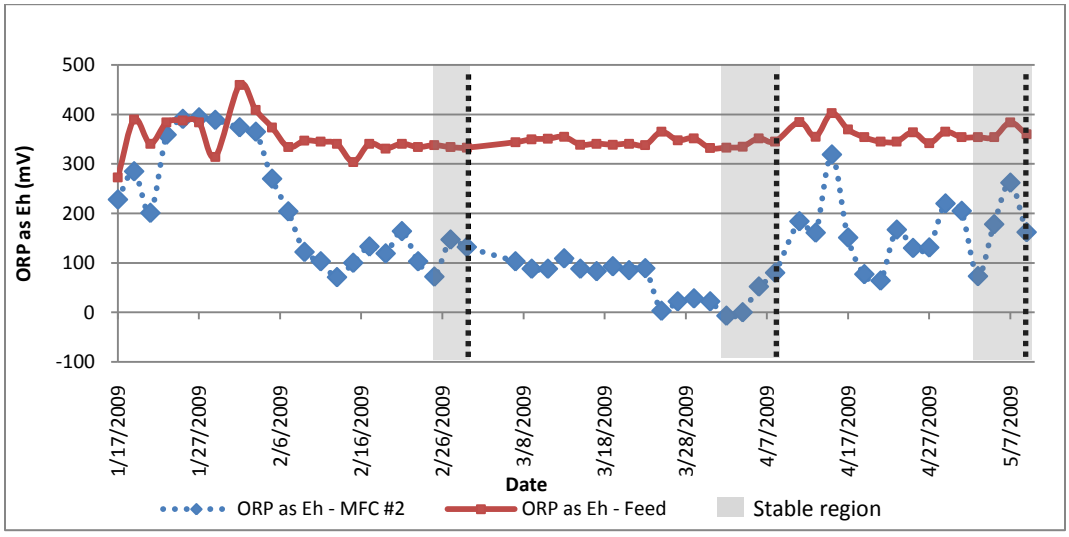

Figure 4.11 Variation of the ORP of the cell feed and discharge during Phases 1-3.

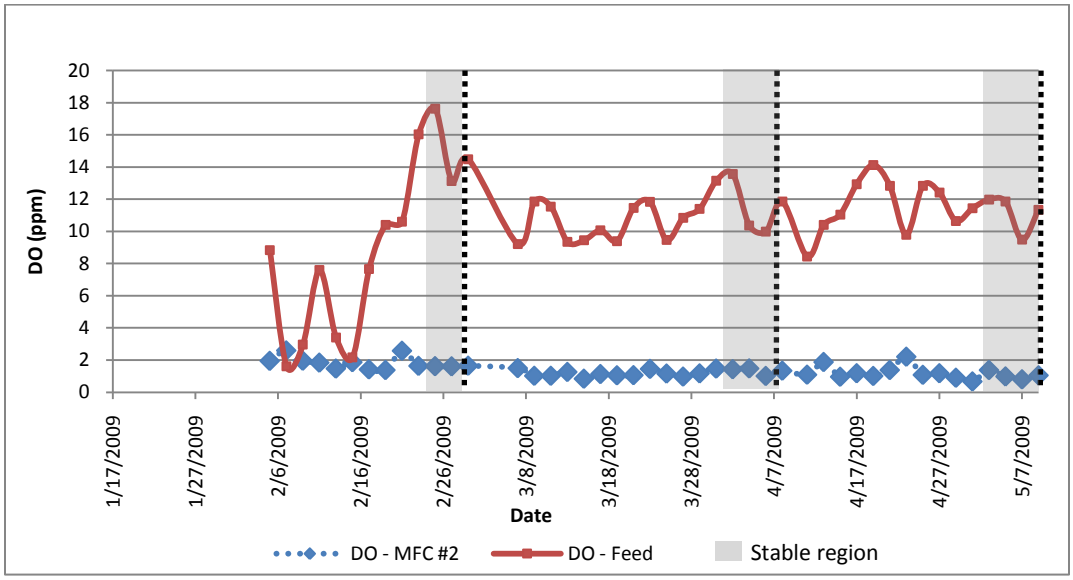

Figure 4.12 Variation of DO of the cell feed and discharge during Phases 1-3.

Table 4.8 pH, ORP, DO during Phases 1-3 once stable current was obtained.

	Phase 1		Phase 2		Phase 3	
	Feed	**Discharge**	**Feed**	**Discharge**	**Feed**	**Discharge**
pH	7.03 ± 0.05	7.59 ± 0.11	7.00 ± 0.07	7.59 ± 0.15	6.99 ± 0.12	8.11 ± 0.17
Eh (mV)	335 ± 5	117 ± 78	341 ± 17	31 ± 82	363 ± 28	169 ± 152
DO (ppm)	15.08 ± 4.53	1.63 ± 0.04	11.44 ± 3.19	1.32 ± 0.41	11.16 ± 2.26	1.05 ± 0.48

The pH of the cell discharge remained stable at 7.6 after the chiller was installed for the remainder of Phase 1 and Phase 2. Upon shifting to Phase 3, however, the pH of the discharge rapidly rose to about 8 within 2-4 days. In relation to the hypothesis postulated in sub-section 4.5.1 regarding the buildup of biomass within the cell during Phase 3 leading to lower current production, it is possible that a larger fraction of acetate removal occurred aerobically, causing even more aerobic biomass accumulation and carbon dioxide production, and therefore more bicarbonate in solution. In other MFC studies, a marked decrease in pH in the anolyte chamber during operation has been observed. [64, 65] This has been attributed mainly to the difference in concentration between protons and other cations (Mg^{2+}, Ca^{2+}, K^{+}). Since Nafion is not selective for protons alone, these other cations could occupy a large fraction of the sulfonic sites on the Nafion backbone, leaving very few active sites for proton exchange and consequently a lower pH and loss in conductivity in the anolyte over time. However, in the current study, it appears that the protons generated by acetate oxidation were rapidly removed either by transport to the cathode or reaction with bicarbonate and/or phosphate buffer. Despite these changes,

the pH range was close enough to neutrality that biological metabolism did not appear to be significantly affected.

The ORP during the start of Phase 1 was high, possibly as a result of reactor acclimation, though it appeared to stabilize after February 9th. The ORP of Phase 2 stabilized relatively quickly at a slightly lower value than Phase 1. In Phase 3, significant variability was observed throughout the run possibly due to shifts in the microbial community. It is known that an ORP above +50mV may reflect the presence of dissolved molecular oxygen which may then be consumed by aerobes or facultative anaerobes. [59] Based on DO and ORP readings from the discharge samples, it appears that slightly aerobic conditions prevailed during all three phases. Although the discharge itself appeared to be aerobic, it should be noted that some stratification of the contents within the fuel cell occurred. This was confirmed when the cell was disassembled on May 13th and significantly more biomass was found to accumulate in the bottom half of the anolyte chamber. On the other hand, the Nafion MEA appeared to have a relatively consistent biofilm thickness regardless of the height. Also, the DO measurement in the drained bulk solution after cell operation was terminated was found to be 0.19 mg/L, much lower than the 1 – 1.5 mg/L typically seen in the discharge samples drawn during cell operation. Stabilization of the DO measurement of the drained bulk solution sample required significantly longer time than a normal discharge due to the higher solids content, meaning that the true DO within the cell during operation was likely even lower than 0.19 mg/L. This may indicate stratification within the cell leading to a gradient in aerobicity (less aerobic in the lower half, aerobic in the upper half).

4.5.3 TSS/VSS Analyses

Total and volatile suspended solids analyses were conducted after homogenization and dilution. After TSS samples were dried overnight and weighed, they were placed in a muffle furnace to burn off all organics and then re-weighed for the VSS content. The variation of the TSS and VSS content during the course of Phases 1- 3 are shown in Figures 4.13 and 4.14, respectively, while a summary of the TSS and VSS values once the current had stabilized is given in Table 4.9.

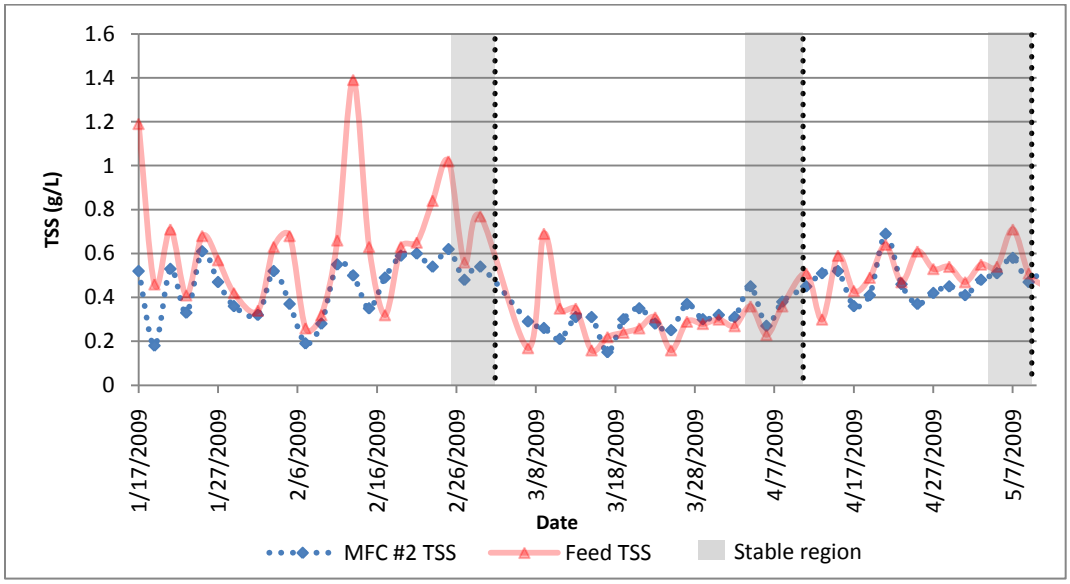

Figure 4.13 Variation of the TSS content of the cell feed and discharge during Phases 1-3

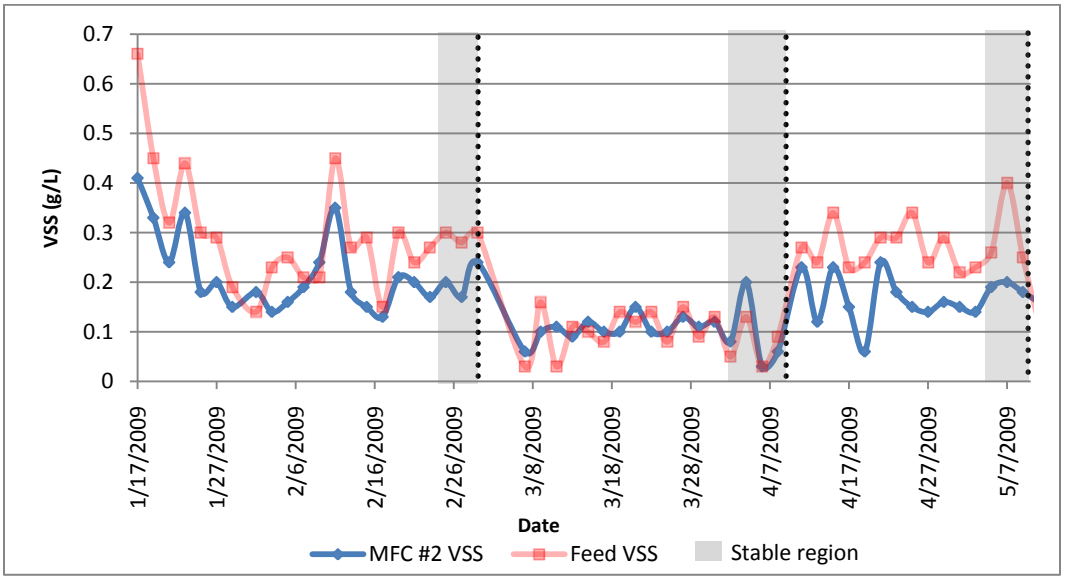

Figure 4.14 Variation of the VSS content of the cell feed and discharge during Phases 1-3

Table 4.9 TSS and VSS content during Phases 1-3 once stable current was obtained.

	Phase 1		Phase 2		Phase 3	
	Feed	**Discharge**	**Feed**	**Discharge**	**Feed**	**Discharge**
TSS (g/L)	0.78 ± 0.45	0.55 ± 0.14	0.31 ± 0.13	0.35 ± 0.16	0.58 ± 0.18	0.51 ± 0.10
VSS (g/L)	0.29 ± 0.02	0.20 ± 0.07	0.08 ± 0.09	0.09 ± 0.15	0.28 ± 0.15	0.18 ± 0.05

In all cases, little significant difference was observed between the feed TSS/VSS and the discharge TSS/VSS at a 95% confidence interval. The discharge appeared black, indicating the presence of biosolids, but the quantity as reflected by the VSS content was small. Typical biomass yields for aerobic degradation of organic compounds are reported to be about 0.40 g VSS/g COD, while anaerobic degradation of acetate to methane produces on the order of 0.05 g VSS/g COD. [66] As will be described in sub-section 4.5.5, approximately 40% of the COD removal was unaccounted for in Phase 1, 85% in Phase 2, and 60% in Phase 3. If the entire difference was due to aerobic growth, it would amount to 1.0, 1.5, and 2.2 g VSS/L for Phases 1, 2, and 3 respectively. Based on the observed VSS in the discharge, it is highly likely that biomass accumulation occurred, especially in Phase 2. This supports the hypothesis that biomass accumulation negatively affected current generation, particularly in Phase 3, where the accumulated biomass generated in Phase 2 would have significantly enhanced the removal of COD by reactions that do not generate current.

4.5.4 Methane Production

Head gas was collected in Tedlar bags and quantified by volume every 4-6 days using liquid displacement and then analyzed for methane, carbon dioxide and nitrogen/oxygen by gas chromatography. The methane generated was then converted into a COD equivalence using Equations 4.7 - 4.9. The variation of the production rate of each gas and the total during Phases 1-3 is shown in Figure 4.15, while a summary of the gas production rate during the stable periods is given in Table 4.10.

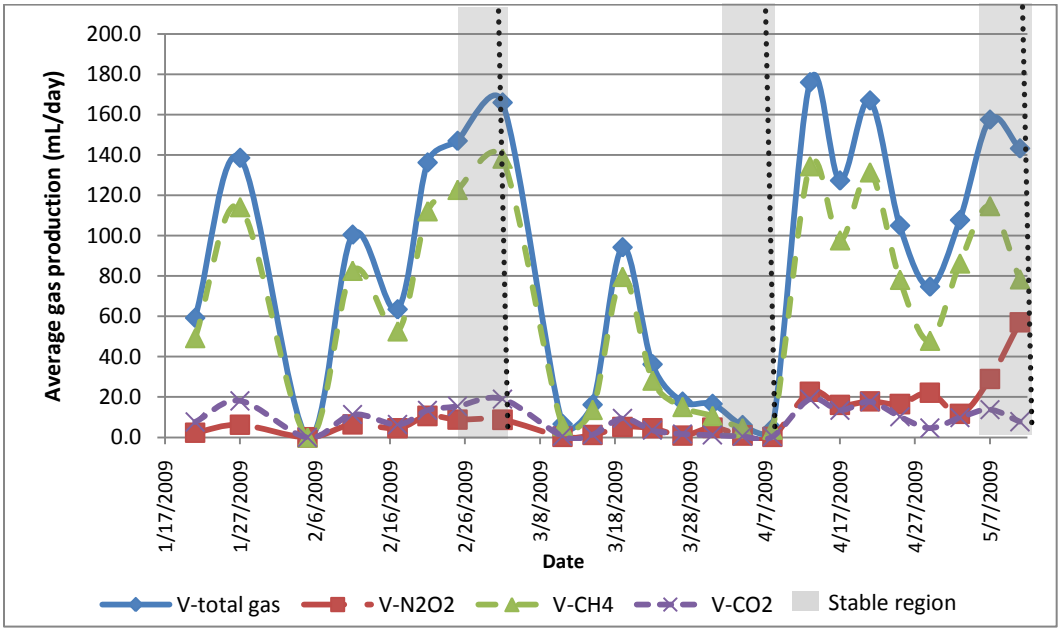

Figure 4.15 **Variation of the rate of gas production by the cell during Phases 1-3**

Table 4.10 **Rate of gas production during Phases 1-3 once stable current was obtained**

	Phase 1	Phase 2	Phase 3
Total gas (mL/day)	156.5 ± 26.3	5.3 ± 2.3	136.2 ± 25.6
CH_4 (mL/day)	130.5 ± 21.5	4.3 ± 1.0	93.2 ± 19.1
CO_2 (mL/day)	17.2 ± 5.0	0.4 ± 0.2	10.4 ± 3.0
N_2/O_2 (mL/day)	8.8 ± 0.2	0.6 ± 1.0	32.6 ± 22.9
CH_4 COD Equivalent (g COD/L-HRT)	2838.9 ± 343.7	58.4 ± 36.1	2159.6 ± 795.9

During Phase 1, gas production in MFC #2 varied significantly before the installation of the chiller on February 17th, but appeared to begin to stabilize after this change was made. Gas production dropped dramatically to near zero soon after the start of Phase 2, rose for a brief period before dropping again near the end of this phase. Gas production increased significantly upon shifting to Phase 3 and thereafter remained high. The drop in gas production in Phase 2 could have been due to two factors: wash out of methanogens and competition by other bacterial species. In anaerobic digesters, the doubling time of methanogens can be on the order of 1-9 days due to their slow growth. [67] Even in an unmixed system such as the MFC where biomass can accumulate, the HRT of 24 h during Phases 1 and 3 may be long enough for the population of methanogens in the MFC to grow significantly. On the other hand, the HRT during Phase 2 was only 12 hours and possibly not long enough for a significant amount of methanogens to be produced. Once the changeover to the longer HRT during Phase 3

occurred, however, methane production recovered almost immediately. These results also suggest that aerobic bacteria appeared to out-compete the anaerobic methanogens for the available acetate during Phase 2, but this situation quickly changed at the higher acetate concentration and HRT during Phase 3.

4.5.5 COD Analysis and Balance

Samples for total and soluble COD analyses were collected from both the feed and discharge once per sampling date. All samples were prepared in triplicate and optical density measurements were converted into COD concentrations through a calibration curve. The total COD values in the feed and discharge were used in the COD balance (Equation 4.12), while the soluble COD in the feed and discharge were used in the calculation of the coulombic efficiency (Equation 4.11). Figures 4.16 and 4.17 show the variation of the total and soluble COD levels, respectively, in the feed and discharge during Phases 1-3. The error bars display 95% confidence intervals based on the triplicate samples. Table 4.11 presents the average total and soluble COD levels over the stable periods of Phases 1-3, along with 95% confidence intervals based on the average COD on each sampling date.

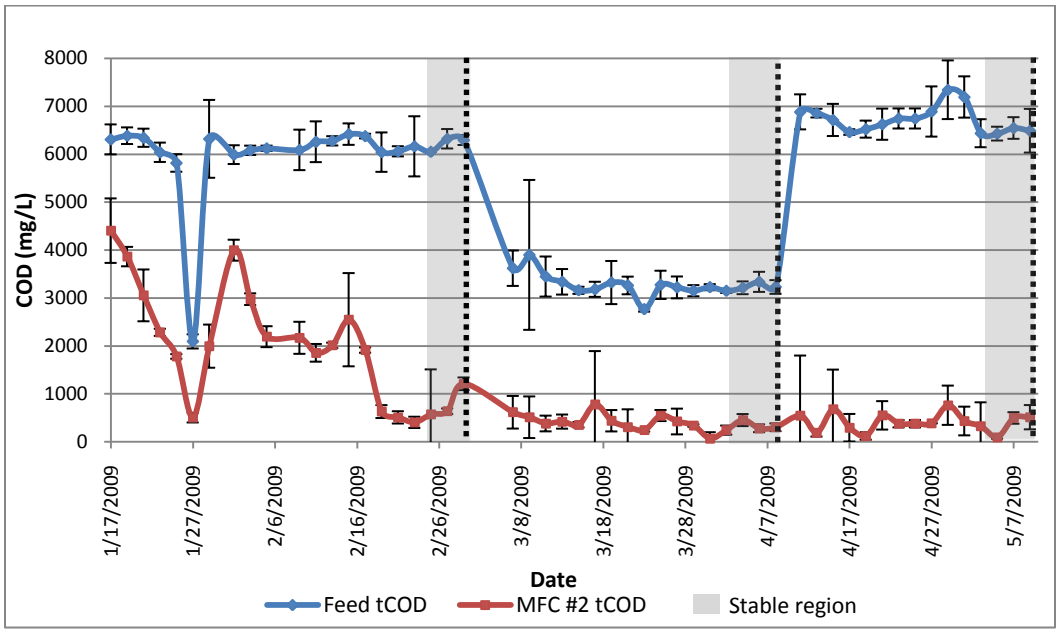

Figure 4.16 Variation of the total COD concentrations in the cell feed and discharge during Phases 1-3

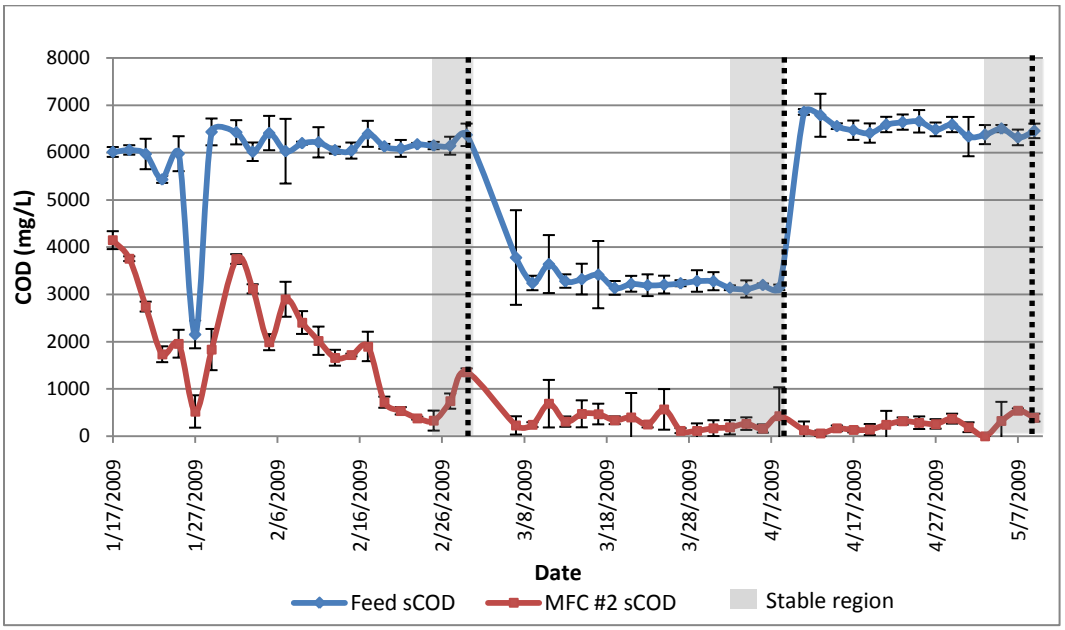

Figure 4.17 **Variation of the soluble COD concentrations in the cell feed and discharge during Phases 1-3**

Table 4.11 **Average total and soluble COD concentrations during Phases 1-3 once stable current was obtained**

	Phase 1		Phase 2		Phase 3	
	Feed	**Discharge**	**Feed**	**Discharge**	**Feed**	**Discharge**
tCOD (g/L)	6.22 ± 0.29	0.81 ± 0.68	3.23 ± 0.15	0.32 ± 0.18	6.48 ± 0.11	0.36 ± 0.38
sCOD (g/L)	6.22 ± 0.16	0.81 ± 1.00	3.15 ± 0.07	0.26 ± 0.23	6.42 ± 0.16	0.31 ± 0.44

The MFC proved to be efficient at reducing COD (as acetate), removing 87%, 91%, and 95% of incoming amount during Phases 1, 2, and 3, respectively. The difference in total and soluble COD was never significant, indicating that little solid biomass was removed from the MFC and so consequently accumulated inside the cell. The low VSS concentrations measured in the discharge supports this hypothesis as well (Table 4.9). Biomass accumulation may have also caused the soluble COD removal during Phase 3 to reach as high as 95% and current production to become substrate- limited, as reflected in the sharp drop in current over a single cycle, as discussed in sub-section 4.5.1. Also, as mentioned in sub-section 4.5.1, the half-saturation constant for acetate in an MFC is 141 mg/L. Since the measured discharge COD concentration of 310 mg/L during Phase 3 corresponds to the level in the bulk solution, the true COD concentration in contact with the active bacteria at the anode was likely lower than 310

mg/L. Given that substrate limitation occurs at bulk concentrations below 282 mg/L [62], it was likely that the MFC became at least partially nutrient-limited.

From knowledge of the soluble COD concentrations in the feed and discharge and the current generated, the coulombic efficiency during each phase was obtained using Equations 4.10 and 4.11. A summary of the coulombic efficiencies during the stable portion of each phase, along with 95% confidence intervals, is given in Table 4.12.

Table 4.12 Average coulombic efficiencies during Phases 1-3 once stable current was obtained

	COD_{Elec} (g/L)	ΔsCOD (g/L)	C_E (%)
Phase 1	0.225 ± 0.004	6.22 ± 0.16	4.24 ± 0.41
Phase 2	0.083 ± 0.001	2.89 ± 0.27	2.85 ± 0.34
Phase 3	0.168 ± 0.004	6.10 ± 0.49	2.75 ± 0.16

Regardless of the feed conditions, the coulombic efficiencies obtained in this study were extremely low. Phase 1 showed the highest coulombic efficiency (4.24% of 6.22 g sCOD/L removed), while Phase 3 yielded the lowest coulombic efficiency at 2.75% of 6.10 g sCOD/L. Clearly, most of the COD reduction in this cell did not involve current production. As a comparison, Liu and Logan achieved a coulombic efficiency of 65% (based on 1 g/L acetate feed) with their flat-plate MFC, although the overall COD removal was only 8%. [14] Shimoyama *et al*. [20] were able to obtain a coulombic efficiency of 28% (based on a 5.8 g/L model organic wastewater feed, COD removal of 93%) using a cassette-type MFC, which closely resembled a flat-plate design. Several factors may have contributed to the low coulombic efficiency. First, operation of a fed-batch reactor with non-continuous flow likely resulted in biomass buildup, creating concentration gradients between the bulk liquid and active biofilm residing near the anode. This would increase the likelihood of diffusion-limiting substrate transport to the active biofilm, resulting in lower substrate concentrations at the active biofilm and decreased current generation. Second, buildup of biomass in the system would increase the bacterial population in the reactor, thereby increasing COD removal rate in the bulk liquid and again decreasing the substrate concentration at the active biofilm. Third, oxygen diffusion from the cathode side and through the Nafion into the anolyte would lead to direct oxidation of the substrate by bacteria and free molecular oxygen in the solution without generating current.

Closing the COD balance requires measurement and/or estimation of the consumption of COD by several sinks, as described in Equation 4.12. Measurable sinks include the total discharge COD and COD consumption due to the formation of methane and current. Oxygen diffusion from the cathode side into the anolyte was estimated based on Equation 4.13 using diffusion coefficients and concentration difference described in sub-section 4.4.4. A summary of the COD removal by measureable and unmeasured sinks is given in Table 4.13, while a graphical summary of the percentage of the total COD in the feed that is removed by each measurable sink is given in Figure 4.18.

Table 4.13 COD removal by measurable and unmeasured sinks during Phases 1-3

	Phase 1	Phase 2	Phase 3
tCOD Discharge MFC (g/L)	0.805	0.319	0.356
Current generation (g/L-HRT)	0.226	0.083	0.168
Methane generation (g/L-HRT)	2.780	0.058	2.160
tCOD unmeasured (g/L-HRT)	2.413	2.771	3.792

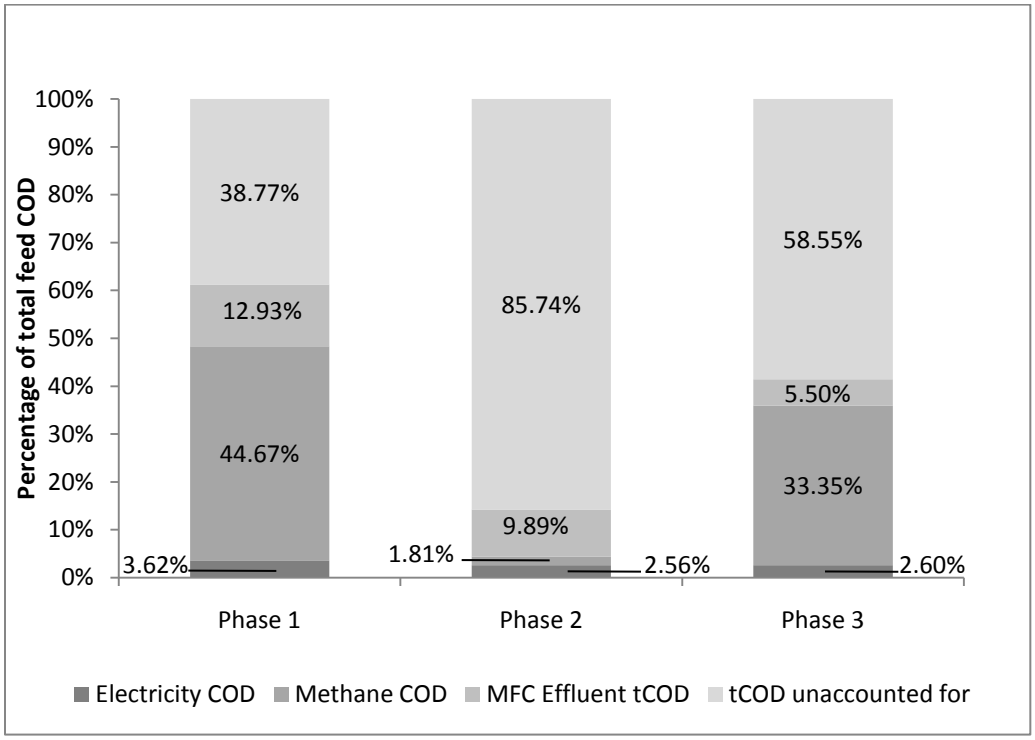

Figure 4.18 Percentage distribution of COD removal by measurable sinks during Phases 1-3

A significant portion of the COD was unmeasured in all phases, particularly Phase 2. This could be due to two possible sinks that cannot be easily measured. As stated previously, oxygen leaking into the anolyte through the Nafion membrane could react directly with the substrate to lower the soluble COD without generating current. Second, biomass that does not leave the cell and accumulates inside due to settling could also account for a significant portion of this unmeasured COD removal.

Using Equation 4.13, the oxygen flux into the anolyte is estimated from parameters obtained from the literature (see sub-section 4.4.4) and an exposed cathodic area of 80 cm^2 to be in the range from 0.51 – 3.08 g/L-day or 7.9 – 47.5% of the total COD fed to the cell. The unmeasured amount of COD removal during Phases 1, 2, and 3 were 38.8%, 85.7%, and 58.6%, respectively. Although the COD loss due to direct reaction with oxygen can account for a large portion in each case, it is likely that a combination of biomass accumulation and oxygen flux accounted for the discrepancies. As a comparison, Virdis *et al*. (2009) [40] closed a COD balance on an MFC with acetate substrate at the anode and nitrate as the terminal electron acceptor at the cathode with the following breakdown of COD removal: ~28% methane gerneration, 45.6% current production, ~22% estimated electrogenic biomass growth, ~4.4%

estimated methanogenic biomass growth. Note that since their study used nitrate as the electron acceptor and both chambers were continuously sparged with helium, no oxygen was assumed to transfer through to the anode chamber.

4.5.6 Acetate Analysis

Lastly, the acetate concentrations in the feed and discharge were determined by ion chromatography. A comparison of the soluble COD concentration determined by standard digestion techniques and the acetate concentration determined by IC and converted to a COD equivalence during Phases 1-3 is given in Figure 4.19.

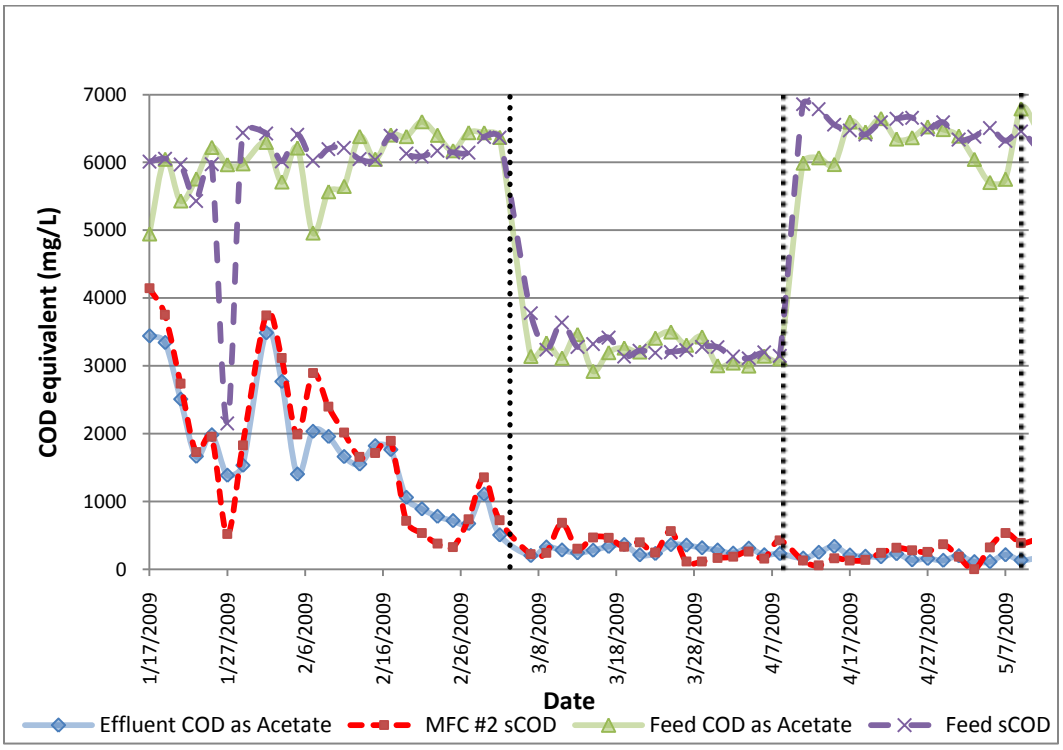

Figure 4.19 Variation of sCOD via IC and sCOD via digestion during Phases 1-3

The concentrations obtained by the two methods tracked each other closely throughout the three phases. The IC method appeared to be steadier day to day with smaller differences between samples, while the digestion method displayed more variability from day to day and between the triplicate samples collected at the same time (see Figure 4.17). Several possible reasons may account for the variability of

the digestion method. First, since digestion glass vials were repeatedly used, they may have become scratched over time. They also may not have been cleaned thoroughly, leading to some error in the optical density readings. Small variations in the volume of digestion solutions added to each sample vial may have also contributed errors. It was observed that the variations in optical density readings for triplicates were similar in magnitude whether a feed or discharge sample was being analyzed and were not proportional to the COD concentration. For example, feed samples from Phase 1 typically gave an optical density readout between 0.250 and 0.270 (arbitrary units), whereas the readings for discharge samples ranged from 0.020 to 0.040. Variations in readings between replicates were observed to be as high as 0.02 or more, accounting for up to 8% of the feed signal, but up to 50% of that of the discharge. The only difference in the handling of the replicates by the IC method was that each was contained in a separate autosampler vial. However, since each is clean and intended for single-use only, fewer measurement errors are expected. It should also be noted that other soluble compounds were detected in the IC column at retention times lower than acetate, but could not be identified as specific compounds. It is likely that these compounds were soluble microbial products such as bacterially produced polymers, lysis products and hydrolysis products. [68]

4.6 Conclusions

A microbial fuel cell with 0.2 mg/cm^2 Pt loading was successfully operated from December 12, 2008 to May 11, 2009. The feed consisted of a synthetic acetate solution supplemented with micronutrients. The cell operated as an upflow fed-batch reactor and was controlled at 0.3 V using a potentiostat. The cell was operated in three phases to observe the effects of substrate concentration and HRT. Several parameters were measured on a routine basis: cell current, wastewater anolyte variables (pH, DO, ORP, TSS/VSS, tCOD, sCOD), head gas volume and methane fraction via GC and acetate concentration via IC. From this data, current and power densities, polarization curves, coulombic efficiencies and COD balances were calculated.

Phase 1 produced the highest current and power density (472.2 ± 8.2 mA/m^2, 141.7 ± 2.4 mW/m^2), although this accounted for only 4.24 ± 0.41 % of the total soluble COD removed. The MFC proved to be an effective technique at removing soluble acetate COD from the reactor, removing 87-95% at an initial loading of 6.44 g/L-day. Little biomass was found in the discharge, as reflected by discharge

TSS and VSS measurement, as well as by the fact that tCOD and sCOD levels in the discharge were similar. This indicated that significant amounts of biomass accumulated within the cell. As a result, substrate was degraded at a faster rate, with a significant portion by reactions that did not generate current. This was particularly evident during Phase 3 when the current dropped much more rapidly within a single feed cycle than during Phase 1 despite operating under identical feed condition. In addition, upon disassembly of the cell, a thick biomass buildup was observed in the lower half of the cell. Significant amounts of methane were detected in Phases 1 and 3, accounting for 44.7% and 33.4% of the total COD removed from the feed. Much less methane was generated during Phase 2, presumably due to the shortened HRT that may have led to washout of the methanogens and/or competition by aerobic bacteria colonized on the cathode biofilm. In all phases, a significant portion of the COD removal remained unmeasured and was suspected to occur due to direct reaction with dissolved oxygen that had leaked from the cathode into the anolyte and to formation of biomass that accumulated within the cell. Lastly, sCOD concentrations obtained from measurement of the acetate concentration by IC were similar to those obtained by a standard method.

Chapter 5
Effect of Catalyst on the Performance of a Microbial Fuel Cell

A key aspect for the successful commercialization of MFCs is not only their power production, but also their materials costs. Perhaps the most significant capital cost of an air-cathode MFC is that associated with the catalyst. Platinum has traditionally been used as the catalyst in PEMFCs and earlier MFCs, although there is a growing interest in less expensive non-precious catalysts for obvious reasons. The development of such a catalyst may ultimately determine the financial viability of MFCs in the future.

This chapter describes the MFC performance obtained using the non-precious nitrogen-doped carbon composite catalyst described in Chapter 3 for oxygen reduction under the optimal feed conditions for power production determined in Chapter 4 (i.e., Phase 1). The results obtained are compared with the performance obtained previously using the platinum catalyst to investigate the effect of cathode catalyst type. The cathode MEAs for the two cells in this chapter were airbrushed with different loadings (1 and 2 mg/cm^2) of non-precious nitrogen-doped carbon composite catalyst into two MFCs (MFC #1 and #2) as a replacement for platinum. Feed conditions were chosen based on the conditions that yielded the highest power production during the experiments with the platinum catalyst (Phase 1). The MFC performance was characterized by the same electrochemical and wastewater measurements as previously used in the case of platinum.

On the basis of the same catalyst loading (mg/cm^2), both cells operating with the non-precious metal catalyst outperformed the platinum cell by producing 151% and 305% more current at 1 mg/cm^2 and 2 mg/cm^2 loading, respectively, while removing 79.6% and 92.2% of soluble COD (as acetate) from each cell, respectively. Coulombic efficiencies were also higher as a result at 6.71% and 12.18% for MFC #1 and MFC #2, respectively. It is unknown as to why the COD removal in the two cells was so different. Removal of reactor biomass in the discharge of MFC #2 seemed to have a positive effect on current production, particularly over the course of a single feed cycle, indicating that biomass removal was important to maintaining consistent current production in a MFC.

Overall, the improved performance of the cell with the non-precious catalyst showed that the potential for further application in MFCs is certainly viable. Also, the proportional increase in current generation

from MFC #1 to MFC #2 due to doubling the catalyst loading indicated that cathodic oxygen reduction was the limiting factor and that further increases in catalyst loading may increase current generation even more.

5.1 Introduction

Platinum is typically used as the cathode catalyst in air-cathode MFCs as it is considered the best known catalyst for oxygen reduction. Based on its success in PEMFCs, its use has naturally crossed over to MFCs as well. Of course, perhaps the primary disadvantage of using a platinum catalyst in any application is cost. Since MFCs to date generate lower power densities than PEMFCs, the cost of platinum (per unit power) is even more significant. Therefore, new non-precious catalysts which can produce similar power densities at a fraction of the cost of platinum are required to improve the attractiveness of MFCs as a practical method of generating power on an industrial scale. Some studies have found that non-precious cathode catalysts such as cobalt tetramethoxyphenylporphyrin (CoTMPP) and iron phthalocyanine (FePc) can achieve similar or even improved fuel performance over traditional platinum catalysts. [38, 69] These findings, albeit preliminary, clearly give promise to inexpensive non-precious catalysts being feasible alternatives to platinum.

Some new approaches to catalyst development for fuel cell applications are focused not only on shifting from precious metal catalysts, but also on incorporating nitrogen groups into the carbon support to make the support itself catalytic for oxygen reduction. [48] By doing so, significantly more surface area is made available for oxygen reduction than the traditional incorporation of metal catalyst onto the surface of a carbon support which does not participate in oxygen reduction.

This chapter focuses on the use of a novel nitrogen-doped carbon composite catalyst for cathodic oxygen reduction in two identical MFCs at different catalyst loadings: 1 mg/cm^2 (MFC #1) and 2 mg/cm^2 (MFC #2). The design of the MFCs is the same as those used in Chapter 4, except that new cathode MEAs containing the carbon composite catalyst were used in place of platinum. To provide a direct comparison against the platinum cell in Chapter 4, the cells were run at the same feed conditions that produced the highest current/power densities for the platinum catalyst (i.e., Phase 1) and their performance was characterized in terms of the same electrochemical (cell voltage, cell current) and

wastewater (pH, ORP, DO, TSS/VSS, total and soluble COD, acetate composition) measurements as in Chapter 4. The coulombic efficiency and COD balance for each cell were also calculated. A polarization curve was also obtained from MFC #2, but could not be obtained for MFC #1, as will be discussed. Conclusions based on the comparison of overall current and power densities, COD removal and COD balance are also drawn.

5.2 Materials

The materials used in this phase of experiments (Phase 4) were the same as those described in Section 4.2, except for those described in the following sub-sections.

5.2.1 Material changes – MFC construction

The stack was separated into two separate MFCs with the same physical design. These cells were operated with different loadings of the N-doped carbon composite catalyst in the cathode MEA synthesized and characterized as described in Chapter 3. MFC #1 was loaded with 1 mg/cm^2 (100 mg total) of the catalyst, while MFC #2 was loaded with 2 mg/cm^2 of the catalyst. In the shift at the end of Phase 3 from the experiments using the platinum catalyst to those using the non-precious catalyst, all cell components were either replaced or cleaned thoroughly. All Delrin and other non-conductive parts were cleaned with detergent and DI water, while the stainless steel mesh and perforated stainless steel plate were cleaned with acetone and rinsed with DI water. The anode and cathode carbon papers were replaced and new Nafion sheets were prepared using the same method described in Subsection 4.2.1. All tubing was replaced as well.

5.2.2 Material changes – Auxiliary equipment

The only addition to the auxiliary equipment was the requirement for new wiring to accommodate the additional MFC. Electrical connection to the MFC was again made using alligator clips, while electrical connection to each dedicated potentiostat was done using banana plugs.

5.2.3 Material changes – Electrical

In order to electrically isolate the two MFCs, another potentiostat (EcoChemie Autolab PGSTAT 30) was used so that each MFC could be controlled independently of the other. In this case, the new potentiostat was dedicated to MFC #1, while MFC #2 was operated using the same equipment and setup as in Phases 1-3. The cell potential in both MFCs was controlled to the same value as in Phases 1-3 (0.3 V). Also, the Autolab potentiostat for MFC #1 had built-in software capable of logging and archiving data without the need for the external eDAQ Ecorder hardware and software. MFC #2 still required the eDAQ Ecorder used previously.

Specifications for the MFC #1 potentiostat are shown in Table 5.1.

Table 5.1 Electrical Equipment Added for MFC #1

MFC #1 Potentiostat/galvanostat	Controls potential of cell at 0.3 V EcoChemie Autolab PGSTAT 30 current range: 10 nA - 2 A voltage range: ±10 V, voltage control through 4 cable sets with standard banana plugs connected to alligator clips digital USB output to lab computer remotely controlled using MUX4 module and GPES software on lab computer continuous data logging and archiving through GPES software

5.3 Experimental Design

Based on the results from Chapter 4 regarding the optimal power generation, Phase 4 was conducted with the same feed procedure and schedule as in Phase 1 (6.44 g/L COD as acetate, 24 hr HRT, 4 hrs/feed cycle). After inoculation for 5 days (May 29th, 2009 – June 3rd, 2009) with a similar mixture of wastewater as during Phase 1, the feed solution was adjusted to the acetate substrate. Cells were operated until the average daily current density varied by less than 5%. For MFC #1, stabilization occurred after 25 days (June 23rd, 2009) while MFC #2 required 35 days (July 3rd, 2009). A computer crash on June 23rd resulted in the loss of all data from MFC #1 between 1:50 pm on June 22nd and 10:06 am on June 23rd. Data were collected after the crash until June 24th and the average current appeared to be unaffected by the crash. Unfortunately, another incident on June 24th appeared to permanently reduce the current generated by MFC#1. Since the next sampling date was to be June 25th, data

collected after the crash could not be used for the COD balance and were thus excluded from the stable data set (period ending June 23rd). On June 24th at approximately 2:00 pm, the current for MFC #1 appeared to drop in half after attempts to fix a bad connection resulted in a suspected prolonged current spike. One of the clips was disconnected while the potentiostat was still active and in voltage control mode. It was suspected that the disconnection of the one clip resulted in an unsustainable current for the bacteria, leading to cell death and partial inactivation of the biofilm. Attempts to recover the current after that point failed. Data were still collected after this period, although they were not included in the stable data set reported here.

5.4 Analytical Parameters

The same analytical techniques as described in Section 4.4 were used in this phase of the experiments. No deviations with regards to the analytical measurements were made.

5.5 Results

This section describes the results obtained from both MFCs during Phase 4. The results are split into the same subsections as in Chapter 4: i) current production, ii) immediate analyses (pH, ORP, DO), iii) solids analysis– TSS/VSS, iv) methane production, v) COD measurement and COD balance, and vi) acetate concentration determination. The criterion for stability was also the same as in Phase 4 (approximately <5% variance in current production over 6 HRTs). Comparisons of these results to those from Phase 1 are made.

5.5.1 Electrochemical Performance

Similar to Phases 1-3, both MFCs during Phase 4 operated with cell potentials controlled to 0.3 V via potentiostats. Both cells were inoculated with a similar mixture of fresh aerobic and anaerobic wastewater before the feed was shifted to the synthetic feed. The feed conditions (concentration, HRT) were chosen based on the conditions which gave the highest current/power densities in Chapter 4,

which was Phase 1. A variation of the current densities from both cells during Phase 4 after shifting to the synthetic feed is given in Figure 5.1, while a plot of the variation of the power densities from both cells is given in Figure 5.2. In each graph, shaded areas for the period when stable behavior was reached are given. Note that the shaded region from June 19th to June 23rd is the stable regime for MFC #1 only, while the shaded region from June 29th – July 3rd is the stable regime for MFC #2 only. A summary of the stable current and power densities for MFCs #1 and 2 and the current/power densities from Phase 1 for comparison is presented in Table 5.2.

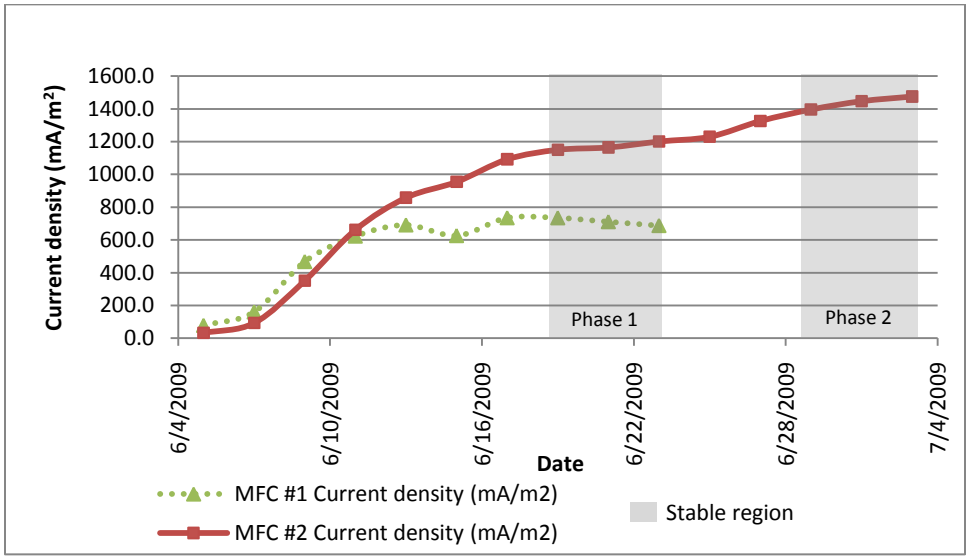

Figure 5.1 **Variation of the current densities generated by MFC #1 and MFC #2 during Phase 4**

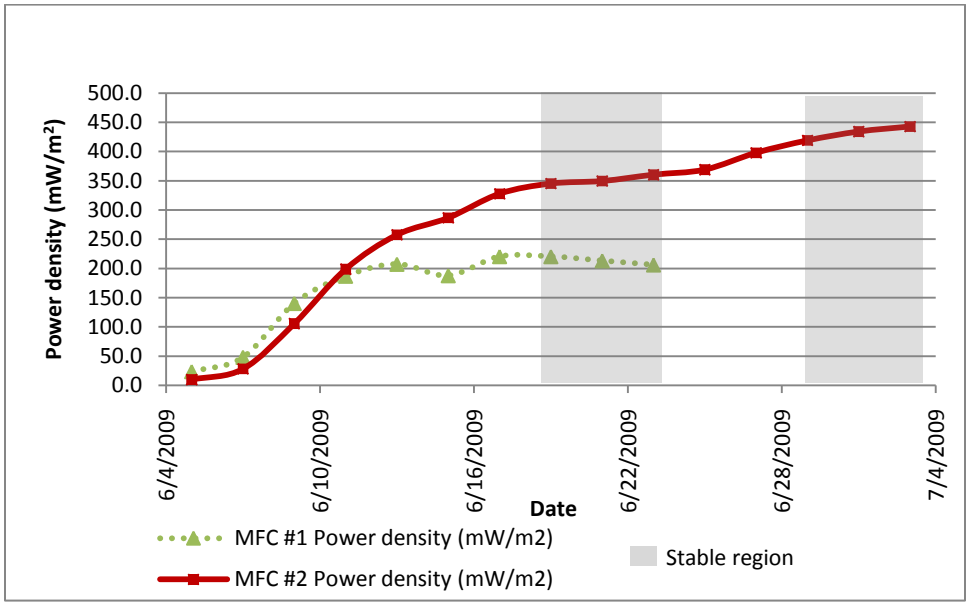

Figure 5.2 **Variation of the power densities generated by MFC #1 and MFC #2 during Phase 4**

Table 5.2 **Average current and power density generation during the stable periods of Phases 1 and 4**

	Avg current density (mA/m^2)	Avg power density (mW/m^2)	COD equivalence (mg/L-HRT)
Phase 4 – MFC # 1	710.7 ± 46.4	213.2 ± 13.9	339.4 ± 22.1
Phase 4 –MFC 2	1439.4 ± 78.7	431.8 ± 23.6	687.5 ± 37.6
Phase 1	472.2 ± 8.2	141.7 ± 2.4	225.5 ± 3.9

During the first few days with synthetic feed, MFC #1 outperformed MFC #2. After 8 days (June 11) of operation with the synthetic feed, MFC #2 began to outperform MFC #1. It is unclear why MFC #1 initially outperformed MFC #2 since its catalyst loading was lower. There may have initially been more electrogenic bacteria present in MFC #1. Also, during the first few days of operation with the synthetic feed solution, COD removal was not yet optimized, with removal of only approximately 50% of the inlet COD from each cell (3.2 g sCOD/L in cell discharge). The COD removal was not high enough for the system to become substrate-limited (K_s of acetate in an MFC application can be up to 181 mg/L). Instead, it may be that the limiting factor during the first 8 days was the extent of the build-up of the biofilm on the anode, not the catalyst loading of the cathode. This would explain the difference in current during the first few days. As the biofilm matured, its ability to pass current presumably increases and eventually it will reach a point where it outstrips the rate at which oxygen

reduction can occur at the cathode. At this point, the current generated by the MFC will reach a plateau and the overall rate becomes limited by the catalyst loading on the cathode. After June 13th, current generation by MFC #1 leveled off to an average current density of 710.7 ± 46.4 mA/m^2, indicating that the cathode catalyst loading had become rate limiting.

As for MFC #2, current continued to increase steadily through June 17th although the increase was not as pronounced from June 17th to June 25th. This was due to the decrease of the sCOD concentration in the bulk solution. The level in the cell discharge had dropped to roughly 250 mg/L close to the conditions where the anode process would become substrate-limited, assuming sCOD was comprised completely by acetate. This hypothesis was also supported by the observations of large drops in the current, with the current ranging between 7.8 – 11.9 mA towards the end of a single feed cycle. On June 25th, large increases in the solids content and total COD level were observed in the cell discharge. After this stage, the maximum current during a single cycle appeared to stabilize at 12 mA although the current at the end of the cycle only dropped to 9.5 mA at its lowest. This indicated that previous biomass accumulation did in fact enable substrate to be consumed more rapidly, but its removal alleviated limitations due to the rapid substrate consumption by processes that did not generate current. The current generated eventually reached an average current density of 1439 ± 78.7 mA/m^2.

As seen from Table 5.2, the current density from both cells using the non-precious metal catalyst exceeds the platinum cell by significant margins, an increase of 50.5% in MFC #1 and 205% in MFC #2. Another interesting observation is that the current density generated by MFC #2 was almost exactly double that by MFC #1, which exactly matches the ratio of their catalyst loadings. This is another indicator that the cathode catalyst loading was in fact the limiting factor for current generation. Since the system appears to be operating under conditions where current generation is linearly proportional to the catalyst loading, even higher current and power could presumably be generated by the MFC if the catalyst loading were increased further. From the point of view of catalyst morphology, a large portion of the surface area of the N-doped carbon catalyst nanoparticles could participate in oxygen reduction since several different types of sites may be active, such as the edge planes, defects and any remaining transition metal in the surface structure [44]. In the platinum catalyst, only the exposed surface area of the platinum particles is available for catalysis, while the carbon support has negligible oxygen reduction capability. Although platinum likely can catalyze oxygen reduction to a greater extent than

N-doped carbon when normalized with respect to the catalyst area, its overall active surface area is likely much lower than that of the N-doped carbon catalyst used in Phase 4.

As already mentioned, a polarization curve was obtained from MFC #2 only since a substantial amount of the biofilm in MFC #1 appeared to become inactivated part way through Phase 4. The polarization and power curves obtained by MFC #2 are compared to those obtained during Phase 1 in Figure 5.3. The internal resistances for Phases 1 and 4 are given in Table 5.3.

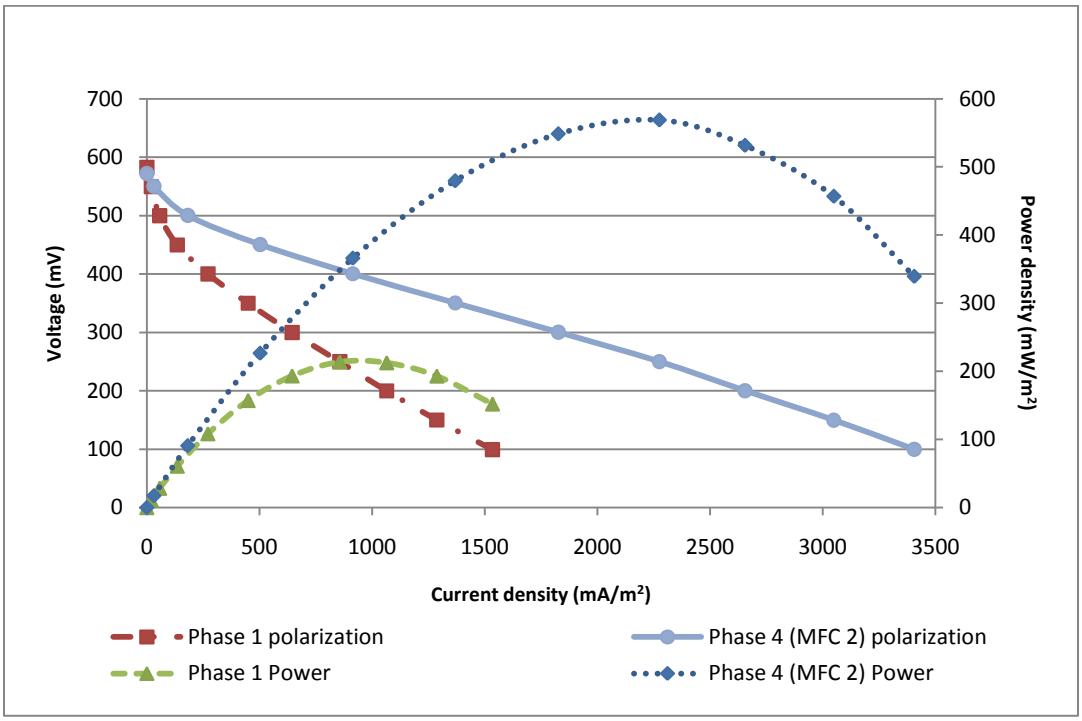

Figure 5.3 **Comparison of the polarization and power density curves generated during Phases 1 and 4 (MFC #2)**

Table 5.3 **Comparison of internal resistances obtained during Phases 1 and 4 (MFC #2)**

	Phase 1	**Phase 4**
Internal resistance (Ω)	37.4	13.7

The polarization and power curves show that MFC#2 during Phase 4 clearly outperformed Phase 1. The maximum power density achieved was 266% higher than that attained during Phase 1. The open circuit voltages were similar in the two cases (583 and 572 mV during Phases 1 and 4, respectively). From the

polarization curves for both phases, mass transfer effects did not appear to play a significant role over the range of current densities studied.

In a previous study, HaoYu *et al*. [38] compared the performances of iron and cobalt phthalocyanine (FePc and CoPc) catalysts supported on pyrolyzed carbon, pyrolyzed cobalt tetramethoxyphenylporphyrin (CoTMPP) catalyst, commercial Pt catalysts and in-house Pt catalysts. They also found that a non-precious metal catalyst (FePc) generated the highest power density. The power densities attained decreased in the following order: FePc (634 mW/m^2), in-house Pt (593 mW/m^2), CoTMPP (483 mW/m^2) and commercial Pt (474 mW/m^2).

5.5.2 Instant Analyses – pH, ORP, DO

As in Phases 1-3, pH, ORP, and DO measurements were conducted on the cell feed and discharge immediately following sampling. The variation of the pH, ORP and DO in both the feed stream and discharge from MFC #1 and #2 during Phase 4 is presented in Figures 5.4 , 5.5, and 5.6, respectively. Periods when stable behavior had been attained (i.e., June 19^{th} - 23^{rd} for MFC #1 and June 29 – July 3^{rd} for MFC #2) are denoted by the shaded regions. The average pH, ORP and DO obtained over the stable periods regime data for MFC #1, MFC #2 and Phase 1are listed in Table 5.4.

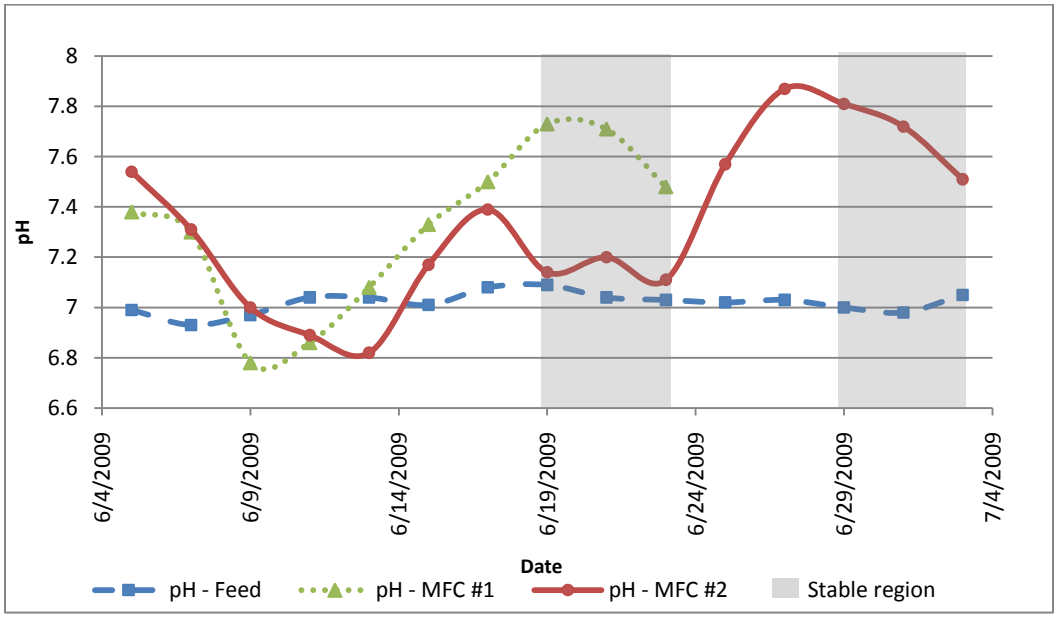

Figure 5.4 **Variation of the pH of the feed and discharge from MFC #1 and MFC #2 during Phase 4**

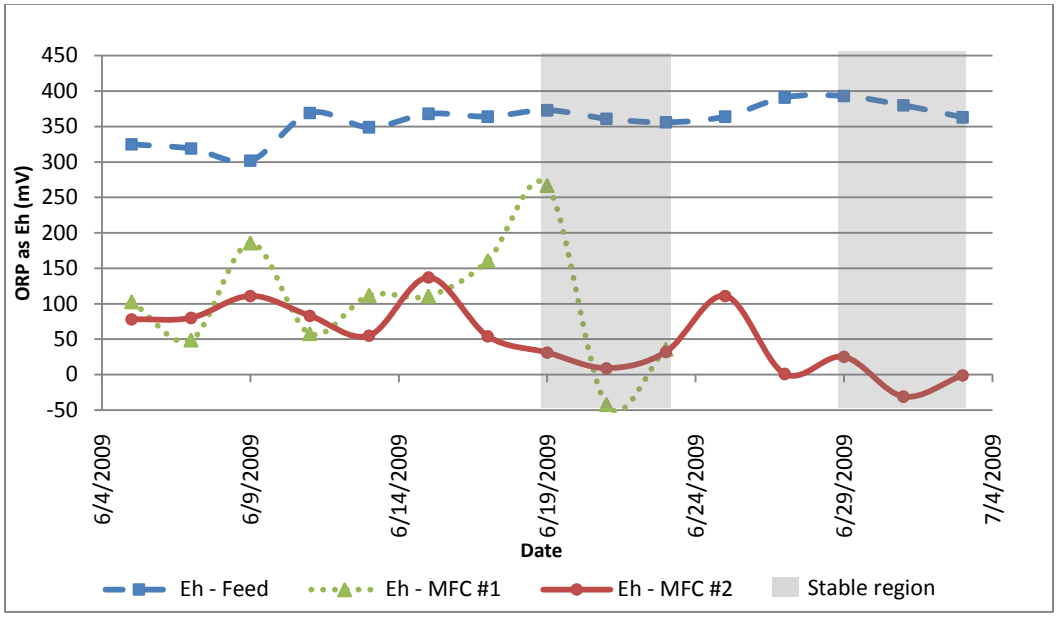

Figure 5.5 **Variation of the ORP of the feed and discharge from MFC #1 and MFC #2 during Phase 4**

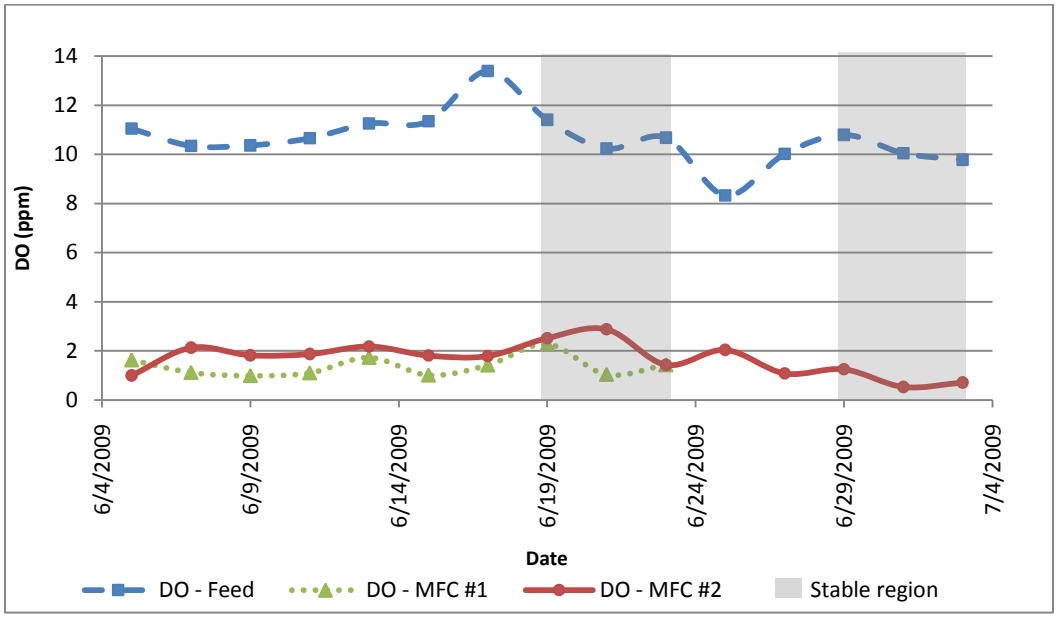

Figure 5.6 **Variation of the DO of the feed and discharge from MFC #1 and MFC #2 during Phase 4**

Table 5.4 **Average pH, ORP and DO obtained over the stable periods of Phase 4 and Phase 1**

	Phase 4 - MFC #1		Phase 4 – MFC #2		Phase 1	
	Feed	**Discharge**	**Feed**	**Discharge**	**Feed**	**Discharge**
pH	7.05 ± 0.06	7.64 ± 0.27	7.01 ± 0.07	7.68 ± 0.30	7.03 ± 0.05	7.59 ± 0.11
Eh (mV)	363 ± 17	87 ± 315	379 ± 29	-2 ± 55	335 ± 5	117 ± 78
DO (ppm)	10.78 ± 1.16	1.58 ± 1.24	10.21 ± 1.04	0.83 ± 0.73	15.08 ± 4.53	1.63 ± 0.04

Since these measurements were started once the shift to the synthetic feed solution was made, it was possible to monitor the change of these parameters during the acclimation phase. The pH of the discharge from both MFC #1 and #2 began to decrease sharply 4 days into feeding with the acetate solution and coincided with the rise in current. These changes may reflect a lag phase associated with electrogenic bacterial growth. In this event, the sharp drop in pH would likely arise from proton generation by the electrogenic oxidation of acetate and the low buffering ability of the solution since the amount of bicarbonate produced during COD removal would still be low (see Subsection 5.5.5). As the rate of COD removal rose, the pH in the discharge from both cells increased as well due to the generation of carbon dioxide and bicarbonate from methanogenic and aerobic degradation of acetate. [66] Examination of Table 5.4 shows that the pH of the cell feed and discharge once the current had stabilized were very similar during both Phase 1 and 4.

The ORP values measured during Phase 4 were more variable than the pH. The redox potential in both cells usually ranged between +50 to +180 mV during the first 2 weeks when the synthetic feed solution had been introduced. MFC #1 experienced a sharp rise in ORP to above 250 mV on June 19th, which fell within the stable period for current production. This caused the mean ORP value during the stable period to be high and the 95% confidence interval about this mean to be very large. If this point is excluded from the data set, the average ORP during the stable regime would drop to -3 ± 55 mV, which is very close to the value obtained during the stable operation of MFC #2. As previously discussed in sub-section 4.5.2, biomass accumulation in the bottom half of the cell may have created a dissolved oxygen gradient whereby the concentration near the bottom of the cell (inlet end of reactor) was very low and most of the dissolved oxygen present would be found near the topdischarge (discharge end). Thus, anaerobic degradation of acetate would be favoured near the bottom and aerobic degradation tends to occur near the top. In this case, the DO content in the discharge from both MFC #1 and MFC #2 was between 0.5 – 2 ppm. Since the ORP also is sensitive to the dissolved oxygen content [59] and significant amounts of methane were produced, it is likely that the ORP in the anaerobic region was low, perhaps in the range from -100 to -400 mV [59].

5.5.3 Solids – TSS/VSS

Solids analyses (TSS/VSS) were conducted on samples collected every 2 days in the same fashion as during Phases 1-3. The variation of TSS and VSS concentrations in the feed and discharge from MFC #1 and MFC #2 during Phase 4 is presented in Figures 5.7 and 5.8,respectively. The average TSS and VSS levels reached once the current had stabilized during Phase 4 and Phase 1 are given in Table 5.5. Of note, samples on July 3rd were discarded due to attachment of the filter paper to the filter seat, resulting in reduction of the filter paper weight. Therefore, the stable regime data for MFC #2 consisted of only the June 29th and July 1st samples.

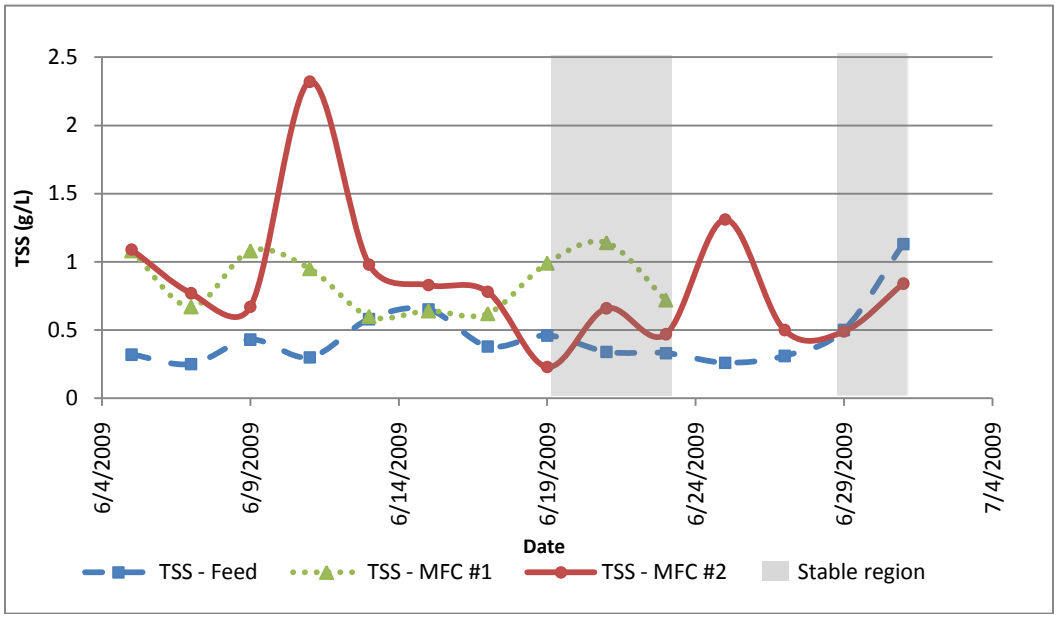

Figure 5.7 **Variation of the TSS content of the feed and discharge from MFC #1 and MFC #2 during Phase 4**

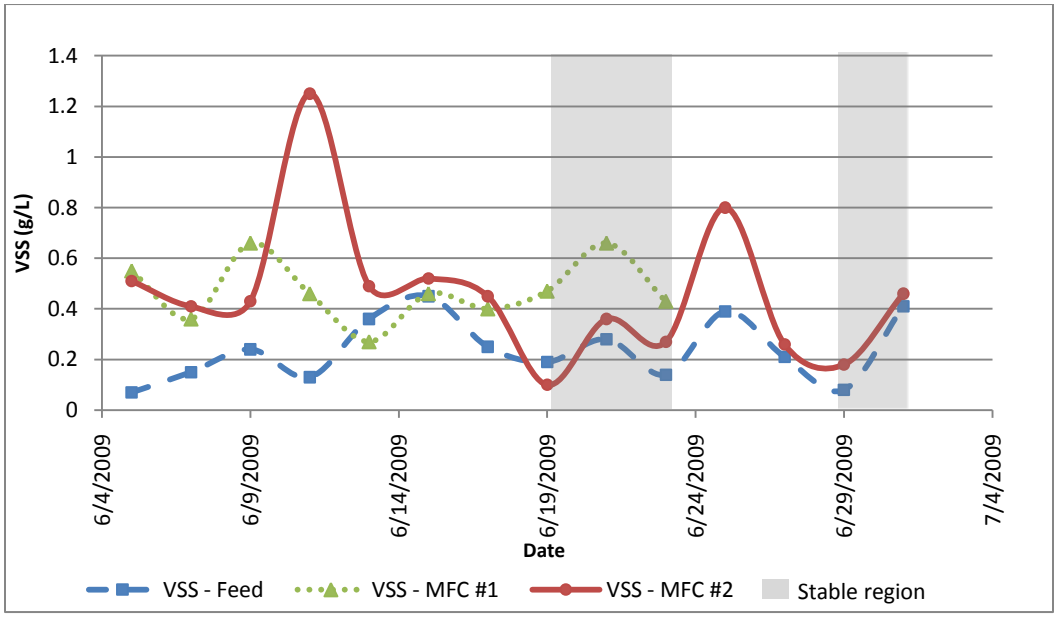

Figure 5.8 **Variation of the VSS content of the feed and discharge from MFC #1 and MFC #2 during Phase 4**

Table 5.5 Average TSS and VSS concentrations obtained over the stable periods of Phase 4 and Phase 1

	Phase 4 – MFC #1		Phase 4 – MFC #2		Phase 1	
	Feed	**Discharge**	**Feed**	**Discharge**	**Feed**	**Discharge**
TSS (g/L)	0.38 ± 0.14	0.95 ± 0.42	0.81 ± 0.87	0.67 ± 0.32	0.78 ± 0.45	0.55 ± 0.14
VSS (g/L)	0.20 ± 0.14	0.52 ± 0.24	0.25 ± 0.46	0.49 ± 0.39	0.29 ± 0.02	0.20 ± 0.07

The average solids content in the discharge streams from both cells during Phase 4 were slightly higher than in Phase 1. As mentioned in sub-section 5.5.2, a marked difference in the current from MFC #2 was observed before and after June 25th as a result of the removal of a significant portion of biomass, as reflected by the spikes in TSS (1.31 g TSS/L), VSS (0.8 g VSS/L) (see Figures 5.7 and 5.8) and the total COD in the discharge (sub-section 5.5.5) on that day. This biomass was likely a mixture of anaerobic and aerobic bacteria that had either sloughed off the cathodic biofilm or accumulated in the top half of the cell. A significant amount of biomass buildup in each cell likely occurred, as was the case during Phase 1, since the unaccounted portion of COD derived from the COD balances on each cell amounted to 34-35%. This would be equivalent to 0.9 g VSS/L biomass if the entire COD were converted aerobically. Assuming this equivalent biomass concentration to be VSS and based on the difference between the average feed and discharge VSS samples (i.e., 0.32 g VSS/L was accounted for in MFC #1, while 0.24 g VSS/L was accounted for in MFC #2), a maximum theoretical accumulations of 0.58 g VSS/L (1.45 g COD/L) in MFC #1 and 0.66 g VSS/L (1.65 g COD/L) in MFC #2 are obtained. No visual inspection of the anode and cathode of either cell was possible to confirm the extent of biomass buildup since experimental runs using the same biofilm were to be conducted after Phase 4 was completed.

5.5.4 Methane Production

Head gas samples were collected every 4 days and analyzed in a similar manner as during Phase 1-3. The only exception occurred on July 3rd when a 2-day sample for MFC #2 was collected to coincide with the end of the run. The variation in the rate of production of methane from MFC #1 and MFC #2 during Phase 4 are shown in Figures 5.9 and 5.10, respectively. The periods when current production

had stabilized are shaded in grey. The average gas generation rates reached when current had stabilized during Phase 4 and Phase 1 are listed in Table 5.6.

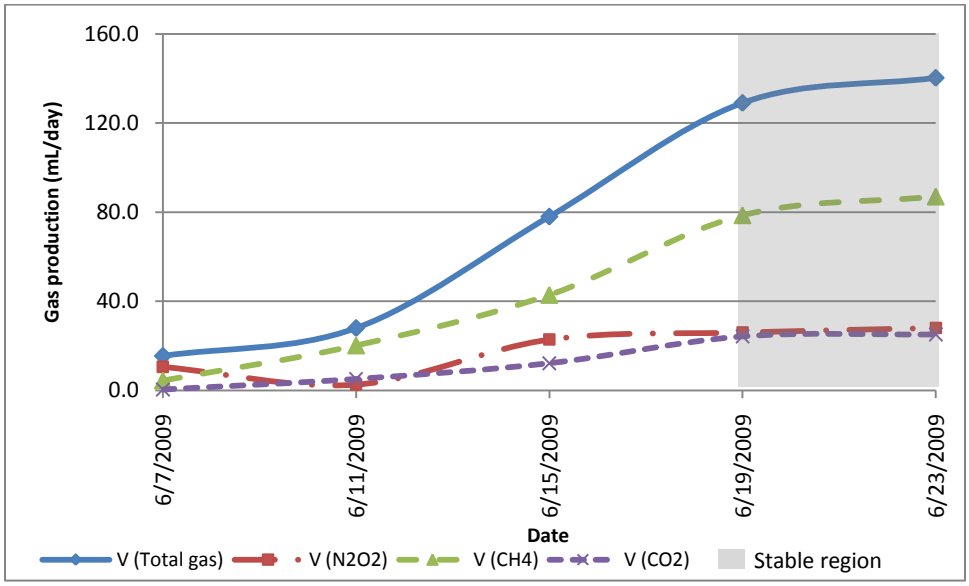

Figure 5.9 Variation of the production rate of gases from MFC #1 during Phase 4.

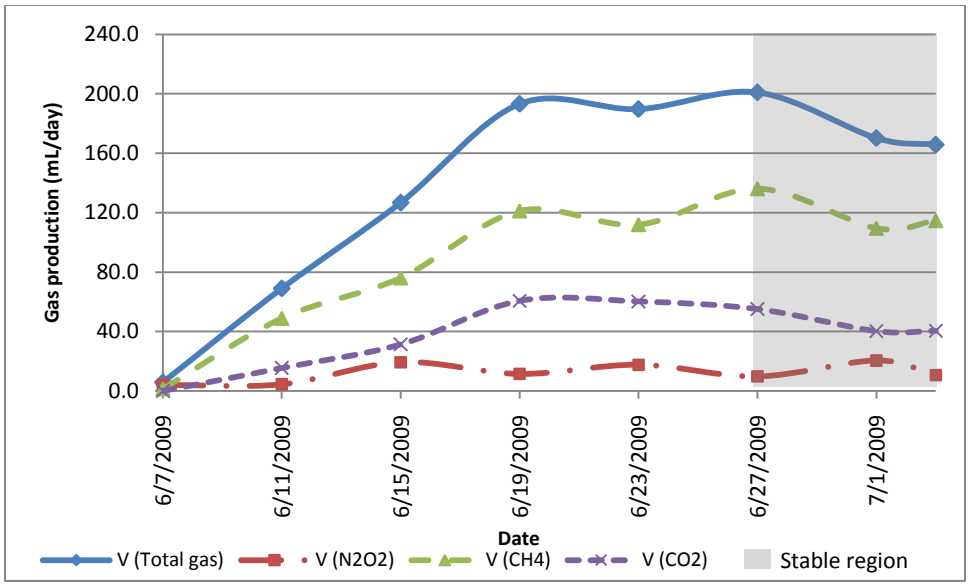

Figure 5.10 Variation of the production rate of gases from MFC #2 during Phase 4

Table 5.6 Average gas production rates obtained over the stable periods of Phase 4 and Phase 1

	Phase 4 – MFC #1	**Phase 4 – MFC #2**	**Phase 1**
Total gas (mL/day)	134.6 ± 8.0	176.8 ± 37.6	156.5 ± 26.3
CH_4 (mL/day)	82.8 ± 6.0	117.4 ± 27.7	130.5 ± 21.5
CO_2 (mL/day)	24.7 ± 0.6	44.0 ± 16.6	17.2 ± 5.0
N_2/O_2 (mL/day)	27.1 ± 1.4	15.3 ± 11.6	8.8 ± 0.2
Methane COD Equivalent (g COD/L-HRT)	1858.3 ± 204.6	2379.3 ± 101.4	2838.9 ± 343.7

The average gas production rate of 176.8 ± 37.6 mL/day from MFC #2 during the stable period was higher than from both MFC #1 and Phase 1 during the comparable period. Although the current generated by MFC #2 stabilized 8 days later than MFC #1, MFC #2 was already producing nearly 200 mL/day of gas on June 19th, the beginning of the stable region for MFC #1. A similar difference in acetate COD removal was found between MFC #1 and MFC #2 (as seen in Subsection 5.5.5). It is unclear why methane production by MFC #2 was so much higher, considering that the only difference between the two cells was the cathode catalyst loading. A study by Virdis *et al*. [39] found that a higher proportion of available COD was converted into methane at a controlled anodic potential of -200 mV than at an anodic potential of -100 mV (40.1% vs. 28.8%), while the current produced was similar. The amount of biomass produced also declined as the anodic potential became more negative. The potential at the cathode was not controlled, while the cell potential and power produced were not reported in this study. Although the cell voltage was always controlled in our study, it may have been that the anodic potential of MFC #2 was lower than that of MFC #1 so that more energy was available for growth and methane production. A separate test using a three-electrode setup to determine the anodic and cathodic potentials would provide some additional insight into this phenomenon. One would expect the VSS concentration of the discharge from MFC #2 to have been higher than that from MFC #1 to reflect increased biomass growth, although this was not always the case in the results shown in Figure 5.8. MFC #2 exhibited much more variability in the solids content from sample to sample than did MFC #1. Significant discharges of biomass in other feed cycles may have occurred when no sampling was done. It was also found that the CO_2/CH_4 ratio in both cells was much higher than in the platinum cell from Phase 1. Since methanogens can also metabolize carbon dioxide to methane, and since lower methane yields were detected compared to Phase 1, it is likely that the population of methanogens in each cell

was lower than that in Phase 1, decreasing the conversion of carbon dioxide to methane. Whether this was a product of the non-precious catalyst, differences in microbial community, or both could not be determined based on the data available.

5.5.5 COD Analysis and Balance

Samples for total and soluble COD analyses were collected from the discharge of both cells and feed stream in the same manner as in Phases 1-3. Portions of the samples for total COD measurement were added to the digestion solution on the same day. Samples for soluble COD analysis were preserved and refrigerated until one week worth of samples had been collected, at which point a portion of each was added to the digestion solution. Figure 5.11 presents the variation of total COD and Figure 5.11shows the variation in the soluble COD content in the feed stream and discharge from MFC #1 and MFC #2 during Phase 4. As before, the period when the current had stabilized for each cell as shaded in grey. A summary of the average tCOD and sCOD content over the stable period for Phases 4 and 1 is given in Table 5.7.

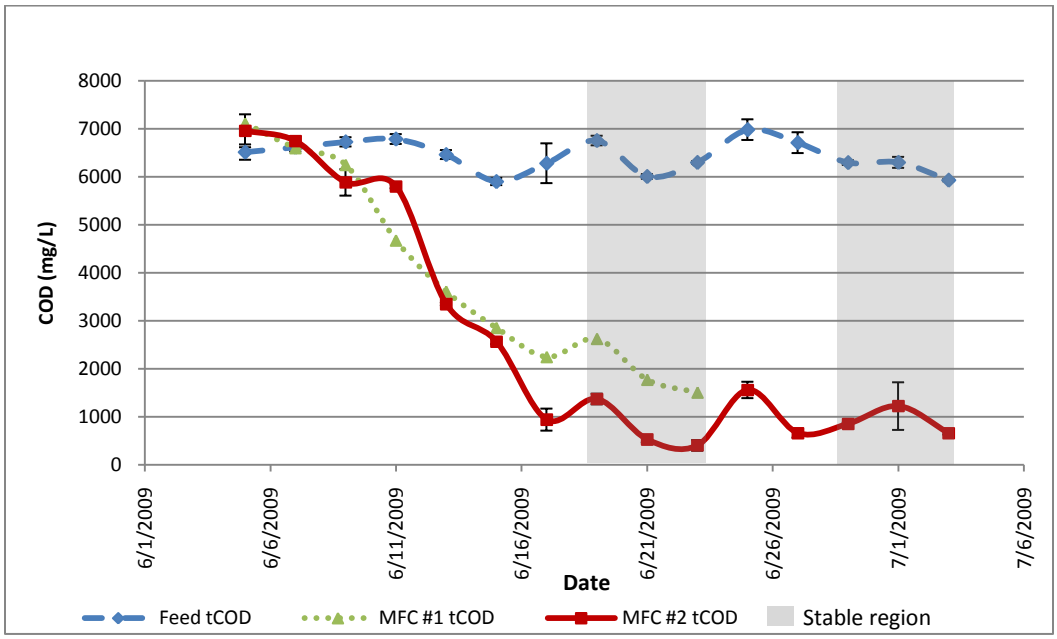

Figure 5.11 Variation of the total COD content of the feed and discharge from MFC #1 and MFC #2 during Phase 4

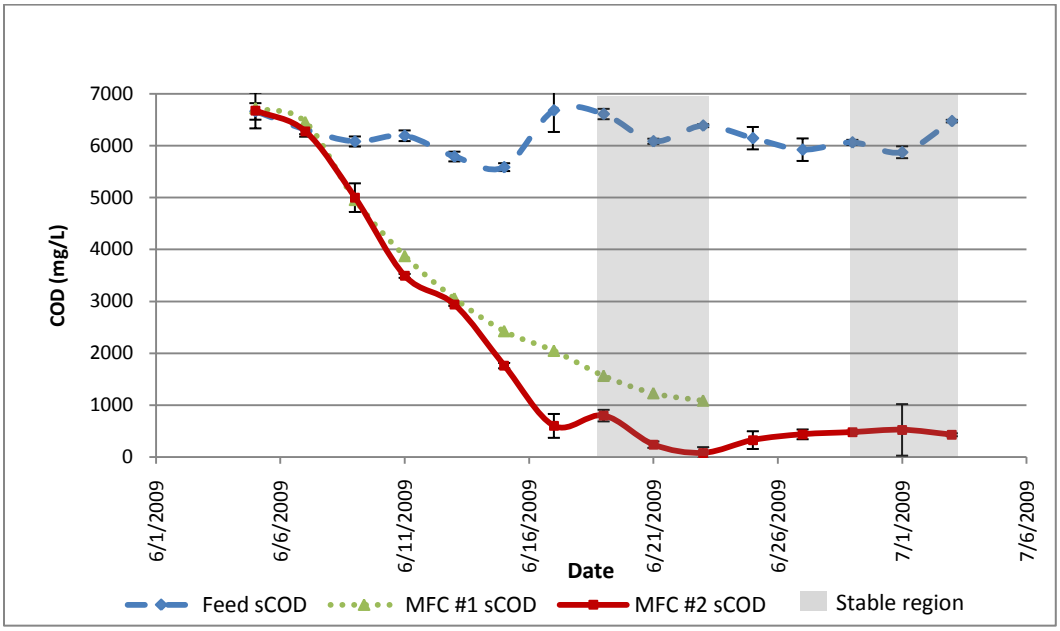

Figure 5.12 **Variation of the soluble COD content of the feed and discharge from MFC #1 and MFC #2 during Phase 4**

Table 5.7 **Average tCOD and sCOD concentrations obtained over the stable periods of Phase 4 and Phase 1**

	Phase 4 – MFC #1		Phase 4 – MFC #2		Phase 1	
	Feed	**Discharge**	**Feed**	**Discharge**	**Feed**	**Discharge**
tCOD (g/L)	6.34 ± 0.74	1.97 ± 1.15	6.18 ± 0.42	0.91 ± 0.56	6.22 ± 0.29	0.81 ± 0.68
sCOD (g/L)	6.36 ± 0.52	1.30 ± 0.48	6.14 ± 0.60	0.48 ± 0.09	6.22 ± 0.16	0.81 ± 1.00

Both cells were effective at degrading acetate from the feed, with MFC #1 removing 79.6% and MFC #2 removing 92.2% of soluble COD. Unlike Phases 1-3, there was a significant difference between the total and soluble COD concentrations in the discharge of each cell. Visual inspection of the discharge from both cells showed that they were generally darker than those produced in Phases 1-3, indicating the presence of biomass. This finding was confirmed through the TSS and VSS analyses that showed higher levels than those obtained during Phase 1. At times, large amounts of biomass were found in samples collected from MFC #2 (e.g., on June 11th and 19th), as well as smaller amounts in several samples from MFC #1. Significant amounts of biomass were likely removed at other times during Phase 4 when samples were not collected. As briefly described in sub-section 5.5.4, the discharge from MFC #1 contained significantly more total and soluble COD dischargethan did the discharge from MFC

#2, amounting to a difference of 1.06 g tCOD/L and 0.82 g sCOD/L. Although MFC #1 had been operating for less time than MFC #2 when its current production had stabilized (8 days less), a clear difference in the COD removal rate was evident as of June 17th. It is possible that the faster COD removal in MFC #2 may have been due to the anodic potential being lower in MFC #2 than MFC #1, permitting increased methane generation and biomass growth. It should be noted though that the discharge tCOD and sCOD levels in the discharge from MFC #1 were still decreasing at the end of the run. Given more time, COD removal from MFC #1 would likely have increased further.

With the soluble COD now known for the feed and discharge, the average coulombic efficiencies obtained once current production had stabilized during Phase 4 and Phase 1 could be calculated and compared as given in Table 5.8.

Table 5.8 Average coulombic efficiencies obtained over the stable periods of Phase 4 and Phase 1

	COD_{Elec} (g/L)	ΔsCOD (g/L)	C_E (%)
Phase 4 – MFC #1	0.339 ± 0.022	5.06 ± 0.44	6.71 ± 0.88
Phase 4 – MFC #2	0.688 ± 0.038	5.66 ± 0.69	12.18 ± 1.29
Phase 1	0.225 ± 0.004	6.22 ± 0.16	4.24 ± 0.41

Both MFCs exhibited improved coulombic efficiencies over that obtained Phase 1, with MFC #1 and MFC #2 attaining levels of 6.71% and 12.18%, respectively, versus 4.24% during Phase 1. Most of the difference in soluble COD removal by MFC #1 and MFC #2 was due to methane production (0.52 g/L CH_4 of 0.60 g/L total COD removal difference.

A summary of the COD sinks (based on concentration) for each cell in Phase 4 is given in Table 5.9, while a percentage breakdown is presented in Figure 5.13. Once again, examination of the COD balances shows that by far most of the COD is removed by reactions that do not generate current in both MFC #1 and MFC #2.

Table 5.9 COD removal by measured and unmeasured sinks during Phase 4 and Phase 1

	Phase 1	MFC #1	MFC # 2
tCOD discharge (g/L)	0.805	1.968	0.909
Current generation (g/L-HRT)	0.226	0.339	0.641
Methane generation (g/L-HRT)	2.780	1.858	2.379
tCOD unmeasured (g/L-HRT)	2.413	2.188	2.247

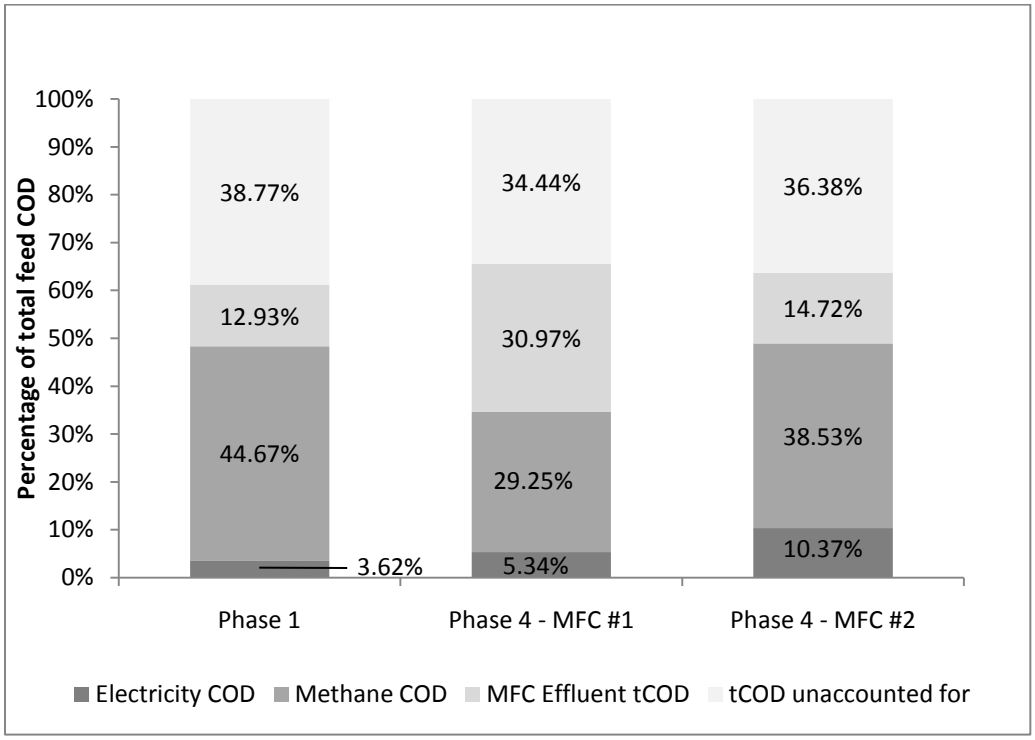

Figure 5.13 Percentage distribution of measurable COD sinks during Phase 4 and Phase 1

MFC #1 showed a lower percentage COD removal by methane generation than MFC #2 and Phase 1 due to its lower soluble COD unmeasured COD portion in both MFC #1 and MFC #2 were very similar and amounted to 34-36% of the total feed COD. This portion was also very similar to that obtained in Phase 1. The oxygen flux through the Nafion once again may have likely contributed significantly to the unmeasured COD removal, accounting for between 7.9 – 47.5% of the total feed COD, as determined by the method described in sub-section 4.5.5. A rise in the amount of oxygen penetrating into the anolyte causes biomass growth and accumulation within the cell to increase significantly.

5.5.6 Acetate Analysis

Lastly, the feed stream and discharge from MFC #1 and MFC #2 were analyzed for acetate concentration by IC as per Phases 1-3 to yield the results shown in Figure 5.14. The soluble COD as determined by the digestion method is included as a comparison.

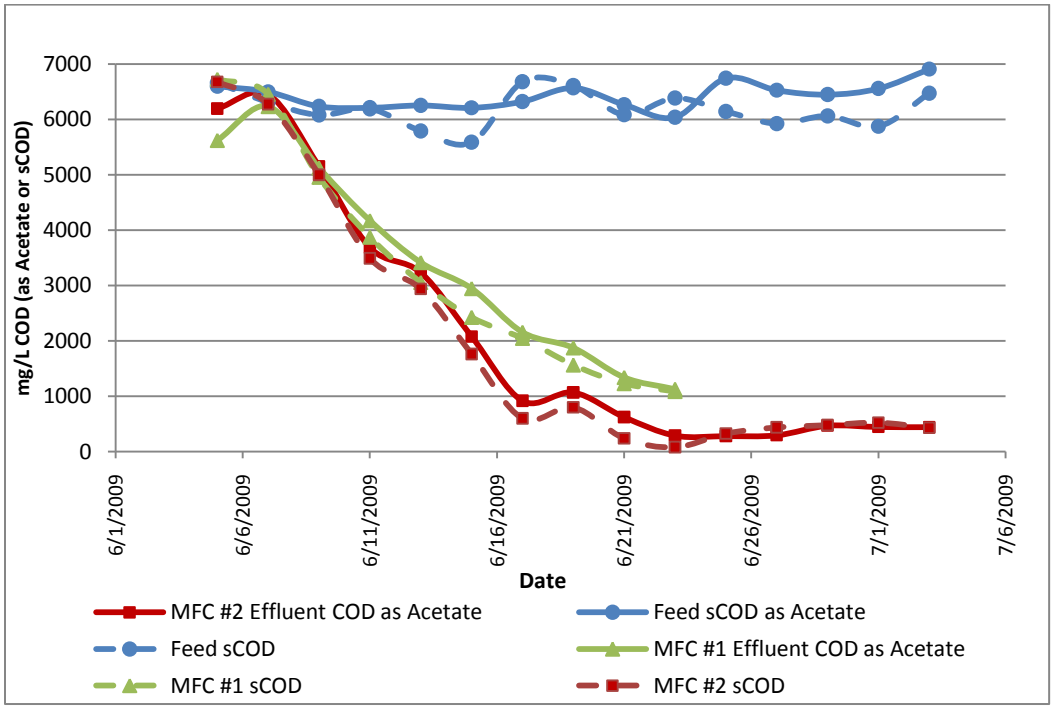

Figure 5.14 Variation of sCOD via IC and sCOD via digestion during Phase 4

The two methods showed similar trends although the IC method generally exhibited slightly higher and more stable discharge concentrations. The IC method also yielded feed concentrations that were higher than those obtained by digestion and closer to the expected 6.44 g COD/L loading level. The likely reasons for this difference were discussed in Subsection 4.5.6.

5.6 Conclusions

Two microbial fuel cells were successfully run using non-precious cathode catalysts at the feed conditions that had given the highest current production during the experiments when the platinum catalyst was used (Phase 1). The two cells were structurally the same as the cell used in the platinum tests except that the platinum catalyst was replaced with 1 mg/cm^2 and 2 mg/cm^2 of an N-doped carbon composite cathode catalyst chosen based on their oxygen reducing capability as determined in Chapter 3. Both cells were monitored for the same electrochemical and wastewater parameters as were the cells with the platinum catalyst to provide direct comparisons.

Both MFCs with non-precious metal cathode catalysts produced higher current and power densities than did those based on the platinum catalyst. MFC #1 produced an average current density of 710.7 ± 46.4 mA/m^2 and average power density of 213.2 ± 13.9 mW/m^2 when its performance had stabilized, while MFC #2 produced 1439.4 ± 78.7 mA/m^2 and 431.8 ± 23.6 mW/m2. This represented current/power increases of 151% and 305% by MFC #1 and MFC#2, respectively, over that attained during Phase 1. It was also found that the current/power produced varied proportionally to the loading of the non-precious metal catalyst, providing strong evidence that the overall MFC performance was limited by the cathodic reaction under these conditions. These results also suggested that even higher power densities could be attained if the catalyst loading on the cathode is increased further. Both cells were also effective at degrading acetate from the feed by removing 79.6% and 92.2% of soluble COD from MFC #1 and MFC #2, respectively.

Significant quantities of biomass were found in the discharge from both cells, as confirmed by TSS and VSS analyses. This led to higher total COD concentrations in the discharge compared to that obtained during Phase 1. As a result of the increased current production, higher coulombic efficiencies were also obtained during Phase 4 – 6.71 ± 0.88 % by MFC #1 and 12.18 ± 1.29 % by MFC #2 compared to 4.24 ± 0.41 % during Phase 1. Despite the increased coulombic efficiency, most of COD removal occurred by reactions that do not generate current. MFC #1, however, produced much less methane than did MFC #2 and the cell during Phase 1 due to an increased production of biomass COD.

Chapter 6
Conclusions and Recommendations

A summary and discussion of conclusions drawn from this study are presented in this section.

6.1.1 Electrical Power Generation

The N-doped catalyst prepared with ethylenediamine (EDA) as the nitrogen precursor exhibited higher catalytic activity than the catalyst prepared with polyaniline (PANI). The EDA catalyst produced a half-wave potential for the ORR of 0.57 V compared to 0.43 V for the polyaniline catalyst. However, the expected half-wave potential should have been higher at 0.65-0.70 V based on previous studies reported in the literature. SEM analysis of the EDA-based catalyst revealed a fluffy, bulbous and highly porous structure. EDAX analysis revealed the presence of 4.87 wt% O, 3.57 wt% N, 1.25 wt% Fe and 1.26 wt% Co, while XRD revealed the presence of elemental Fe and Co and possibly Fe_xCo_y
The experiments on a 0.2 mg/cm^2 platinum cathode showed that MFC operation with a longer HRT and higher feed concentration (i.e., Phase 1) generated more current and power (141.7 ± 2.4 mW/m^2) from than at a lower HRT and lower feed concentration (i.e., 104.0 ± 5.2 mW/m^2 during Phase 2). However, when the feed conditions were changed back to those of Phase 1, the original power density was not recovered. In fact, it remained virtually the same as in Phase 2 at 105.7 ± 2.7 mW/m^2. The fraction of the consumed acetate that generated current always remained low regardless of the operating conditions.

Upon replacement of the platinum catalyst with the N-doped catalyst, the current and power was found to rise significantly. With a 1.0 mg/cm^2 catalyst loading, the generated power density rose to 213.2 ± 13.9 mW/m^2, or 50.5% higher than the baseline established in Phase 1. Loading another MFC with twice the amount of the same non-precious metal catalyst caused the power to double as well to 431.8 ± 23.6 mW/m^2. This proportional increase in power density provided strong evidence that cathodic oxygen reduction was the main factor limiting current production.**OK As expected, the coulombic efficiencies in the non-precious catalyst MFCs rose in near proportion to the increase in current generation to 6.71% and 12.18% for 1.0 mg/cm^2 and 2.0 mg/cm^2 catalyst loadings, respectively.

6.1.2 Wastewater Treatment

In all operating runs, the MFCs were able to achieve high acetate removal, i.e., 87 %, 91%, and 95% during Phases 1, 2, and 3, respectively, and 79.6% and 92.2% with the 1.0 mg/cm^2 and 2.0 mg/cm^2 loadings of the non-precious catalyst. The pH of the discharge was slightly basic, varying between 7.6 and 8.2 over the course of the experiments. The ORP and DO levels indicated that dissolved oxygen was still present in the discharge. Measurements of the COD content in the solids indicated that little biomass left the reactor in all phases. This resulted in more biomass accumulation in the system and may have contributed to a low fraction of COD removal by current-generating reactions.

As discussed earlier, the coulombic efficiencies were always found to be low, peaking at 12.18% for the 2.0 mg/cm^2 non-precious catalyst loading. For all runs, oxygen leakage through the membrane from the cathode into the anolyte appeared to contribute a significant portion of COD reduction, estimated to be as high as 3.08 g/L-day, or approximately 50% of the total removal.OK It is suspected that most of this COD reduction contributed to aerobic biomass production, resulting in less COD available for current generation. Also, under the conditions of the higher HRT and acetate feed concentration, methane generation also caused a significant portion of COD removal, amounting to 30-50% of total COD removed. At the lower HRT and feed concentration, almost no methane was generated despite COD removal remaining near 90%. It was suspected that the methanogens were washed out from the cell and aerobic bacteria on the biofilm attached to the Nafion on the cathode side of the anolyte accounted for the COD removal.

6.1.3 Implications for MFC Design and Operation

The design of the MFC was a flat-plate type with baffles in the anolyte chamber. Although this cell was originally intended to be operated in downward flow mode, this configuration made it difficult to collect methane samples without creating a vacuum where the methane gas could be drawn out of the Tedlar bag. Therefore an upflow design was chosen. With this design and the non-continuous feed schedule without internal mixing, it was difficult to control of the biomass within the cell, it was not possible to visually inspect the reactor for biomass buildup. Disassembly of the cell after Phase 3 revealed a significant buildup of biomass, supporting this hypothesis, however results taken after a

replication run of the non-precious catalyst similar to the feed conditions in Phase 3 found little biomass.

The desire to obtain a COD balance also affected the way in which the MFC was operated. Operation of the cell by recycling some of the discharge stream back into the feed would have required a separate storage chamber in which some COD removal may also occur, thereby confounding the COD balance. From a power production point of view, continuous flow would shear off some of the biomass accumulated on the biofilm, particularly the portion that would have died or become inactive. Also since the generated current from fed-batch tended to decrease with time, continuous flow would likely result in a higher average current. On the other hand, continuous operation of a pump would reduce the net power produced by the cell as a whole. Clearly there must be a balance struck between operating closer to continuous flow, while minimizing pump requirements.

Some problems with regards to sampling and wastewater analysis (e.g., ORP and DO) were also incurred due to the upflow mode. Stratification of the bacteria may have occurred within the MFC, leading to an anaerobic zone near the influent and aerobic zone near the effluent, although it could not be confirmed due to the configuration of the cell. Since there was no way of obtaining a sample from the anaerobic zone, the discharge from the aerobic zone had to suffice. Although the discharge indicated the presence of dissolved oxygen, the significant amounts of methane in the off-gas also indicated anaerobic conditions.

With regards to the N-doped catalyst chosen, the ORR performance was still not as high as expected despite repeated attempts to synthesize it. However due to time constraints, we could only use the best available catalyst at that time in the cathode MEA. Approximately one month after the MFC began operating with the N-doped catalyst, another student in the fuel cell group was able to produce a catalyst with activity comparable to the best values reported in the literature values. Given more time, the improved catalyst could have been installed and better performance attained.

6.2 Recommendations

The improvements that could be made to the design and operation of the MFC can be divided into the following categories: catalyst, material and design and stacking/scale-up considerations.

6.2.1 Catalyst Improvements

The proportional rise in generated current with increase in catalyst loading suggests that still higher current can be obtained with the same catalyst by further increasing the loading level. However, it must also be kept in mind that at some point the consequent increase in catalyst layer thickness will impede oxygen transport to the point that it becomes a limiting factor. As mentioned in Subsection 6.1.3, an even more active non-precious catalyst was obtained by another student, but could not be tested in the MFC. Operation of the cell using this catalyst is also recommended.

6.2.2 Material and Design Improvements

With the difficulty encountered in attempting to obtain the highest current densities while monitoring the various modes of COD consumption, future studies should focus only on one of these two main objectives. By choosing to optimize current densities without as much concern for closing a COD balance, an MFC can easily be run with a continuous flow and a recycle stream. This configuration will promote shearing of excess biomass from the biofilm, provide some turbulence within the reactor and consequently minimize concentration gradients between the bulk phase and the active biofilm near the anode. It is still possible to operate a cell in continuous flow mode while measuring the various COD sinks although the implementation of a recycle stream may not be possible unless a second system is set up as a control.

In the MFC, baffle design combined with the upflow configuration were likely contributing factors to the accumulation of biomass in the system. Therefore, operation of the cell without baffles and in a downward flow configuration may be beneficial. Cross-flow operation, in which the feed flows normal to the anode biofilm rather than parallel to it, is also a possibility. This would help increase turbulence within the cell.

With regard to material selection, the brittle carbon paper on both the anode and cathode sides can be replaced with flexible and thicker carbon cloth. Such a cloth may help increase the surface area available for the catalyst layer on the cathode to adhere, while it will allow more area for the active

biofilm to proliferate on the anode side. With regard to the expensive Nafion membrane, recent research has examined the use of J-cloth as a replacement for proton conductivity while maintaining an oxygen transfer barrier with promising results. [70] Such a change could also be tested on the present configuration and, if successful, would also eliminate the need for hot-pressing of the cathode. In doing so, the cathode could become a detachable component that could be replaced more easily at a lower cost than the Nafion MEA. To reduce the oxygen diffusion through the cathode into the anolyte chamber, two methods can be applied. More than one J-cloth layer could be applied to replace the Nafion membrane or the outward facing side of the cathode could be sprayed with four gas diffusion layers containing Teflon to improve water retention while reducing excess oxygen flux through the Nafion, as discussed in the literature review.

One other technique that has not been explored is the synthesis of a catalyzed carbon cloth in the same fashion as the catalyzed carbon black powder. The transition metals and ethylenediamine would be adsorbed directly into the carbon cloth itself, pyrolyzed and then acid-treated to yield the final product. Since carbon cloth is more durable than carbon paper, it would more likely withstand the catalyst synthesis process. Hot-pressing of the catalyst to a Nafion layer is not necessary in an MFC, unlike the situation with a PEMFC. Therefore, the catalyzed carbon cloth can have a layer of the catalyzed carbon black sprayed on and then hot-pressed.

6.2.3 Stacking and Scale-Up

The present flat-plate cell configuration was chosen since it is compatible with the stackable design used in PEMFCs. In theory, this design can be stackable, however a distributor and flow channels for the air to reach all the cathodes would be required in between the anolyte chambers but the distance between the anode and cathode would have to be kept to a minimum to minimize ohmic overpotentials. It may be possible to create support frames between adjacent cathodes which are hollow and are exposed on the top and bottom, allowing air to travel cross-flow across the cathode. A fan placed underneath the stack can provide flow as shown in Figure 6.1.

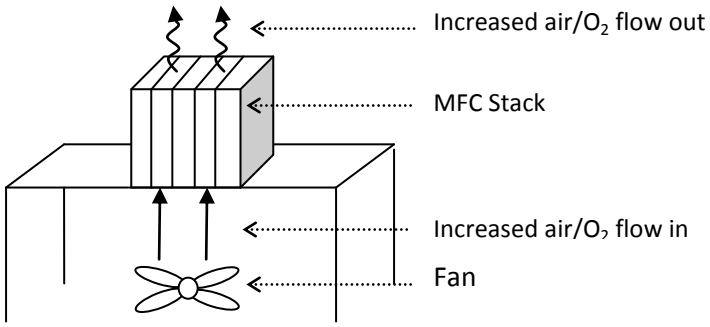

Figure 6.1 MFC Stack with fan installed underneath

A similar design could also be immersible into a wastewater tank although instead of an exposed cathode, the anode would be entirely exposed to wastewater while the catholyte chamber would be sealed except for air vents. This design was implemented by Shimoyama et al. [20], as described in the literature review. One drawback they observed was that the power produced by the stack amounted to only 63% of the sum of the individual cell power densities. Research into the cause of this phenomenon is warranted as well.

References

1. Sterlicchi, J. "Obama's Stimulus Bill Green Lights Green Spending", Accessed September 21st, 2009, from http://www.businessgreen.com/business-green/news/2236575/obama-stimulus-bill-green.

2. Rabaey, K., K. van de Sompel, L. Maignien, N. Boon, P. Aelterman, P. Clauwaert, L. de Schamphelaire, H.T. Pham, J. Vermeulen, M. Verhaege, P. Lens, and W. Verstraete., "Microbial Fuel Cells for Sulfide Removal". Environmental Science & Technology, 2006, 40, pp. 5218-5244.

3. Virdis, B., K. Rabaey, Z. Yuan, and J. Keller,"Microbial Fuel Cells for Simultaneous Carbon and Nitrogen Removal"., Water Research, 2008, pp. 3013-3024.

4. Bullen, R. A.,T.C. Arnot, J.B. Lakeman, and F.C. Walsh,., "Biofuel Cells and Their Development". Biosensors and Bioelectronics, 2006, 21, pp. 2015-2045.

5. Ramasamy, R. P., Z. Ren, M.M. Mench, and J.M. Regan,., "Impact of Initial Biofilm Growth on the Anode Impedance of Microbial Fuel Cells", Biotechnology and Bioengineering, 2008, 101 (1), pp. 101-108.

6. Pichoreanu, C. I.M. Head, K.P. Katuri, M.C.M. van Loosdrecht, K. Scott, "A Computational Model for Biofilm-based Microbial Fuel Cells", Water Research, 2007, 41, pp. 2921-2940.

7. Oh, S., B. Min, and B.E. Logan, "Cathode Performance as a Factor in Electricity Generation in Microbial Fuel Cells", Environmental Science and Technology, 2004, 38, pp. 4900-4904.

8. Rozendal, R.A., H.V.M. Hamelers, and C.J.N. Buisman, "Effects of Membrane Cation Transport on pH and Microbial Fuel Cell Performance", Environmental Science and Technology, 2006, 40, pp. 5206-5211.

9. Min, B., O.B. Román, and I. Angelidaki, "Importance of Temperature and Anodic Medium Composition on Microbial Fuel Cell (MFC) Performance", Biotechnology Letters, 2008, 30, pp. 1213-1218.

10. Fan, Y., H. Hu, and H. Liu,, "Sustainable Power Generation in Microbial Fuel Cells Using Bicarbonate Buffer and Proton Transfer Mechanisms", Environmental Science and Technology, 2007, 41, pp. 8154-8158.

1. Marcus, A.K., C.I. Torres, and B.E. Rittmann, "Conduction-Based Modeling of the Biofilm Anode of a Microbial Fuel Cell", Biotechnology and Bioengineering, 2007, 98 (6), pp. 1171-1182.

2. Cheng, S., H. Liu, and B.E. Logan, "Power Densities Using Different Cathode Catalysts (Pt and CoTMPP) and Polymer Binders (Nafion and PTFE) in Single Chamber Microbial Fuel Cells", Environmental Science and Technology, 2006, 40, pp. 364-369.

3. Dentel, S.K., B. Strogen, and P. Chiu, "Direct generation of electricity from sludges and other liquid wastes", Water Science and Technology, 2004, 50 (9), pp. 161-168.

4. Liu, H., R. Ramnarayanan, and B.E. Logan, "Production of Electricity during Wastewater Treatment Using a Single Chamber Microbial Fuel Cell", Environmental Science and Technology, 2004, 38, pp. 2281-2285.

5. Feng, Y., X. Wang, B.E. Logan, and H. Lee, "Brewery Wastewater Treatment Using Air-Cathode Microbial Fuel Cells", Applied Microbiology and Biotechnology, 2008, 78, pp. 873-880.

6. Lu, N., S-G. Zhou, L. Zhuang, J-T. Zhang, and J-R., Ni, "Electricity Generation from Starch Processing Wastewater Using Microbial Fuel Cells", Biochemical Engineering Journal, 2009, 43, pp. 246-251.

7. Min, B. and B.E. Logan, “Continuous Electricity Generation from Domestic Wastewater and Organic Substrates in a Flat Plate Microbial Fuel Cell”, Environmental Science and Technology, 2004, 38, pp. 5809-5814.

8. Catal, T., K. Li, H. Bermek, and H. Liu, “Electricity Production from Twelve Monosaccharides Using Microbial Fuel Cells”, Journal of Power Sources, 2008, 175, pp. 196-200.

9. Lee, H-S., P. Parameswaran, A. Kato-Marcus, C.I. Torres, B.E. Rittmann, “Evaluation of Energy-conversion Efficiencies in Microbial Fuel Cells (MFCs) Utilizing Fermentable and Non-fermentable Substrates”, Water Research, 2008, 42, pp. 1510-1510.

20. Shimoyama, T. et al., “Electricity Generation from Model Organic Wastewater in a Cassette-Electrode Microbial Fuel Cell”, Applied Microbiology and Biotechnology, 2008, 80, pp. 325-330.

2. Spellman, F.R., “Mathematics Manual for Water and Wastewater Treatment Plant Operators”, 2004, CBC Press, Boca Roca, FL, pp. 305.

22. Virdis, B., K. Rabaey, Z. Yuan, and J. Keller, “Microbial Fuel Cells for Simultaneous Carbon and Nitrogen Removal”, Water Research, 2008, 42, pp. 3013-3024.

23. Liang, P. X. Huang, M-Z. Fan, X-X. Cao, and C. Wang,, “Composition and Distribution of Internal Resistance in Three Types of Microbial Fuel Cells”, Applied Microbiology and Biotechnology, 2007, 77, pp. 551-558.

24. Beaumont, V. “Investigation of Microbial Fuel Cell Performance and Microbial Community Dynamics During Acclimation and Carbon Source Pulse Tests”, Unpublished Master’s Thesis, 2007, University of Waterloo, Waterloo, Ontario, Canada.

25. You, S., Q. Zhao, J. Zhang, J. Jiang, and S. Zhao,, “A Microbial Fuel Cell Using Permanganate as the Cathodic Electron Acceptor”, Journal of Power Sources, 2006, 162, pp. 1409-1415.

26. Ringeisen, B.R., E. Henderson, P.K. Wu, J. Pietron, R. Ray, B. Little, J.C. Biffinger, and J.M Jones-Meehan,, “High Power Density from a Miniature Microbial Fuel Cell Using Shewanella oneidensis DSP10”, Environmental Science and Technology, 2006, 40, pp. 2629-2634.

27. Liu, H. and B.E. Logan, “Electricity Generation Using an Air-Cathode Single Chamber Microbial Fuel Cell in the Presence and Absence of a Proton Exchange Membrane”, Environmental Science and Technology, 2004, 38, pp. 4040-4046.

28. Fan, Y., H. Hu, and H. Liu., “Enhanced Coulombic Efficiency and Power Density of Air-cathode Microbial Fuel Cells with an Improved Cell Configuration”, Journal of Power Sources, 2007, 171, pp. 348-354.

29. Aelterman, P. et al., “Continuous Electricity Generation at High Voltages and Currents Using Stacked Microbial Fuel Cells”, Environmental Science & Technology, 2006, 40, pp. 3388-3394.

30. Srinivasan, S., “Fuel Cells: From Fundamentals to Applications”, 2006, Springer Science + Business Media, New York, NY, pp. 240.

31. Vasquez, L.O., “Fuel Cell Research Trends”, 2008, Nova Science Publishers, New York, NY, pp. 405.

32. Ahmad, Z., “Principles of Corrosion Engineering and Corrosion Control”, 2006, Butterworth-Heinermann, Oxford, UK, pp. 74.

33. Zhang, J., “PEM Fuel Cell Electrocatalysts and Catalyst Layers: Fundamentals and Applications”, 2008, Springer-Verlag London Ltd., London, UK, pp. 92.** no page**

34. Paulus, U.A., T.J. Schmidt, H.A. Gasteiger, and R.J. Behm, “Oxygen Reduction on a High-Surface Area Pt/Vulcan Carbon Catalyst: A Thin-Film Rotating Ring-Disk Electrode Study”, Journal of Electroanalytical Chemistry, 2001, 495, pp. 134-145.

35. Basu, S., “Recent Trends in Fuel Cell Science and Technology”, 2007, Springer, New York, NY, pp. 12-23.

36. Leimin, X., L. Shijun, Y. Lijun, and L. Zhenxing, “Investigation of a Novel Catalyst Coated Membrane Method to Prepare Low-Platinum-Loading Membrane Electrode Assemblies for PEMFCs”, Fuel Cells, 2009, 9 (2), pp. 101-105.

37. Garland, N. and J. Marcinkoski, “Fuel Cell System Cost – 2008”, 2008, DOE Hydrogen Program Record, Department of Energy, USA.

38. HaoYu, E., S. Cheng, K. Scott, and B. Logan, “Microbial Fuel Cell Performance with Non-Pt Catalysts”, Journal of Power Sources, 2007, 171, pp. 275-281.

39. Shao, Y., G. Yin, J. Wang, Y. Gao, and P. Shi, “In Situ Deposition of Highly Dispersed Pt Nanoparticles on Carbon Black Electrode for Oxygen Reduction”, Journal of the Electrochemical Society, 2006, 153 (7), pp. A1261-A1265.

40. Jahnke, H., M. Schonbron, and G. Zimmerman, “Organic Dyestuffs as Catalysts in Fuel Cells”, Topics in Current Chemistry, 1976, 61(133), pp. 133-181.

41. Faubert, G., G. Lalande, R. Côté, D. Guay, J.P. Dodelet, L.T. Weng, P. Bertrand, and G. Dénès, “Heat-Treated Iron and Cobalt Tetraphenylporphyrins Adsorbed on Carbon Black: Physical Characterization and Catalytic Properties of These Materials for the Reduction of Oxygen in Polymer Electrolyte Fuel Cells”, Electrochimica, Acta., 1996, 41 (10), pp. 1689-1701.

42. Lalande, G., R. Côté, G. Tamizhmani, D. Guay, J.P. Dodelet, L. Dignard-Bailey, L.T. Weng, and P. Bertrand, “Physical, Chemical and Electrochemical Characterization of Heat-Treated Tetracarboxylic Cobalt Phtyhalocyanine Adsorbed on Carbon Black as Electrocatalyst for Oxygen Reduction in Polymer Electrolyte Fuel Cells”, Electrochimica Acta., 1995, 40 (16), pp. 2635-2646.

43. Weng, L.T., P. Bertrand, G. Lalande, D. Guay, J.P. Dodolet, “Surface Characterization by Time-of-Flight SIMS of a Catalyst for Oxygen Electroreduction: Pyrolyzed Cobalt Phthalycyanine-on-Carbon Black”, Applied Surface Science, 1995, 84, pp. 9-21.

44. Niwa, H., K. Horiba, Y. Harada, M. Oshima, T. Ikeda, K Terakura, J. Ozaki, and S. Miyata, “X-ray Absorption Analysis of Nitrogen Contribution to Oxygen Reduction Reaction in Carbon Alloy Cathode Catalysts for Polymer Electrolyte Fuel Cells”, Journal of Power Sources, 2009, 187, pp. 93-97.

45. Jaouen, F., S. Marcotte, J-P. Dodelet, and G. Lindbergh, “Oxygen Reduction Catalysts for Polymer Electrolyte Fuel Cells from the Pyrolysis of Iron Acetate Adsorbed on Various Carbon Supports”, Journal of Physical Chemistry B, 2003, 107, pp. 1376-1386.

46. Sirk, A.H.C., S.A. Campbell, and V.I. Birss, “Oxygen Reduction by Sol Derived [Co, N, C, O]-Based Catalysts for Use in Proton Exchange Membrane Fuel Cells, Electrochemical and Solid State Letters, 2005, 8 (2), pp. A104-A107.

47. Yeager, E. “Electrocatalysts for O_2 Reduction”, Electrochimica Acta, 1984, 29 (11), pp. 1527-1537.

48. Nallathambi, V., J-W. Lee, S.P. Kumaraguru, G. Wu, B.N. Popov, “Development of High Performance Carbon Composite Catalyst for Oxygen Reduction Reaction in PEM Proton Exchange Membrane Fuel Cells”, Journal of Power Sources, 2008, 183, pp. 34-42.

49. Zoski, C.G. “Handbook of Electrochemistry”, 2007, Elsevier Science, Amsterdam, Holland, pp. 451.

50. Goldstein, J., D.E. Newbury, P. Echlin, D.C. Joy, C.E. Lyman, E. Lifshin, and L. Sawyer, “Scanning Electron Microscopy and X-Ray Microanalysis”, 2003, Plenum Publishers, New York, NY, pp. 1.

51. Chung, F.H., D.K. Smith, “Industrial Applications of X-Ray Diffraction”, 1999, CRC Press, New York, NY, pp. 5.

52. Kelsall, R.W., I.W. Hamley, and M. Geoghegan, “Nanoscale Science and Technology”, 2005, John Wiley & Sons, Weinheim, Germany, pp. 108.

53. Thomas, F.G. and G. Henze, “Introduction to Voltammetric Analysis: Theory and Practice”, 2001, CSIRO Publishing, Collingwood, pp. 23.

54. Wang, J. “Analytical Electrochemistry”, John Wiley and Sons, New York, NY, pp. 113.

55. “2009 Hydrogen Program and Vehicle Technologies Annual Merit Review - Non-Precious Metal Catalysts”, 2009, Los Alamos National Laboratory, slide 1.

56. Kim, B.H., I.S. Chang, and G.M. Gadd, “Challenges in Microbial Fuel Cell Development and Operation”, Applied Microbiology and Biotechnology, 2007, 76, pp. 485-494.

57. Mohan, S.V., R. Saravanan, S.V. Raghavulu, G. Mohanakrishna, and P.N. Sarma,, “Bioelectricity Production from Wastewater Treatment in Dual Chambered Microbial Fuel Cell (MFC) Using Selectively Enriched Mixed Microflora: Effect of Catholyte”, Bioresource Technology, 2008, 99, pp. 596-603.

58. Torres, C.I., A.K. Marcus, and B.E. Rittmann, “Proton Transport Inside the Biofilm Limits Electrical Current Generation by Anode-Respiring Bacteria”, Biotechnology and Bioengineering, 2008, 100 (5), pp. 872-881.

59. Gerardi, M.H. “The Microbiology of Anaerobic Digesters”, 2003, Wiley, Somerset, NJ, pp. 13-25.

60. Logan, B.E. “Microbial Fuel Cells”, 2008, John Wiley & Sons, Hoboken, NJ, pp. 47.

61. Haug, A.T., and R.E. White, “Oxygen Diffusion Coefficient and Solubility in a New Proton Exchange Membrane”, Journal of The Electrochemical Society, 2000, 147 (3), pp. 980-983.

62. Liu, H., S. Cheng, and B.E. Logan, “Production of Electricity from Acetate or Butyrate Using a Single-Chamber Microbial Fuel Cell”, Environmental Science & Technology, 2005, 39, pp. 658 – 662.

63. Esteve-Nunez A, M. Rothermich, M. Sharma, D. Lovley, “Growth of Geobacter sulfurreducens under nutrient-limiting conditions in continuous culture”, Environmental Microbiology, 2005, 7, pp. 641–648.

64. Clauwaert, P, D. van der Ha, N. Boon, K. Verbeken, M. Verhaege, K. Rabaey, and W. Verstraete, “Open Air Biocathode Enables Effective Electricity Generation with Microbial Fuel Cells”, Environmental Science & Technology, 2007, 41, pp. 7564 – 7569.

65. Rozendal, R.A., H.V.M. Hamelers, and C.J.N. Buisman, "Effects of Membrane Cation Transport on pH and Microbial Fuel Cell Performance", Environmental Science & Technology, 2006, 40, pp. 5206-5211.

66. Tchobanoglous, G., F.L. Burton, and D.H. Stensel, Metcalf & Eddy, "Wastewater Engineering: Treatment and Reuse", 2003, McGraw- Hill, Boston, MA, pp. 567-580.

67. Wise, D.L. "Bioprocessing and Biotreatment of Coal", 1990, CRC Press, New York, NY, Pp. 341.

68. Laspidou, C.S. and B.E. Rittmann, "A Unified Theory for Extracellular Polymeric Substances, Soluble Microbial Products, and Active and Inert Biomass", Water Research, 2002, 36, pp. 2711- 2720.

69. Cheng, S., H. Liu, and B.E. Logan, "Power Densities Using Different Cathode Catalysts (Pt and CoTMPP) and Polymer Binders (Nafion and PTFE) in Single Chamber Microbial Fuel Cells, Environmental Science and Technology, 2006, 40, pp. 364 – 369.

70. Fan, Y., H. Hu, and H. Liu, "Enhanced Coulombic Efficiency and Power Density of Air-Cathode Microbial Fuel Cells with an Improved Cell Configuration", Journal of Power Sources, 2007, 171, pp. 348-354.

Appendices

Appendix A
Abbreviations

Table A.1 Abbreviations

COD	Chemical Oxygen Demand
DCMFC	Dual-Chamber Microbial Fuel Cell
DO	Dissolved Oxygen
EDA	Ethylenediamine
EDAX	Energy-Dispersive X-Ray Spectroscopy
GC	Gas Chromatography
HRT	Hydraulic Residence Time
IC	Ion Chromatography
MEA	Membrane Electrode Assembly
MFC	Microbial Fuel Cell
ORP	Oxidative-Reductive Potential
ORR	Oxygen Reduction Reaction
PANI	Polyaniline
PEMFC	Proton Exchange Membrane Fuel Cell
SCMFC	Single-Chamber Microbial Fuel Cell
SEM	Scanning Electron Microscope
TSS	Total Suspended Solids
VSS	Volatile Suspended Solids
XRD	X-Ray Diffraction

Appendix B

Synthesis and Characterization Procedures

1. Polyaniline-based Catalyst Synthesis Procedure

Carbon black preparation

- Treat 10g of carbon black (CB) in 500mL of concentrated (6M) HCl solution to remove metal impurities present on the carbon.
- Wash the HCl-treated CB with DI-water and then air-dry.
- Immerse CB in 250mL of 70% HNO_3 solution at 80C° for 8 hours in order to introduce carboxyl groups onto the carbon surface.
- Wash functionalized CB with DI water and then dry.

Polymerization & Complex Formation

- Dissolve 1g of CB in approximately 200ml of 1M HCl solution.
- Dissolve 1 mL of aniline into the CB/HCl solution.
- Mix two solutions while stirring and then leave for 30 min.
- Add 0.613g of APS into 1M HCl, then add the solution drop-wise (one every 4-5 seconds) into CB/aniline mixture while constant stirring to oxidize the absorbed aniline species and form carbon radicals to initiate polymerization.
- Stir the solution for 1 hour at room temperature.
- Filter the sample (this may take >1 hour for a 1g CB sample) and then rinse residue with water.
- Add filtered solids into a flask, add 20-30 mL water and sonicate for 1-2 min.
- Add 0.845g of cobalt acetate with the PANI in 50 mL ethanol to form a complex with polyaniline coated onto CB; stir mixture.
- Bring solution to a boil, cover loosely and keep boiling for 1 hour.
- Filter the sample and rinse residue with water.
- Place filtered solids on an aluminum tray and leave to dry in an oven at 40-50ºC overnight.

2. Ethylenediamine-based Catalyst Synthesis Procedure

- Dissolve 1.0 g of untreated CB in 250 mL ethanol by sonicating for 30 min and then stirring for 1-2 hrs.
- At the same time, COMPLETELY dissolve 0.25 g of $Co(NO_3)_2$ and $FeSO_4$ into 250 mL of EtOH. It is essential that this solution be completely dissolved before adding to CB.
- Combine CB and metal solution and stir for a minimum of30 min
- Dissolve 4 mL EDA into 20 mL of EtOH
- Add EDA solution drop-wise to the stirred CB-metal solution and then cover the flask loosely
- Raise mixture temperature to 80ºC and stir for 30 min
- With temperature maintained at 80ºC on a hot plate, remove cover and allow the ethanol to evaporate almost completely. Once the ethanol has almost completely evaporated, remove mixture from the hot plate and place in oven (40-50ºC) overnight to completely dry.
- Grind sample with mortar and pestle
- Pyrolyze @ 850-900ºC for 1 hr as per pyrolysis procedure
- Grind sample again with mortar and pestle
- Acid treat using 100 mL of 0.5 M H_2SO_4
- Filter sample through glass fiber filter and rinse residue with DI water until pH is 6-7. Use pH paper to check
- Transfer solids onto aluminum dish and let dry overnight
- Grind sample again with mortar and pestle
- Place sample batch into an airtight 20 mL vial and store in a cool, dry place.

3. Pyrolysis procedure (Ar)

- **Ensure that all samples to be pyrolyzed are ground beforehand**
- Open window to outside in DWE 2533 and place exhaust gas tube through to the outside
- Carefully unseal process tube from end caps
- Place sample inside process tube using rod and move to middle of tube
- Seal both ends of process tube using glass end caps
- Plug in both N_2 and Ar gas flow controllers; display should stabilize at 100 mL/min within 1 min
- Close N_2 gas line via the following steps:
    - turn N_2 gas cylinder tank valve clockwise until tight
    - turn N_2 gas cylinder regulator coarse and fine adjustment knobs in "closed" direction
    - turn N_2 valves upstream and downstream of the gas flow controller clockwise
    - verify that N_2 gas line is closed by reading N_2 gas flow controller
- Open Ar gas line via the following steps:
    - turn Ar gas cylinder tank valve fully counter-clockwise
    - turn Ar gas cylinder regulator coarse and fine adjustment knobs in "open" direction
    - turn Ar valves downstream of the gas flow controller fully counter-clockwise
    - verify that Ar gas line is open by reading Ar gas flow controller and by checking organic capture flask for bubbles

      **Note that Ar gas flow controller reading must be divided by 1.45 to attain true Ar flow rate (i.e. 100 mL/min displayed flow = 100/1.45 = 68.96 mL/min true flow)
- Allow 20 min for purge with Ar prior to operating furnace. Operation of furnace with any O_2 still present will cause oxidation of the catalyst and significant gas production and possibly burst gas seals
- Set mini-mite furnace program for 1 hr ramp up to 900ºC, 1 hr hold @ 900ºC and then furnace shutdown.
- Pyrolyze sample for 1 hr at 900ºC.
- After pyrolysis, allow purge with Ar gas for an additional 15 min. Open the furnace lid to allow for quicker cooldown.
- Close Ar gas line using same procedure for closing the N_2 gas line and allow furnace to cool for 1 hr.

- After cooled, take pyrolyzed sample out of boat and put into a 20 mL jar.
- When ready, transfer the sample to a 250 mL flask and add 100 mL of 0.5 M H_2SO_4 while stirring.
- Place the flask sealed a rubber stopper into fume hood and boil for more than 4 hours and top with DI water as necessary
- Filter the sample, rinse with water and dry overnight in an oven at 50ºC.

Appendix C

Sampling and Solution Preparation Procedures

1. Sampling Procedure

SAMPLE AS CLOSE TO THE BEGINNING OF NEXT FEED CYCLE, 30 MINUTES MAXIMUM TIME!!

- Switch the pump into manual mode:
  - Switch the pump to off mode (flick the switch one notch up)
  - Press the manual button on the digital timer until 'ON' mode is operative (one press).
  - After the "Cycle" light on the remote timer has turned off, switch the pump back to feed mode (switch in the direction of the checkmark)

- For the discharge samples, label the following (w/ removable tape):
  - two 40 mL vials with a generic "1" or "2".
  - two 40 mL vials with "1a" and "2a".
  - two 40 mL vials with the following nomenclature: Date, MFC #, Sample type. (i.e. Se25-1-S for September 25th, MFC #1, Soluble sample)

- For the feed sample, label (w/ removable tape):
  - one 40 mL vial with "F",
  - one 40 mL vial with "Fa",
  - one 40 mL vial with the following nomenclature: Date, 'F', Sample type. (i.e. Se25-F-S for September 25th, Feed, Soluble sample)

**At this point, if the Tedlar bag is to be removed for sampling, follow procedure 5. If not, follow procedure 6.

Exchange of Tedlar bags and sampling Tedlar bag volumes

- Take 2 emptied Tedlar bags and record empty volumes as follows:
  - Fill a 500 mL graduated cylinder with DI water up to the 400 mL mark and note the water volume.
  - Fully immerse one of the empty Tedlar bags and record the volume difference. Using a piece of masking tape, label the bag with the MFC #, the collection period (beginning date and end date) and the empty volume.
  - Repeat the previous two steps for the 2nd bag.
  - To properly remove a filled Tedlar bag from the MFC, seal the bag by extending the nipple valve and turning it clockwise about ¼ turn (the dot on the nipple should line up with the lines on the neck).

- Crimp the gas line by using a C-clamp on the flex tubing.
- Use a ratchet to loosen the hose clamp and remove the bag.
- Replace the old bag with a new one and tighten the hose clamp.
- Check the seal by gently pulling on the flex tubing with one hand and the nipple with the other. The connection should be snug.
- Uncrimp the gas line and open the Tedlar bag by unlocking the valve (turn ¼ turn counter-clockwise) and shortening the nipple (should be 1 cm long when in the open position).
- Repeat procedure for the 2nd bag.
- To measure gas volume collected in bag, fill a 2000 mL graduated cylinder to 1200 mL with DI water. Record initial volume.
- Remove masking tape label from the bag. Push bag into the cylinder and use the blunt end of a sampling spoon to ensure it is completely immersed. **Be sure to not use anything sharp as it will pierce the bag.** Record the volume difference.
- Repeat procedure for the 2nd bag.
- Take filled bags down to CPH 1324 for GC analysis.

- Seal the Tedlar bags by extending its nipple valves (the long position is the "CLOSED" position). This is crucial to prevent gas loss from the bags during sampling.
- Crimp the flex tubes leading to the waste jar with C-clamps and remove C-clamps from the sample ports.

Collection of Discharge Samples

- Place sample vial 1 under MFC #1 sample port with the tube touching the bottom of the vial and sample vial 2 under MFC #2 sample port with the tube touching the bottom of the vial.
- Place a small beaker underneath both sample ports.
- Press the 'reset' button to manually activate the pump. Collect any residual discharge into the waste beaker.
- Immediately after the residual discharge has been emptied, put the sample vials underneath the appropriate sampling port and collect samples. **Since the pump is still operative during this transition, the exchange must be fast.**
- Often, only about 5 mL can be collected with each pump cycle. After the first cycle is completed, press the reset button again and collect more sample. The total amount of sample collected should reach to at least the 3rd barcode line on the sample vial (i.e., ~ 15 mL). Once this amount has been obtained, immediately shut off the pump by putting the pump switch to "Off" (as in step 2a).

- Immediately take DO and ORP readings for both samples according to *bi-daily analysis* procedure.
- Reapply the C-clamps on the sample port, then remove the waste jar C-clamps to allow for proper discharge of discharge.

- Turn pump back on by shifting to the checkmark.
- Open the Tedlar bags by shortening the nipple valves. This will put the bags into the "OPEN" position.
- Close the incubator.

Collection of Feed Sample:

- Open the rubber stopper covering the bottle.
- Take the syringe and feed tubing and insert into the bottom of the bottle; then raise it about 1 cm from the bottom to ensure that no settled iron precipitates are collected.
- Extract about 20 mL of feed and empty into the feed sample vial.

- Check the datalogger to ensure that the current readings are not oscillating. If they are, open the circuit for the affected MFC using the potentiostat, check the connections carefully and set potentiostat back into controlled voltage mode. After sampling has been completed, check again to ensure no oscillation is occurring. If oscillations occur, repeat this step and wait 15 min to ensure signal has restabilized.

2. Solution Preparation Procedures

40x concentrated mineral solution preparation

- To prepare a 40x mineral solution, add about 900 mL DI water to 1 L volumetric flask.
- Place a funnel on top of the flask.
- Bring the minerals to the weighing balance.
- Turn on balance and wait for number display to appear.
- Place weighing paper on balance and press "Tare" to zero the scale.
- Measure out the appropriate mass of minerals as shown in Table C.1.

Table C.1: Mineral mass concentrations for 40x stock solution (based on 6.44 g/L COD loading)

Compound	Mass (g/L)
$MgCl_2*6H_2O$	25.76
$CoCl_2$	2.147
$ZnSO_4$	1.168
$CuSO_4$	1.069
$CaCl_2$	0.4293
$MnCl_2*4H_2O$	2.024

- Once the appropriate amount of mineral has been weighed, add it into the flask and tap the weighing paper to ensure that all the mineral has been added.
- Repeat procedure for the remaining minerals.
- After the last addition, use a squirt bottle of DI water to wash any remaining solids in the funnel into the flask.
- Remove the funnel and use the DI water bottle to wash any remaining solids on the flask neck.
- Fill the flask up to the 1 L line with DI water.
- Cap the flask and invert the flask to mix the solution. Wait until the air pocket reaches the bottom of the flask before returning the flask to the upright position. Repeat 9 more times.
- Add a magnetic stirrer to the flask, place the flask on a stir plate and stir the solution for 10 minutes.
- Transfer the solution to a labeled 1 L Nalgene bottle, twist on the cap tightly and store in the refrigerator.

Stock solution preparation

- Remove the concentrated mineral solution from the refrigerator.
- Repeat steps 2-10 from the concentrated mineral solution preparation procedure with the following exception regarding the appropriate mass of minerals as shown in Table C.**2**.

Table C.2 Mass concentrations for stock solution (g/L)

Compound	Phase 1	Phase 2	Phase 3
NaAce (COD)	8.365 (6.44)	8.365 (6.44)	8.365 (6.44)
NH_4Cl	1.0733	2.1466	1.0733
$FeCl_3*6H_2O$	0.03	0.06	0.03
KH2PO4**	0.2652	0.5304	0.2652
K2HPO4**	0.5312	1.0624	0.5312
Mineral sol'n (mL)	50	100	50

** 5 mM buffer strength

- Pipette appropriate volume of the concentrated mineral solution into the flask.
- Repeat steps 11-13 of the concentration mineral solution preparation procedure.
- To prepare 2 or 4 L of solution, add the appropriate amount of DI water (1-3 L) into a suitable container and then add the 1 L mineral/stock solution flask into the bottle.
- Take the bottle to DWE 3506 for pH adjustment; also bring the 50% NaOH bottle, a Pasteur pipet and pipet bulb.
- Turn on pH probe by pressing "measure". If the reading is not between 6.9 and 7.1, recalibrate probe.
- Add the NaOH solution one drop at a time until pH stabilizes at 7.
- Take the bottle back down to DWE 2524 and place it in the chiller.
- Snugly insert the rubber stopper back onto the bottle.

Zobell's solution (for ORP analysis)

- Fill 100 mL volumetric flask with 75 mL of DI water and put a funnel on top.
- Add chemicals to the flask as per Table C.3.

Table C.3 Mass concentrations for Zobell's solution (based on 100 mL)

Compound	Mass (g/L)
$K_4Fe(CN)_6*3H_2O$	0.1267
$K_3Fe(CN)_6$	0.0987
KCl	0.7455

- Add DI water to the 100 mL line and mix thoroughly. Transfer solution into 100 mL Nalgene bottle and store in the refrigerator.

Appendix D

Analytical Procedures

1. Bi-daily Analyses – pH, ORP, DO, TSS/VSS, tCOD

DO & ORP

1. Turn on DO and ORP meters.
2. Calibrate both meters using appropriate solutions: pH 4 and 7 buffers, Zobell's solutions fro ORP.

   2a. To check ORP meter:

   - Press "Mode" to mV scale. Immerse probe in the bottle of Zobell's solution.
   - The reading should be between +230 to +245 mV; if not, prepare more Zobell's solution as per procedures.
   - Press "Mode" again to mVscale.
3. Immerse DO probe in the MFC #1 sample vial and stir.
4. Take lowest DO reading, record DO reading on sheet.
5. Rinse with distilled water, dry with a Kimwipe
6. Repeat procedure for MFC #2 and feed vials; rinse with distilled water again.
7. Follow steps 3-5 for the ORP measurement.

pH and filter drying

1. Take samples to DWE 3506 for pH measurement.
2. Remove the pH probe from the buffer solution and rinse with DI water.
3. Immerse probe into MFC #1 sample and stir until reading stabilizes.
4. Repeat procedure for all samples.
5. Afterwards, remove all filter tray samples from the oven and place into a dessicator.
6. Take samples to CPH 1324 for homogenization and tCOD measurement.

Separation/"total" sample preservation/tCOD

- Label 9 COD vials, 3 samples x 3 (triplicate analysis) for tCOD (i.e. Se25-F-T1).
- Bring all labeled sample vials (3 full and 3 empty), 3 extra unlabelled vials (9 total) and COD vials to CPH 1324.
- Pour a sample into each plastic sample cup.

- Turn the rheostat for the homogenizer to 30, rinse with DI water, turn on homogenizer and homogenize a sample for 1 minute.
- After turning off homogenizer, put sample in the DI water cup and rinse for 10 seconds. Rinse the unit again using a squirt bottle of DI water to dislodge any solids left and use a paper towel to wipe dry.
- Repeat procedure for other samples
- Once sample has been homogenized, dilute it 9:1 for tCOD analysis.
- Once samples have been diluted, swirl cup to mix contents and pipette 2.5 mL into the appropriate labeled COD vial. Repeat this procedure for all 9 vials.
- Dilute the remaining undiluted sample in half by pipetting 12 mL of the remaining sample into the appropriate generic labelled sample vial (i.e. "1a" for MFC #1), using 3 x 4 mL increments. Add an identical amount of DI water.
- Repeat dilution step for other two samples.

TSS/VSS, "Soluble" sample preservation

- Bring the 3 generic sample vials (generic label 1a, 2a, Fa) and the 3 empty soluble labeled vials (6 total) to DWE 3506.
- Collect the 6 TSS dishes from the previous day, the 6 pre-dried aluminum dishes and the 6 VSS dishes from the dessicator.
- Place a piece of filter paper in each of the dishes, weigh and record the resulting mass.
- Once weighed, place dishes in the muffle furnace using thick cloth gloves and a large tweezer. Heta @ 550ºC for 12 min.
- Also weigh the VSS dishes
- After at least 12 min, remove dishes and cool down in the dessicator for 30 min.
- Prepare as follows:
    - Place the soluble feed sample vial in the unit, use a rubber stopper to ensure that the funnel spout is inside the rim of the vial.
    - Seal the bottom portion with the glass dome.
    - Apply the rubber-bottom filter seat on top of the glass container and place filter paper in the middle of the filter seat using tweezers.
    - Apply the ceramic funnel top and seal the filter paper tightly using the clamp.
    - Pipette 10 mL of soluble sample into the funnel and turn on vacuum pump
    - Remove clamp and place filter paper in appropriate aluminum dish using tweezers
    - Repeat steps c-f for the replicate sample, keeping the same soluble sample vial. Transfer sample label tape to new vial.
    - Pour the remaining liquid into the funnel and turn on vacuum pump. This will filter the remainder of the sample.
    - Remove the soluble sample vial and cap it.
    - Rinse the apparatus thoroughly with DI water, particularly the inside of the funnel spout.
    - Repeat preparation steps for the other two samples.
- Place aluminum dishes in oven and allow to dry at 105ºC for at least 24 hrs.
- After placing dishes in oven, preserve the remaining soluble samples by adding 2 drops of concentrated H_2SO_4 to sample vials to bring pH below 2 and refrigerate.
- Take 6 new aluminum dishes and 6 filter papers, put one paper in each dish, etch the bottom of the dish with next day's nomenclature (e.g., Se25-F-1) and leave to dry in the oven until next sampling day.

2. Other Analyses – GC, sCOD , IC

GC – Equipment Operation

- Turn on the computer beside the GC unit and let Windows boot up.
- Turn the helium feed to the GC unit on by turning the main valve completely counter-clockwise followed by the line-feed valve counter-clockwise a ¼ turn. Do not adjust the 2nd valve alone as this controls the He pressure.
- Turn the GC unit on (switch on bottom left side).
- Lift the cover on the unit up again.
- Ensure the helium is reaching the GC unit by using the small bottle of DI water inside the machine (take cap off DI water and put small metal tube sticking out of the unit into the DI water, watch for bubbles, recap DI water when done), close the cover on the GC unit.
- Find the current switch having 'high', 'off' and 'low' settings; the switch which should be initially in the middle (off) position, should now be set to 'low'.
- Open the 'PeakSimple' software on the computer and wait for it to load.
- Go to File → Open Control File and select test2.con from the list; let this control file load.
- Right-click and select 'Channel details' from the dropdown list.
- Ensure that the Run time is 2.8 minutes.
- Right-click and select 'postrun' from the dropdown list.
- Change the file and run names to : Greg_mndyMFC_air_00.CHR and Greg_mndyMFC.LOG.
- Once the 'Run' button on the GC unit is lit up (green), use the empty syringe beside the unit to draw 3 x 1 mL of air to "wash" the syringe, then draw another 1 mL of air as a sample and inject it into the unit. Once the sample has been injected, push the green 'Run' button. Wait 5 seconds after the light turns off and then quickly remove the needle.
- Let the unit run for the 2.8 minutes required for analysis.
- Repeat last step once more.
- Right-click and select 'postrun' from the dropdown list.
- Change the run name to : Greg_mndy_MFC1_00.CHR.
- Once the 'Run' button is lit up, take a gas sample by inserting needle into rubber septum of the Tedlar bag and drawing gas out. Draw out 3 x 1 mL to prime the needle and get rid of any excess air. Then draw the needle out one more time to collect a 1 mL sample. *Exercise

caution when inserting needle so that the bag is not punctured!* Now inject the sample into the unit. Once the sample has been injected, push the green 'Run' button. Wait 5 seconds after the light turns off and then quickly remove the needle.

- Repeat procedure for 2nd and 3rd replicates of MFC #1.
- Change the run name to Greg_mndy_MFC1_00.CHR.
- Repeat procedure for all replicates of MFC #2.
- Close the 'PeakSimple' software and select 'Save all' when prompted to save before exiting.
- Open the 'Peak329' folder (shortcut on desktop) and select the yrmndyMFC.LOG file associated with the samples just run, copy it and paste it into the appropriate folder (desktop as well).
- Turn the current switch on the GC unit to 'off' (center setting), turn off the GC unit and shut off helium feed by turning the main then the line-feed valves clockwise until snug.

COD Reagent Preparation

COD Sulphuric Reagent

- Empty the COD sulphuric reagent bottle into the appropriate waste container.
- Weigh out 5.5 g of silver sulphate and add it to the COD sulphuric acid reagent bottle.
- Place a magnetic stirrer in the bottle, place bottle on a balance and tare again to zero.
- Add 1 kg of sulphuric acid to the bottle – add 500 mL first and weigh; then slowly add acid up to 1 kg.
- Place bottle on stir plate overnight to allow salts to dissolve.
- Store bottle on shelves below the fume hood.

COD Digestive Chromate Reagent

- Empty the COD digestive chromate reagent bottle into the appropriate waste container and rinse with DI water.
- Weigh out 10.216 g of potassium dichromate and add it to the COD digestive chromate reagent bottle.
- Weigh out 33.3 g of mercuric sulphate and add it to the COD digestive chromate reagent bottle.
- Add 500 mL of DI water, cap the bottle, swirl the mixture to dissolve the salts; if needed, use a metal or plastic stirring rod to break up salt chunks; DO NOT shake since bottle is not well sealed.
- Add 167 mL of sulphuric acid, cap the bottle and swirl the mixture to mix well; CAUTION: The bottle will become very hot.
- Add 333 mL of DI water, cap the bottle and swirl the mixture to mix well.
- Store bottle on shelves below the fume hood.

1000 mg/L COD Standard

- Empty any remaining 1000 COD Standard.
- Weigh out 850 mg of potassium hydrogen phthalate (‘KHP’) and add it to the 1000 COD standard bottle.

- Add 1 L of DI water, cap the bottle, shake mixture for 2-4 min and place in standards refrigerator.

COD Analysis

- Carry all preserved samples (fresh and out of the fridge) to CPH 1324.
- For soluble COD analysis, dilute soluble samples as shown (on top of 2x dilution during original sampling):

Table D.2 Sample dilution for sCOD analysis

	Feed	MFC #1	MFC #2
Expected COD (mg/L)	6440	500	500
Dilution	5x (10x total)	2.5x (5x total)	2.5x (5x total)
Sample/water ratio (mL/mL)	2 mL/8 mL	4 mL/6 mL	4 mL/6 mL

**This is just a recommendation. It may be necessary to adjust the dilution ratio to accommodate lower expected COD readings.

- Collect enough COD digestion vials for all samples and standards (# of samples x3 plus 2 or 10 for standards); label the vials with labeling tape.
- For standards vials, label the COD concentration (i.e. S-1000 for the 1000 Cod standard or S-0 for the DI water blank).
- For sample vials, label with the sample nomenclature, (e.g.,. Se25-F-S1 denotes September 25th-Feed-Soluble replicate 1).
- If either COD reagent has been remixed or the 1000 mg/L standard has been remixed since the last digestion, prepare the following COD dilution standard series.
- Remove six 50 mL flasks and the 1000 mg/L COD standard from the refrigerator.
- Add the following volumes using an auto-pipette to obtain the proper dilution (/50 mL).

Table D.3 Dilution ratios for COD standards

Final conc.(mg/L)	10	25	50	100	300	500	1000
Standard added (X mL / 50 mL)	0.5	1.25	2.5	5	15	25	-

  - If reagents and standards are unchanged since the last digestion, prepare only the 1000 mg/L COD standard and a blank (DI water) for digestion.

- Use the 5 mL pipette to transfer 2.5 mL of each of the COD standards (2 or 10 counting the blank) and samples into the appropriate COD digestion vials.

- Use the 5 mL pipette to transfer 3.5 mL of COD sulphuric acid reagent into each vial; perform by pouring just enough reagent from the bottle into a glass beaker and using pipette to transfer from beaker to vials; this step should be carried out under the fume hood
- Use the 5 mL pipette to transfer 1.5 mL of COD digestive chromate reagent into each vial; perform by pouring just enough reagent from the bottle into a glass beaker and using pipette to transfer from beaker to vials; this step should be carried out under the fume hood.
- Seal each of the COD digestion vials with a clean cap, shake the vials until all the salt on the bottom has been dislodged and place vial in a test tube rack.
- Carry the vials to DWE 3506 and place the vials in the COD digestion block heater, turn on with the temperature set at 150ºC, set the timer for 2 hours, empty any diluted samples and standards and wash the Nalgene cups and glass beakers used. After 1-2 hours, reset the timer to 2 hrs to ensure a full 3 hour digestion.
- After the full digestion (3 hours), turn off the COD digestion block heater, carefully remove the vials, cool them in the test tube rack for 20-30 min and move vials to workbench.
- Use ethanol and Kimwipes to clean the outside of each of the COD digestion vials.
- Use the HACH spectrophotometer to obtain optical density (OD) readings for each COD sample and standard.
    - Turn on the spectrophotometer, press zero and enter when prompted for the program.
    - Using the COD blank, zero the machine by placing it in the vial port, cover with the black tube cover and press "Zero".
    - Read each COD optical density value by placing sample in the vial port and covering it with the black tube cover, digital readout will be given.
    - Record all COD values in the logbook.
- Once COD values are obtained, place the COD digestion vials containing sample and standards in the storage test tube racks with older samples.

COD calculation

Feed COD (g/L): Reading x 10

Discharge COD (g/L): Reading x 10

Once again, this may have to be adjusted based on dilution ratio

VFA by IC Standard Solution Preparation

- Remove the IC standard bottle from the refrigerator in DWE 3506.
- Use a 3 mL syringe and needle to extract the required volume **DO NOT remove the cap as the contents are filled with N_2 gas to keep contents anaerobic.**
- Standard solution contains 10 mM (600 mg/L) HAc; dilute standard solution to 60 mg/L as follows:
    - Extract 1 mL of the standard solution using 5 mL pipette and add to 10 mL flask
    - Dilute up to 10 mL using MilliQ water and cap the flask.
    - Place the standard solution back into the refrigerator.

VFA by IC Sampling Procedure

- Bring the following to DWE 3506:
    - All samples.
    - Diluted standard solution.
    - 2-3 5 mL syringes and syringe filters.
    - 5-7 autosampler cartridges.
    - 30-39 vials & filter caps.
    - Extra Nalgene cup.
    - Plastic filter cap locking device.
- Separate the feed samples from the discharge samples.
- For the feed samples, pre-dilute by an additional 20 times as follows:
    - Take 4 clear glass vials designated for the IC.
    - Use an autopipette to add 1 mL of sample to 19 mL of MilliQ water in each cup.
- For the discharge samples, pre-dilute an additional 5 times as follows:
    - Take 4 clear glass vials designated for the IC.
    - Use an autopipette to add 4 mL of sample to 16 mL of MilliQ water for each cup.
- Cap the vials as follows:
    - For discharge samples, the generic IC vials are labeled by relative date, then MFC # (i.e. IC 1-1 means the 1st date for MFC #1).
    - For feed samples, the generic IC vials are labeled as relative date, then "F" for feed (i.e. IC 2-F means the 2nd date for the feed).
- Perform pH adjustment of all diluted vials:
    - Turn on pH probe in DWE 3506.

- If pH reading is not between 6.9 and 7.1, recalibrate probe.
- Rinse using DI water and insert into vial.
- Adjust pH using either 50% NaOH (initially), 1 M HCl or 1 M NaOH (towards the end) until the pH is between 2.7 and 3.

- Take adjusted vials back to DWE 3508.
- Place the appropriate number of Dionex plastic vials into the cartridges and label using the sample date, MFC # and replicate. Depending on the number of samples for the week, either 31 or 39 Dionex plastic vials in total will be required based on a duplicate analysis. The order of the vials introduced into the autosampler will be as follows:

Table D.4 Order of vials for 3 and 4 sample IC analysis

3 sample days	B, S,W, B, 4, W, B, 4, W, B, 4, W, B, 4, W, B, 2, W, Shut (31 total)
4 sample days	B, S, 5, W, S, B, 5, W, S, B, 5, W, S, B, 5, W, S, B, 4, W, Shut (39 total)
B = Blank, S = Standard, W = Wash, (Number) = # of consecutive samples, Shut = Shutdown sequence	

- Since the first vial is a blank, add ~3 mL of MilliQ water to the vial and seal using the filter cap
- Add ~3 mL of the diluted standard solution to the 2nd vial.
- Since "W" denotes a wash cycle, add only ~3 mL MilliQ water to the "W" vial.
- For samples, prime the syringe by rinsing it 3 times with MilliQ water, shake off any excess and then rinse with the sample solution 3 times.
- Extract ~ 3 mL from the sample vial. Attach the syringe filter to the end of the syringe and push the sample through the filter into the appropriate plastic vial. Cap the vial using the filter cap and plastic cap tool. First use the holed end to seat the cap and then the flat end to push it down.
- Extract another 3 mL for the duplicate and push it through the same syringe filter into the next plastic vial. Cap using filter cap as in step 13.
- Repeat steps 12-14 for all samples. Keep in mind that after each sample date, discard the syringe filter to prevent cross-contamination. After all samples for one of the cells are analyzed, discard the syringe as well (i.e. after all MFC #1 samples are analyzed, discard the syringe).
- After a cartridge has been filled, place it (in order) into the autosampler so that it does not accidentally tip over while filling other cartridges.

IC Operation procedure – Manual Pre-wash

- Open the 1-methane sulfonic acid (MSA) and acetonitrile (AN) bottles and fill to near the top since each run will require about 1 L of each eluent.
- Open the He gas line valve on the rear wall.
- Move toggle on the Pressure/Sparge switch on the IC column to "Sparge" for both the MSA and AN lines.
- Allow sparging with N_2 gas for 10 min.
- During the sparge, press "Remote" on the UV detector and the UV lamp to "Start" to allow for warm-up of the lamp. After ~1 min, the lamp light will automatically switch to "On".
- Move toggle on the Pressure/Sparge switch back to "Pressure".
- Press the Local/Remote button on the IC column to "Local".
- Using the touchpad on the IC column, begin a wash of the IC column by the following steps:
  - Press '%/#' once, then '1' to select MSA.
  - Press '1-0-0' for 100% MSA, channel 3 (AN) should automatically be set to 0; if it is not:
    - Press '%/#' once then '3' to select AN.
    - Press '0' for 0%, then '%/#' once to accept.
  - Press 'Flo', then '1' to set the flow rate at 1 mL/min.
  - Press 'Start'.
  - Wash for 10-15 min until absorbance is stable, then press 'stop'.
- Repeat step 6, except set AN to 100% and MSA to 0%, wash for 10-15 min again.
- Press the Local/Remote button on the IC column to "Remote".

IC Operation Procedure – Software

- Turn on computer (if not on already).
- Open the software by double-clicking "Shortcut to MenuDx.exe"
- Click 'Schedule' to set/edit the schedule.
- If a schedule template has already been set up, just alter the sample names as per step 4d and leave the rest of the columns the same.
- 1st column is the Sample Name. Based on the vial order in step 7, enter:
  - "Blank" for a blank run.
  - "Standard" for a standard run.
  - "Wash" for a wash run.

- The standard ID for the sample (i.e. Se25-1-1 for September 25th, MFC #1, replicate 1) for a sample run.

- 2nd column defines the Sample Type. For all runs, enter "Sample" from the dropbox.
- 3rd column is not altered.
- 4th column defines the Method. Under the method folder, click "VFA3" as the method, then click "Open". The only exception is for the wash runs; in this case, click "VFAwash" and then "Open".
- 5th column defines the Data file. This contains the name of the file and also where the data will be saved. Before entering this step, make a folder file path for the analysis date as follows: Windows explorer → Peaknet → Data → Greg → "Sample date folder". Once this file folder is created, set it as the destination folder in the Data File column. Name the first sample "VFA_001.DXD", the second "VFA_002.DXD" and so forth. Save the schedule folder as "4_sample". Make another schedule for a 3 sample run and save as "3_sample".
- Click 'Run' on the main menu.
- Load the appropriate schedule (this may take a minute).
- Move toggle on the "Run/hold" button of the autosampler to "Run".
- Click on "Run", then "Start" to begin the analysis. The run can also be stopped using the command: "Run" → "Abort".
- Note that each run lasts about 55 minutes, except for the wash run which requires 20 minutes. Based on this, the 3_sample program should operate for about 27 hours, while the 4_sample program lasts about 36 hours. The best time to run each set would be:
- For 3_sample program, 2-3 pm.
- For 4_sample program, 8 pm.
- After completion of all runs, shut off the He gas flow using the valve on the back wall.
- To read the results of the analysis, go to the main menu and click "Optimize".
- Open the appropriate file from the file folder created previously.
- Press "Print Preview" and check the 2nd page for results.
- To scroll to the next file, click on the 3rd icon in the taskbar (looks like a file folder with a blue arrow pointing to the right).

VFA, COD calculation

Feed [VFA] = Result x 40 Feed [COD] = Feed [VFA] * 1.07

Discharge [VFA} = Result x 10 Discharge [COD] = Discharge [VFA] * 1.07

- Discard the plastic vials and filter caps.

Washing of IC Vials

- Wear full safety gear (gloves, coat, goggles).
- To wash vials, first discard any liquid in the clear sample vials into an appropriate labeled waste container.
- Carry all vials and caps to DWE 3506.
- Place 2 sheets of paper towel on a counter top.
- Take the COD waste jug from the bottom shelf near the lab coats along with the waste bottle and place on the paper towel.
- Carefully pour ~10 mL of COD waste into a sample vial.
- Tilt the vial so that the liquid is almost horizontal, making sure not to let the contents drip out.
- Rotate the vial so that the liquid coats its inside walls (clearly visible due to the liquid viscosity).
- Transfer the waste to the next vial.
- After this has been repeated for all vials, discard the COD waste into the 250 mL waste bottle.
- Now take the vial and fill halfway with tap water.
- Repeat steps 7-9, making sure to dissolve any of the COD waste.
- Discard the waste into the waste bottle.
- Take the vials and caps to the dishwashing room (DWE 3507).
- Rinse all vials and caps 10 times with tap water. Be sure to rinse the exterior as well a few times.
- Rinse all vials and caps 3 times with DI water. Be sure to rinse the exterior as well a few times.
- Rinse all vials and caps 1 time with MilliQ water. Be sure to rinse the exterior as well.
- Take wet vials and place on a drying rack. If time is short, place vials into the oven at 60-70ºC to dry. Otherwise, leave out at room temperature overnight.

Appendix E
Experimental Data

Please see attached CD for experimental data. Data is not available with electronic version.